UNIVERSIDADE FEDERAL DO PARANÁ

ANDRESSA DE ARAUJO SILVA

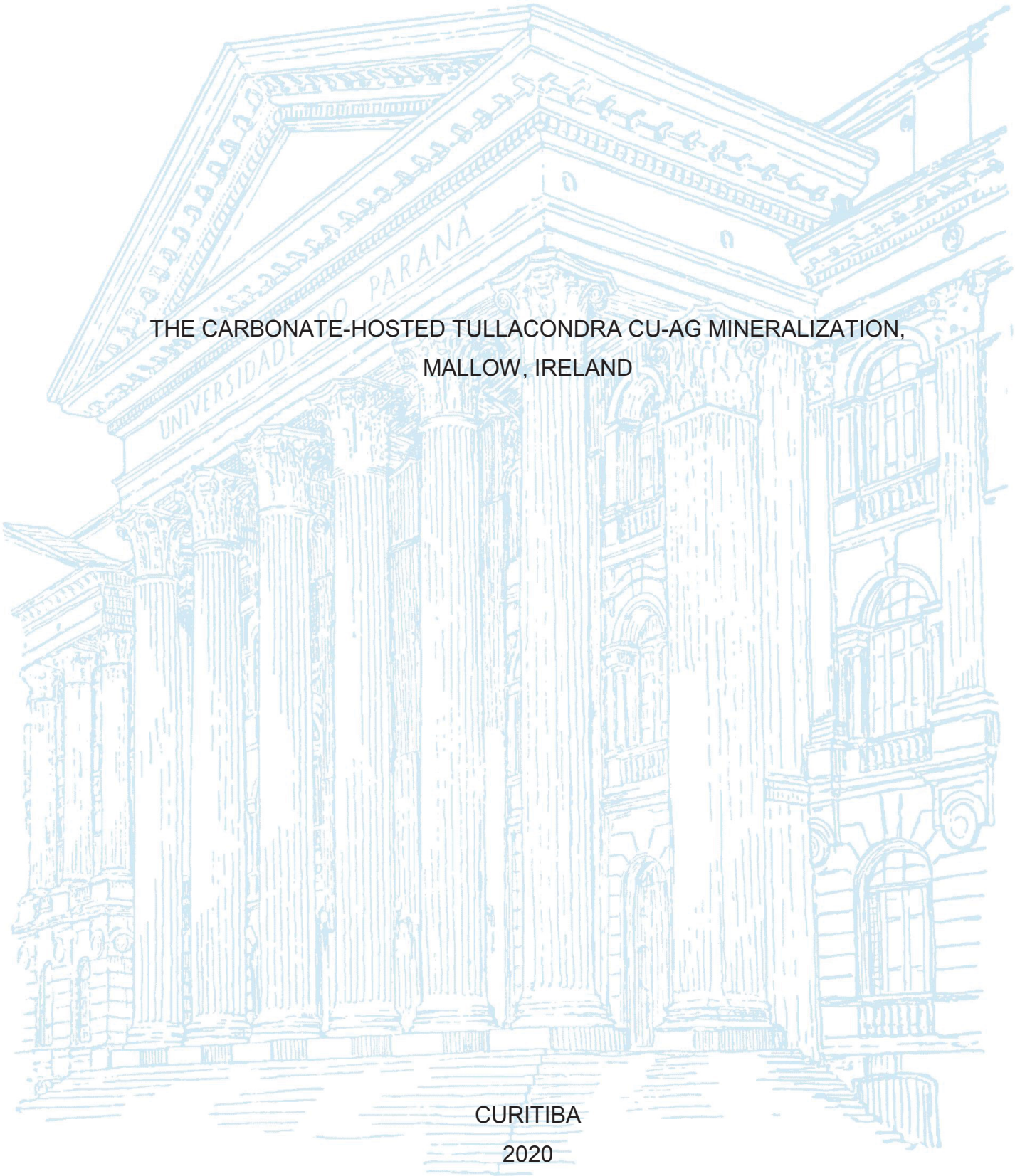

THE CARBONATE-HOSTED TULLACONDRA CU-AG MINERALIZATION, MALLOW, IRELAND

CURITIBA

2020

ANDRESSA DE ARAUJO SILVA

THE CARBONATE-HOSTED TULLACONDRA CU-AG MINERALIZATION, MALLOW, IRELAND

Dissertação apresentada ao curso de Pós-Graduação em Geologia, Setor de Ciências da Terra, Universidade Federal do Paraná, como requisito parcial à obtenção do título de Mestre em Geologia Exploratória.

Orientador: Prof. Dr. Pedro Filipe de Oliveira Cordeiro

Coorientador: Prof. Dr. Leonardo Evangelista Lagoeiro

CURITIBA

2020

Catalogação na Fonte: Sistema de Bibliotecas, UFPR
Biblioteca de Ciência e Tecnologia

S586c Silva, Andressa de Araujo
The carbonate-hosted Tullacondra cu-ag mineralization, Mallow, Ireland [recurso eletrônico] / Andressa de Araujo Silva. – Curitiba, 2020.

Dissertação - Universidade Federal do Paraná, Setor de Ciências daTerra, Programa de Pós-Graduação em Geologia, 2020.

Orientador: Pedro Filipe de Oliveira Cordeiro – Coorientador: Leonardo Evangelista Lagoeiro

1. Sedimentos (Geologia) - Irlanda. 2. Carbonato – reservatórios. 3. Cobre. 4. Prata. I. Universidade Federal do Paraná. II. Cordeiro, Pedro Filipe de Oliveira. III. Lagoeiro, Leonardo Evangelista. IV. Título.

CDD: 552.5809415

Bibliotecário: Elias Barbosa da Silva CRB-9/1894

TERMO DE APROVAÇÃO

Os membros da Banca Examinadora designada pelo Colegiado do Programa de Pós-Graduação em GEOLOGIA da Universidade Federal do Paraná foram convocados para realizar a arguição da dissertação de Mestrado de **ANDRESSA DE ARAUJO SILVA** intitulada: **THE CARBONATE-HOSTED TULLACONDRA CU-AG MINERALIZATION, MALLOW, IRELAND**, sob orientação do Prof. Dr. PEDRO FILIPE DE OLIVEIRA CORDEIRO, que após terem inquirido a aluna e realizada a avaliação do trabalho, são de parecer pela sua APROVAÇÃO no rito de defesa.

A outorga do título de mestre está sujeita à homologação pelo colegiado, ao atendimento de todas as indicações e correções solicitadas pela banca e ao pleno atendimento das demandas regimentais do Programa de Pós-Graduação.

CURITIBA, 23 de Abril de 2020.

Assinatura Eletrônica
23/04/2020 16:00:18.0
PEDRO FILIPE DE OLIVEIRA CORDEIRO
Presidente da Banca Examinadora (UNIVERSIDADE FEDERAL DO PARANÁ)

Assinatura Eletrônica
23/04/2020 16:48:18.0
LENA VIRGÍNIA SOARES MONTEIRO
Avaliador Externo (UNIVERSIDADE DE SÃO PAULO)

Assinatura Eletrônica
23/04/2020 16:52:12.0
ARIADNE BORGO
Avaliador Externo (UNIVERSIDADE FEDERAL DO PARANÁ)

Dedico essa dissertação à minha
mãe, uma pessoa brilhante e a principal
razão das minhas conquistas.

AGRADECIMENTOS

Durante esse período de dois anos de mestrado, tive a honra de estudar um *Irish-type deposit*. Isso só foi possível com o apoio de pessoas daqui do Brasil e de fora também. Por isso, vou dividir os meus agradecimentos em duas partes, uma em português e outra em inglês, para que os meus agradecimentos possam chegar a todos.

Primeiramente, gostaria de agradecer à minha família pelo apoio e incentivo. Sou uma pessoa privilegiada por poder ter como prioridade os estudos e isso eu devo a vocês.

Agradeço à UFPR e ao Programa de Pós-graduação em Geologia pela oportunidade de estudar e avançar na minha pesquisa.

Agradeço ao professor Pedro Cordeiro, o melhor orientador, amigo e psicólogo que eu poderia ter. Sou privilegiada também por ter encontrado essa pessoa e acredito que qualquer um que cruzar seu caminho é uma pessoa de sorte. Agradeço aos professores Leonardo Lagoeiro, Germán e Cadu que me ajudaram de alguma maneira durante esses dois anos.

Agradeço aos funcionários do LAMIR que de algum modo me ajudaram nas análises petrográficas e químicas.

Agradeço aos meus colegas Anderson Matias, Laisa Stingelin e Júlia Oliveira pelas discussões sobre os depósitos irlandeses.

Agradeço aos estudantes que fizeram ou fazem parte do LabGeol pela companhia e cafés nesses dois anos. Em especial, àqueles que estiveram mais engajados em melhorar o nosso programa de pós-graduação. Agradeço ao Matheus Silva (Chris) pela companhia e carinho desse último ano.

Agradeço aos membros do UFPR SEG Student Chapter, pelas reuniões, viagens e atividades que fizemos juntos durante esses dois últimos anos de UFPR. Meus agradecimentos vão, em especial, às alunas Ana Clara Müller e Nathalia Lemes por tomarem frente do grupo.

Aos membros do Clube de Dança da UFPR, principalmente ao pessoal do forró que me ajudou a descontrair muitas vezes.

À CAPES pela bolsa de pesquisa e que sem ela não teria conseguido seguir com meus estudos. Infelizmente, estamos em momentos dificeis para os pós-graduandos e para ciência brasileira. Espero que isso mude.

ACKNOWLEDGEMENTS

I would like to thank the iCrag and the researchers Patrick Meere, Sean Johnson and Richard Unit for the academic support and for reviewing my various abstracts submitted to different conferences and my paper.

I am also grateful to Loretta Corcoran and Antonio Simonetti for carrying out our micro-X-ray fluorescence analysis at the University of Notre Dame and their availability for reviewing my dissertation.

Special thanks are also given to Bob Kozyrski of the Diversified Asset Holdings Pty Ltd for supporting my travel to Ireland making possible a visit to the Tullacondra quarry and core shed. I would like to thank John and Maire Hickey, the lovely couple who hosted me during my time in Ireland.

“Tú eres una mujer libre, eres libre de irte de fiesta, eres libre de irte de una isla y eres libre de irte del planeta si te apetece” (La Casa de Papel, Dir. Diego Ávalos, Perf. Alba Flores e Ursula Corbero, Nextflix, 2019)

RESUMO

O depósito de Cu-Ag de Tullacondra está localizado no sul da Irlanda dentro do *Irish Midlands,* e contém aproximadamente 4,2 Mt de 0,7% de cobre e 27,5 g/t de prata. Apesar de seu tamanho pequeno e baixas concentrações de minério, o depósito de Tullacondra ocorre no mesmo contexto metalogenético que importantes depósitos de Zn-Pb (Navan, Lisheen e Silvermines) localizados também no *Irish Midlands.* Entretanto, a relação metalogenética entre os depósitos de cobre do sul da Irlanda com os demais depósitos da bacia carbonática irlandesa não é bem conhecida e requer investigações mais detalhadas. Com esse propósito, análises petrográficas, geoquímicas, de imageamento de μXRF e modelamento geológico foram realizadas. Os resultados desse estudo detalhado indicam que o depósito de Tullacondra apresenta de controles estratigráficos e estruturais semelhantes aos depósitos de Zn-Pb irlandeses. Nossa investigação mostra que a mineralização de Tullacondra foi controlada principalmente pela *Tullacondra Fault*, uma falha normal de direção EW, e por uma zona fraturada relacionada a *relay ramps.* Secundariamente, a mineralização de Tullacondra é controlada pela estratigrafia. Os minerais de ganga do depósito são calcita, quartzo, feldspato e muscovita, e consistem em menores proporções de barita, monazita, zircão, rutilo, apatita, clorita, ilmenita, hematita e hidrocarbonetos. Os minerais de minérios são compostos por sulfestos e sulfossais de arsênio e cobre. Análises geoquímicas mostram que a concentração de SiO_2 diminui enquanto CaO aumenta da base para o topo. Isso é resultado da transgressão marinha que ocorreu durante a deposição das rochas hospedeiras. Além disso, óxido de magnésio está localmente elevado nos corpos de minério distais devido a uma dolomitização pré-mineralização. A abundância de minerais de arsênio e Cu, Ag, As, Sb, and Zn é elevada próximo a *Tullacondra Fault* diminuindo com a distância. Em contraste com modelo antigo, propõe-se que o depósito Tullacondra consiste em três corpos de minério *stratabound* e uma zona vertical fraturada mineralizada. Adicionalmente, os estágios de principal mineralização são formados por duas assembleias minerais distintas: (1) calcocita, bornita, e calcopirita disseminadas, paralelas ao acamamento e hospedadas em dissolution seams; e (2) arsenopirita, tennantita, e calcopirita disseminadas, paralelas ao acamamento e hospedadas em dissolution seams. Em um estágio posterior à mineralização principal, esses minerais de minério foram remobilizados e mineralizaram em veios. Além disso, o desenvolvimento de *dissolution seams* anteriormente a mineralização foi importante para canalizar o fluido mineralizante, mas falhou ao evoluir em zonas de brechas de dissolução. Por isso, o processo não resultou na acumulação de quantidades econômicas de sulfetos.

Keywords: depósitos de Cu-Ag. Depósitos hospedados em carbonatos. *Irish-type. Irish Midlands.*

ABSTRACT

The Tullacondra Cu-Ag deposit is located in southern Ireland within the Lower Carboniferous Irish Midlands, and contains approximately 4.2 Mt of 0.7% copper and 27.5 g/t silver. Despite its small size and low grades of Cu and Ag, the Tullacondra deposit occurs in the same metallogenetic context as other major Zn-Pb deposits (Navan, Lisheen and Silvermines) located in the Irish Midlands. However, its exact metallogenic relationship relative to the copper deposits from southern Ireland and Irish Midlands is not well known and requires detailed investigation. In this regard, petrography, geochemical analysis, μXRF imaging, modeling geological modeling were carried out. The results from this detailed study indicate that the Tullacondra deposit consists of similar structural and stratigraphic controls, metal affinities, and mineral zonation compared to Zn-Pb deposits within Ireland. Our investigation shows that mineralization within the Tullacondra deposit is primarily controlled by the EW-trending normal Tullacondra Fault, and by fractured zone related with its relay ramp (damage zone), and is secondarily influenced by stratigraphy. The gangue minerals are calcite, quartz, feldspar and muscovite, and minor barite, monazite, zircon, rutile, apatite, chlorite, ilmenite, hematite and bitumen. The ore minerals consist of copper and arsenic sulfides and sulfosals. Geochemical analysis show that SiO_2 content decreases and CaO increases upward due to the marine transgression during the deposition of the host rocks. Additionally, magnesium oxide is locally enriched in the distal orebodies due to the local pre-ore dolomitization. The abundances of arsenic minerals and Cu, Ag, As, Sb, and Zn are elevated proximal to the fault decreasing outward the Tullacondra Fault and upward. In contrast to prior formational models, we propose that the Tullacondra deposit consists of three stratabound orebodies and a vertical mineralized fractured zone (damage zone). Additionally, the main ore stages is marked by mineralization of two assemblage minerals: (1) disseminated, parallel bedding and dissolution seam-hosted chalcocite, bornite, and chalcopyrite; (2) disseminated, parallel bedding, and dissolution seam-hosted arsenopyrite, tennantite, and chalcopyrite. In a Late-ore stage, these ore minerals were remobilized and formed vein-hosted chalcocite, bornite, chalcopyrite, and tennantite. Moreover, the development of dissolution seams during the pre-ore stage was important for channeling mineralizing fluid flow but this failed to evolve into fully brecciated zones, and thus this process did not result in the accumulation of economic amounts of sulfides.

Keywords: Cu-Ag deposit. Carbonate-hosted deposit. Irish-type. Irish Midlands.

LISTA DE FIGURAS

LISTA DE TABELAS

LISTA DE ABREVIATURAS OU SIGLAS

LISTA DE ABREVIATURAS DE MINERAIS

apy	- arsenopirita	cct	- calcocita	py	- pirita
bn	- bornita	chc	- calcedônia	qz	- quartzo
cal	- calcita	cv	- covelita	tnt	- tenantita
ccp	- calcopirita	dol	- dolomita		

Fonte: Whitney and Evans (2010)

LISTA DE ABREVIATURAS DE UNIDADES E LITOLOGIAS

BS	- Ballyvergin Shale	OC	- Oolitic Calcarenite
Fm	- Formação	ORS	- Old Red Sandstone
LLS	- Lower Limestone Shale	TL	- Tullacondra Limeston
Ls	- Limestone	TS	- Transition Series
LSC	- Lower Shaly Calcarenite	USC	- Upper Shaly Calcarenite
LTS	- Lower Transition Series	UTS	- Upper Transition Series

LISTA DE ABREVIATURAS DE INSTITUIÇÕES, EQUIPAMENTOS, MÉTODOS ANALÍTICOS E OUTROS

μXRF - Microfluorescência de raios-X
BSR - Bacteriogenic sulfate reduction
CEST - Center for Environmental Science and Technology
DEGEOL - Departamento de Geologia da Universidade Federal do Paraná
DH - Drill hole
E - Leste
EDS - Espectroscopia por energia dispersiva
ENE - Leste-nordeste
EW - Leste-oeste
GSI - Geological Survey Ireland
iCrag - Irish Centre for Research in Applied Geosciences
ICP-AES - Inductively Coupled Plasma - Atomic Emission Spectrometry
ICP-MS - Inductively Coupled Plasma - Mass Spectrometry
LAMIR - Laboratório de Análises de Minerais e Rochas

LAPEM - Laboratório de Pesquisa em Microscopia
LOI - Loss on ignition
MEV - Microscopia Eletrônica de Varredura
MVT - Mississippi Valley-Type deposits
N - Norte
NE - Nordeste
NNW - Norte-noroeste
NS - Norte-sul
Petrog. - Petrografia
RGB - Red, Green, Blue
S - Sul
SEDEX - Sedimentary exhalative deposits
SEM - Scanning Electron Microscopy
SSE - Sul-sudeste
SW - Sudoeste
TSR - Thermochemical Sulfate Reduction
UFPR - Universidade Federal do Paraná
W - Oeste
WSW - Oeste-sudoeste
W - OESTE
WSW - Oeste-sudoeste

LISTA DE SÍMBOLOS

% - Porcentagem
‰ - Por mil
< - Menor que
> - Maior que
$\delta^{34}S$ - Isótopo de enxofre
µA - Microampere
Ag - Prata
Al - Alumínio
Al_2O - Óxido de alumínio
As - Arsênio
Ba - Bário
Bi - Bismuto
C - Carbono
Ca - Cálcio
CaO - Óxido de cálcio
Cd - Cádmio
Ce - Cério
Co - Cobalto
Cr - Crômio
Cs - Césio
Cu - Cobre
Dy - Disprósio
Er - Érbio
Eu - Európio
Fe - ferro
g/t - grama por tonelada
Ga - Gálio
Gd - Gadolínio
H_2S - Ácido Sulfídrico
Hf - Háfnio
Hg - Mercúrio
Ho - Hólmio
In - Índio
K - Potássio
K_2O - Óxido de potássio
kV - Kilovolt
La - Lantânio
Li - Lítio
Lu - Lutécio
Mg - Magnésio
MgO - Óxido de Magnésio
Mn - Manganês
Mo - Molibdênio
Mt - Milhões de toneladas
Nb - Nióbio
Nd - Neodímio
Ni - Níquel
O - Oxigênio
Os - Ósmio
P - Fósforo
Pb - Chumbo
ppm - Parte por milhão
Pr -Praseodímio
Q1 - primeiro quartil
Q2 - segundo quartil
Q3 - terceiro quartil
Rb - Rubídio
Re - Rênio
Sb - Antimônio
Sc - Escândio
Si - Silício
SiO_2 - Óxido de silício
Sm - Samário
Sn - Estanho
Sr - Estrôncio
Ta - Tântalo
Tb - Térbio
Te - Telúrio
Th - Tório
TiO_2 - Óxido de titânio
Tl - Tálio
Tm - Túlio
U - Urânio
V - Vanádio
W -Tungstênio
Y - Ítrio
Yb - Itérbio
Zn - Zinco
Zr - Zircônio

SUMÁRIO

1. INTRODUÇÃO

A presente dissertação refere-se ao estudo petrográfico e geoquímico de amostras do depósito de Cu-Ag de Tullacondra localizado a NNW e a 10 km da cidade de Mallow no condado de Cork, sul da Irlanda (Fig. 1). Descoberto em 1973, esse depósito contém uma zona enriquecida em cobre, com aproximadamente 3,6 Mt a 0,7% de Cu e 27,5 g/t de Ag, e, ainda, uma zona enriquecida em prata com cerca de 0,6 Mt a 150 g/t Ag e 0,6% Cu (Wilbur e Royall, 1975; Wilbur e Carter, 1987).

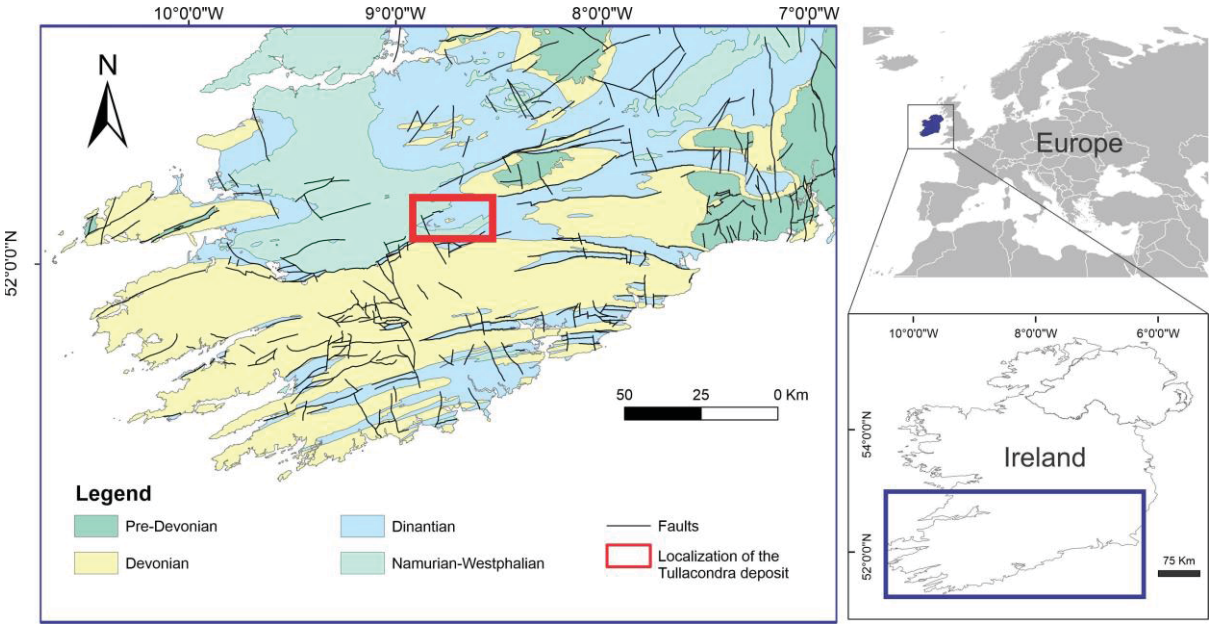

Figure 1 - Figura de localização do depósito de Tullacondra. Dados disponíveis no site do Serviço Geológico da Irlanda (GSI, 2020).

O depósito de Tullacondra é hospedado em calcarenitos e folhelhos de unidades do Carbonífero Inferior que também hospedam importantes depósitos de Zn e Pb, tais como os depósitos de Navan, Lisheen e Silvermines (Fig. 2). De acordo com Singer (1995), esses depósitos contêm uma das maiores reservas de Zn e Pb do mundo com cerca de 110 Mt em Navan (Ashton *et al*., 2015), 22 Mt em Lisheen (Shearley *et al*., 1996), e 17 Mt em Silvermines (Andrew *et al*., 1986b). Além dos Depósitos de Zn-Pb a plataforma carbonífera irlandesa contêm depósitos de Cu-Ag, tais como Aherlow, Gortdrum e Ballyvergin com 6 Mt, 3,8 Mt e 2,3 Mt, respectivamente (Andrew, 1986a; Steed, 1986). Esses depósitos apresentam similaridades com depósitos irlandeses de Zn e Pb, como por exemplo, ambos os

casos mostram controle estrutural de falhas com *trend* NE a ENE e dolomitização associada diretamente ou indiretamente com a mineralização (Andrew 1986b; Steed, 1986; Wilbur e Carter, 1986; Anderson *et al*., 1998; Hitzman *et al*., 2002; Johnston, 1999; Kyne *et al*., 2019; Lang *et al*., 2020; Torremans *et al*., 2018; Wilkinson *et al*., 2005). Entretanto, os depósitos de Cu-Ag são subeconômicos e os processos que permitiram a formação de depósitos de Cu-Ag ao invés de depósitos de Zn-Pb são pouco entendidos. Além disso, outros depósitos de Zn-Pb fora da Irlanda se assemelham com *Irish-type*, tais como os depósitos da Província Vazante-Paracatu em Minas Gerais (Cordeiro *et al*. 2018; Monteiro *et al*. 2006), e poderiam também conter reservas de Cu-Ag não exploradas. Assim, o entendimento da mineralização em Tullacondra pode auxiliar nos esforços de exploração de cobre e prata, e determinar potencial desconhecido do *Irish Ore field* e de outras Províncias minerais de Zn-Pb para depósitos de cobre.

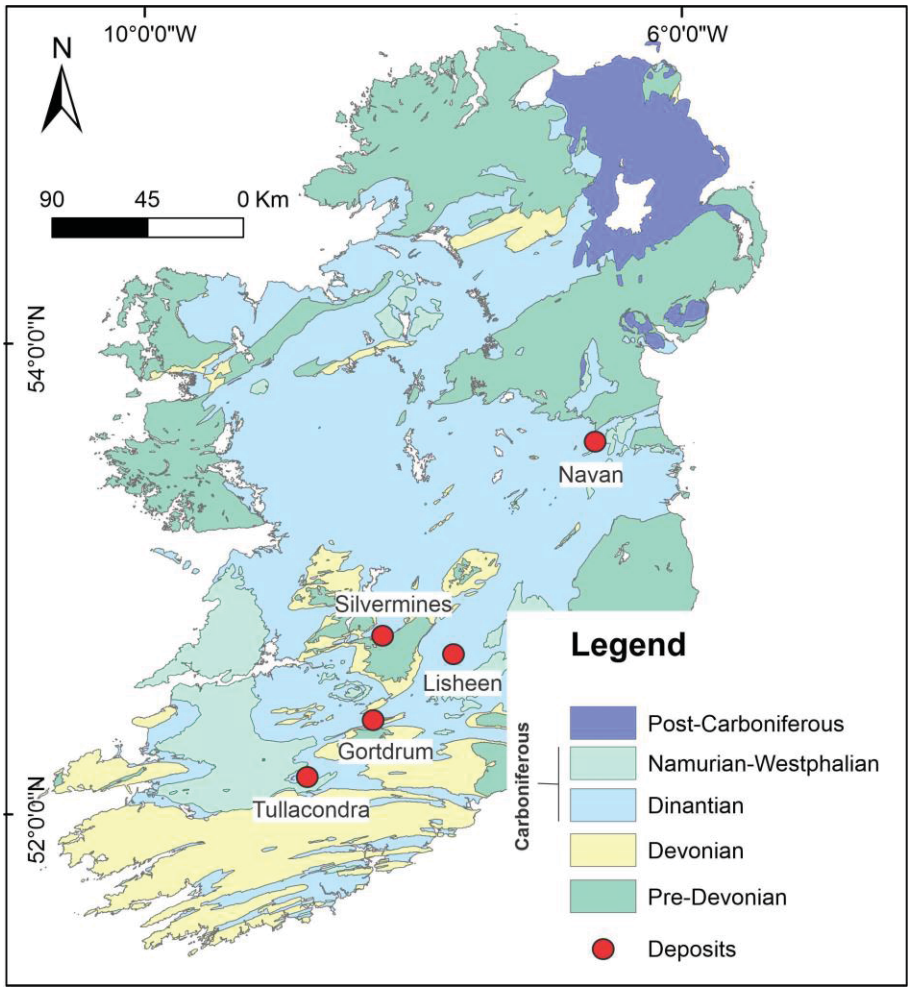

Figure 2 - Mapa da Irlanda mostrando a localização dos depósitos de Zn-Pb de Navan, Lisheen e Silvermines, e de Cu de Tullacondra e Gortdrum. Dados disponíveis no site do Serviço Geológico da Irlanda (GSI, 2020).

Portanto, com a finalidade de um detalhamento da mineralização de cobre e prata do depósito de Tullacondra, descrições e *assays* de furos de testemunhos**,** química de rocha total, petrografia, análises de MEV-EDS e mapeamento semi-qualitativo de micro-fluorescência de raios-X foram realizados. Com esses dados, nós mostramos mais similaridades entre os depósitos de Zn-Pb do *Irish Ore field* e o depósito de Tullacondra, provando que ambos os depósitos fazem parte de um mesmo contexto metalogenético. Além disso, com base nos dados interpretados e na bibliográfia disponível sobre depósitos da *Irish Midlands,* um modelo genético é proposto.

1.1 ESTRUTURA DA DISSERTAÇÃO

Essa dissertação é estruturada em: (1) Introdução – o capítulo introdutório inclui também a justificativa, objetivo geral e específico, além dos métodos empregados; (2) Contexto geológico – o contexto geológico é subdividido em Geologia Regional e Geologia do depósito de Tullacondra. Na Geologia Regional, é mostrado a evolução estratigráfica e tectônica da bacia carbonática irlandesa durante Paleozoico. Na Geologia do depósito de Tullacondra, especifica-se a evolução geológica local, mostrando as denominações estabelecidas para região de Tullacondra em comparação com o que é citado regionalmente; (3) Resultados e discussões – este capítulo é ilustrado na dissertação em forma de artigo. O artigo é intitulado “The carbonate-hosted Tullacondra Cu-Ag Mineralization, Mallow, Ireland” e se encontra na seção de “Resultados e Discussões”. No artigo são mostradas as principais feições dos corpos de minérios de Tullacondra, tais como dimensões, controles estruturais e estratigráficos, texturas e tipos de minérios, minerais de ganga, e comportamento geoquímico. As normas de citação do artigo obedecem as regras da revista a qual pretendemos submeter, a *Economic Geology;* (4) Considerações finais – neste capítulo são abordadas as últimas considerações, o que incluem planos futuros para essa pesquisa e recomendações; (5) Referências; Anexos – os anexos mostram os dados geoquímicos e os dados químicos de Cu e Ag e estratigráficos usados para o modelamento geológico.

1.2 JUSTIFICATIVA

Os depósitos hospedados na bacia carbonática irlandesa fazem parte de uma classe mundial de depósitos de Zn-Pb, conhecida como *Irish-type*, e o estudo mais detalhado sobre a gênese de depósitos de cobre associados deve complementar o que já se sabe sobre esse modelo. Além disso, Tullacondra oferece uma oportunidade unica de entender a transição entre sistemas hospedados em carbonatos *Irish-type* e SEDEX. Isso porque, a mineralização em ambos os casos é associada ao fundo marinho, e os depósitos de *Irish-type* são considerados transicionais entre o tipo SEDEX e MVT (Wilkinson, 2013).

É importante destacar ainda que o entendimento da mineralização de cobre e prata associada com aquelas de zinco e chumbo do *Irish Ore field* pode auxiliar na exploração e prospecção de depósitos de cobre ainda não descritos na Província de Zn-Pb da Irlanda ou de outras províncias de Zn-Pb similares.

1.3 OBJETIVO GERAL

O objetivo é compreender os processos metalogenéticos de formação do depósito de Cu-Ag de Tullacondra. Assim, será discutido se, com base no que já se é entendido sobre os depósitos *Irish-type* de Zn-Pb, os depósitos de Cu-Ag podem estar inseridos no mesmo contexto metalogenético que os grandes depósitos de Navan, Lisheen e Silvermines.

1.3.1 Objetivo específico

Os objetivos específicos incluem:

a) Caracterizar os principais corpos de minério, incluindo principais minerais de minério, unidades hospedeiras, controles estruturais e estratigráficos;
b) Determinar as principais alterações hidrotermais, feições texturais e suas relações com a mineralização;
c) Determinar a sequência paragenética dos minerais de minério e ganga;

d) Determinar o comportamento geoquímico das rochas hospedeiras e dos diferentes corpos de minério, estabelecendo as possíveis zonações químicas e minerais, e em que contexto essas zonações se formaram;
e) Correlacionar os resultados obtidos nesse estudos, com estudos de outros depósitos de Zn-Pb e de Cu-Ag na Irlanda;
f) Determinar um modelo metalogenético para o depósito de Tullacondra com base nos resultados e pesquisa bibliográfica.

1.4 METODOLOGIA

Ao longo do desenvolvimento deste trabalho foram realizados levantamento bibliográfico e compilação de dados geológicos dos depósitos hospedados em rochas do Carbonífero do centro e sul da Irlanda, em especial do depósito de Tullacondra. Esse trabalho investigou 48 amostras coletadas do galpão de testemunhos da Diversified Asset Holdings Proprietary Limited pertencendo a furos de testemunhos da parte oeste, central e leste do depósito de Tullacondra, identificados como M73-3 (com 24 amostras e 130m de profundidade), M73-11 (14 amostras e 160m de profundidade), e M73-19 (10 amostras e 95m de profundidade), respectivamente. A identificação do furo segue a ordem: M de Mallow (cidade onde o depósito se encontra), 73 referente ao ano em que o furo foi feito (1973) e 3, 11 e 19 são as sequências de cada furo em relação aos demais. As amostras são identificadas ainda por um terceiro componente relacionado à profundidade em que a amostra foi coletada em pés. A amostra M73-3-27, por exemplo, estava a 27 pés de profundidade. A coleta de amostras foi feita de modo a representar todas as diferentes unidades mineralizadas.

Assim, petrografia, análises geoquímicas de elementos maiores e traços, e imageamento por microfluorescência de raios-X foram realizadas com o intuito de caracterizar petrologicamento e geoquimicamente o depósito de Tullacondra. Além disso, um modelamento geológico com análises geoquímicas de Cu e Ag dos anos 70 disponibilizadas pelo Serviço Geológico Irlandês (GSI) de 35 furos foi feito para caracterizar os principais corpos de minério.

1.4.1 Análise petrográfica

As amostras foram coletadas, cortadas e fotografadas pelo professor orientador durante seu trabalho de pós-doutorado da região centro-sul da Irlanda. Destas amostras, foram confeccionadas 42 lâminas polidas no Laboratório de Análises de Minerais e Rochas (LAMIR) do Departamento de Geologia (DEGEOL) da UFPR. Em seguida, procedeu-se a descrição das seções polidas via microscópio petrográfico de luz transmitida e refletida para caracterização da paragênese mineral do Laboratório de Pesquisa em Microscopia (LAPEM), também do DEGEOL, e do LAMIR. As amostras foram fotografadas em escala microscópica com o auxílio do *Software AxioVision* e de máquina fotográfica pertencente ao DEGEOL. Para minerais não identificados por microscopia óptica, analises semi-quantitativas pelo MEV-EDS (Microscopia Eletrônica de Varredura com Espectroscopia por energia dispersiva) foram feitas no LAMIR.

1.4.2 Geoquímica

Análise geoquímica de rocha total de 43 amostras para elementos maiores e traços foram realizadas pela ALS Global. Anteriormente, essas amostras foram moídas no LAMIR utilizando moinho de disco AMP1 com panelas revestidas por carbeto de tungstênio (WC) e com controle de contaminação moendo sílica.

As análises químicas na ALS Global estão disponíveis no Anexo I e incluíram: (1). ICP-AES através de ataque em solução ácida (*four acid digestion*) permitiu a determinação de elementos maiores e Ag, Cd, Co, Cu, Li, Mo, Ni, Pb, Sc, e Zn enquanto *Loss on ignition* (LOI) foi determinado através de *furnace*; (2) ICP-MS que permitiu a determinação de Ba, Ce, Cr, Cs, Dy, Er, Eu, Ga, Gd, Hf, Ho, La, Lu, Nb, Nd, Pr, Rb, Sm, Sn, Sr, Ta, Tb, Th, Tm, U, V, W, Y, Yb, e Zr, elementos que foram primeiramente atacados por soluções de ácido hidroclorico, hidrofluórico e nítrico; (3) Arsênio, Bi, Hg, In, Re, Sb, Sc, Te, e Tl também foram analisados por ICP-MS mas através de *aqua regia digestion*; (4) Carbono e enxofre total foram determinados por *induction furnace.* Embora todos os óxidos estejam dentro do limite de detecção, alguns metais apresentam amostras acima e/ou abaixo do limite. Os limites de detecção dos elementos traços ilustrados nesse trabalho são: Ag (0,5-100 ppm), As (0,1-250 ppm), Cu (0,2-10000 ppm), S (0,01-50 %), Pb (2-10000 ppm), Sb (0,05-250 pmm) e Zn (2-10000 ppm).

1.4.3 Mapeamento qualitativo por Micro-Fluorescência de Raios-X

Quatorze amostras de *offcuts* foram selecionadas representando diferentes unidades e estilos de mineralização do depósito de Tullacondra a fim de elaborar mapas elementares semi-qualitativos da superfície dessas amostras. O instrumento utilizado foi Edax Orbis micro-XRF do *Center for Environmental Science and Technology* (CEST) na *University of Notre Dame.* Parâmetros analíticos incluem tamanho do feixe de 30 µm, voltagem de 40 kV e corrente de 300 µA (Çimen *et al*. 2019 e Corcoran *et al*. 2019). Métodos estão detalhados em (Corcoran et al., 2019). Os elementos mapeados foram Cu, S, Al, Fe, Ca, P, As, K, Mg, Mn, Si, Ti e Zn, e imagens ternárias de RGB para Cu, Al e Ca foram geradas usando o software *ImageJ*. Essas imagens ilustram as diferentes texturas dos minerais de minério. Esses mapas serão aproveitados também em futuras publicações.

Tabela 1 – Relação entre amostras e análises petrográficas (petrog), MEV-EDS, geoquímicas (assay) e de micro-fluorescência de raios-X realizados nesse trabalho. Na tabela é mostrado também o resultado da química de rocha total dos elementos plotados nos diagramas das Figuras 16-17.

Sample	Petrog.	EDS	Assays	micro-XRF	SiO2 (%)	Al2O3 (%)	CaO (%)	MgO (%)	Fe2O3 (%)	K2O (%)	TiO2 (%)	Cu (ppm)	Ag (ppm)	As (ppm)	Sb (ppm)	Zn (ppm)	Pb (ppm)	Co (ppm)
M73-3-027	X		X		7.29	1.1	28.3	17.55	0.94	0.41	0.05	5130	<0.5	4.2	2	6	3	15
M73-3-039	X		X		5	0.76	50.1	0.57	0.77	0.28	0.03	>10000	20.2	8.6	14.6	12	5	23
M73-3-069	X		X		7.21	0.27	51.6	0.48	0.32	0.12	0.01	463	0.5	11.5	0.73	8	2	7
M73-3-094	X	X	X	X	38.5	0.5	34.1	0.38	0.43	0.19	0.02	782	3.1	0.9	0.17	3	3	62
M73-3-119	X	X	X	X	61.1	15.1	6.13	1.33	2.27	4.91	0.78	9000	46.6	8.3	0.39	23	4	20
M73-3-132	X		X		23	2.28	40	0.88	1.02	0.71	0.09	3510	14.5	2.1	0.22	9	4	23
M73-3-143	X		X		69.1	8.01	9.59	0.72	2.31	2.56	0.33	>10000	1.4	44.3	1.93	15	3	46
M73-3-154	X	X	X		26.4	3.67	35.7	0.75	1.21	1.19	0.16	2450	13.1	80.6	12.35	17	5	31
M73-3-162	X	X	X	X	39.2	7.56	20.1	4.9	2.02	2.51	0.31	4010	3.7	97.6	77	55	3	45
M73-3-196	X	X	X	X	7.38	1.06	28.4	18.7	2.07	0.35	0.06	6930	0.7	8	4.4	3	5	27
M73-3-203	X		X		3.83	0.71	29.9	19.55	1.47	0.25	0.02	1650	<0.5	3.9	0.63	3	<2	14
M73-3-218	X	X	X		7.42	1.08	28.3	17.7	1.55	0.35	0.04	654	<0.5	1.7	0.22	3	2	17
M73-3-233	X	X	X		63	15.5	3.32	2.89	2.51	4.74	0.83	2470	<0.5	70.2	0.7	33	<2	45
M73-3-241	X		X		8.94	0.63	28.2	17.05	1.4	0.24	0.04	65	<0.5	4	0.32	3	6	39
M73-3-254	X	X	X		58.8	20.4	0.39	2.14	4.26	5.89	0.92	41	<0.5	28.7	0.64	46	8	24
M73-3-283	X	X	X		9.58	0.54	27.8	17.1	1.11	0.23	0.02	9	<0.5	48.5	0.66	3	<2	38
M73-3-293	X	X	X		18	2.25	24	15	1.12	0.77	0.11	21	<0.5	2	0.09	6	2	22
M73-3-318	X	X	X		52.1	13.45	8.85	2.79	3.37	4.3	0.61	7120	<0.5	13.2	0.9	34	6	20
M73-3-328	X	X	X	X	57.7	12.9	5.46	3.89	3.31	4.22	0.57	>10000	<0.5	22.2	1.15	26	4	51
M73-3-347	X	X	X		81.8	8.26	0.79	0.51	1.78	2.71	0.53	9830	1.7	72.7	25.6	34	3	92
M73-3-364		X	X		62.9	3.5	8.91	5.88	0.95	1.19	0.47	3510	2.4	15	0.76	6	5	108
M73-3-374	X	X	X		66	6.76	6.39	4.47	1.16	2.25	0.35	1350	<0.5	23.6	5.99	16	2	96
M73-3-393	X	X	X	X	50.2	11.9	7.5	5.61	3.23	3.89	0.61	>10000	1.5	>250	>250	422	6	56
M73-3-412	X	X	X		90.5	4.24	0.82	0.66	0.62	1.42	0.2	18	<0.5	0.5	0.12	6	2	129
M73-11-290	X		X	X	27.2	6.58	31.5	1.43	2.35	1.95	0.27	15	<0.5	>250	1.07	89	45	35
M73-11-296	X		X		60.9	8.17	12.1	0.9	1.28	2.37	0.34	5250	45	17.2	0.13	12	3	46
M73-11-310			X		35.1	8.67	22.9	1.43	2.43	2.64	0.38	>10000	>100	22.4	0.07	20	13	32
M73-11-319	X		X	X	5.79	0.89	51	0.65	1.12	0.28	0.05	1520	0.9	12.9	0.47	8	16	13
M73-11-336	X		X		17.45	3.07	41.2	1.1	1.59	0.91	0.13	375	<0.5	16.2	0.16	15	21	26
M73-11-347	X		X		7.59	0.97	50.2	0.61	1	0.33	0.05	6420	30	3.7	0.06	6	7	29
M73-11-359	X		X		5.27	0.8	50.7	0.82	1.12	0.29	0.03	2540	8	4.3	0.24	8	10	26
M73-11-404	X		X		7.33	0.86	49.1	1.05	1.48	0.3	0.05	843	0.6	15.1	0.1	10	16	12
M73-11-422			X	X	32	7.62	26.3	1.63	2.7	2.58	0.39	>10000	57.6	10.3	0.23	26	11	19
M73-11-431			X		29.7	1.4	31.5	1.67	6.17	0.1	0.08	1070	1	0.5	0.07	33	2	55
M73-11-442			X		71	10.4	4.71	0.63	1.49	3.42	0.51	>10000	>100	>250	>250	640	4	62
M73-11-450			X		86.4	6.06	0.97	0.14	0.39	2.56	0.17	5910	26	155.5	3.25	21	8	133
M73-11-498	X		X	X	52.6	9.46	6.28	1.21	3.8	3.51	0.55	13	<0.5	1.6	0.37	18	5	47
M73-11-510	X		X		65.6	3.55	8.19	1.31	1.84	1.48	0.14	6	<0.5	0.7	<0.05	9	3	98
M73-19-072	X		X	X	18.05	4.32	41.8	0.79	2.26	1.33	0.24	8460	12.3	9.5	2.29	22	21	42
M73-19-133	X	X	X	X	13.05	1.45	46.2	0.67	1.61	0.49	0.09	>10000	79	10.2	0.27	8	9	33
M73-19-142	X																	
M73-19-172	X																	
M73-19-249	X		X	X	75.1	11.8	0.91	0.58	1.09	3.95	0.68	>10000	95.5	>250	>250	697	5	132
M73-19-257	X	X	X	X	75.9	11.05	1.87	0.94	1.49	3.77	0.56	7050	45.3	>250	146.5	448	7	132
M73-19-264	X																	
M73-19-271	X																	
M73-19-279	X																	
M73-19-296	X		X		87.2	3.63	4.03	0.43	0.66	1.74	0.06	1280	3.6	>250	119	99	5	268

1.4.4 Modelamento geológico

O modelamento geológico, que incluiu o modelamento da geologia do depósito e da geometria dos corpos de minério, foi realizado no *software Leapfrog* baseado em banco de dados geoquímicos para Cu e Ag de 35 dos quase 100 furos de testemunhos feitos ao longo dos 30 anos de pesquisa na área de Tullacondra. O banco de dados utilizados nessa pesquisa foi compilado originalmente pela empresa *Munster Base Metals* de 1969 a 1986 da área de Tullacondra com base em análises

químicas em amostras coletadas ao longo de 35 furos de sondagem. Esses dados estão disponibilizados atualmente pelo Serviço Geológico da Irlanda (GSI) e disponíveis nos anexos II e III.

2 CONTEXTO GEOLÓGICO

2.1 GEOLOGIA REGIONAL

O embasamento das rochas hospedeiras do depósitos irlandeses consistem em rochas metassedimentares e metavulcânicas Pré-Devonianas (Phillips e Sevastopulo, 1986). Essas rochas foram formadas, dobradas e falhadas devido ao surgimento e fechamento do Oceano Iapetus durante a Orogenia Caledoniana (Phillips e Sevastopulo, 1986; Matte, 2001). Entre o Devoniano e o final do Carbonífero Inferior, o ambiente tectônico da região tornou-se extensional, o que permitiu a deposição da plataforma carbonática irlandesa. A base da sequência das rochas sedimentares da Irlanda inicia-se com espessas camadas de arenitos e lamitos verdes, cinza e vermelhos, finos a médios da unidade *Old Red Sandstone* (ORS), depositadas no final do Devoniano ao longo da Bacia de *Munster* no sul da Irlanda (Johnston, 1999). Conglomerados e arenitos conglomeráticos ocorrem localmente (Hitzman e Large, 1986; Phillips e Sevastopulo, 1986). Graham (1983) sugeriu como origem para as ORS leques desenvolvidos nas terminações de sistemas fluviais. Sobrejacentes aos arenitos do ORS deu-se início à deposição da plataforma carbonática irlandesa no início do Carbonífero (Fig. 3, estágio *Courceyan*) com carbonatos do Grupo Navan. No sul e centro das *Midlands*, o Grupo Navan é lateralmente equivalente por sedimentos marinhos de carbonatos argilosos e folhelhos denominados como *Lower Limestone Shale* (Philcox, 1984). Sopreposto ao Grupo Navan encontram-se carbonatos micríticos do Complexo *Waulsortian* que abrangem depósitos do *Courceyan* Médio no sul ao começo do *Chadian* no NE (Fig. 3) (Lees, 1961; Hitzman e Large, 1986). Muitas das mineralizações que ocorrem em rochas carbonáticas na Irlanda estão litoestratificamente restritas a rochas do *Waulsortian* e do Grupo Navan, ou em seu equivalente lateral *Lower Limestone Shale,* como no caso de Tullacondra (Johnston, 1999).

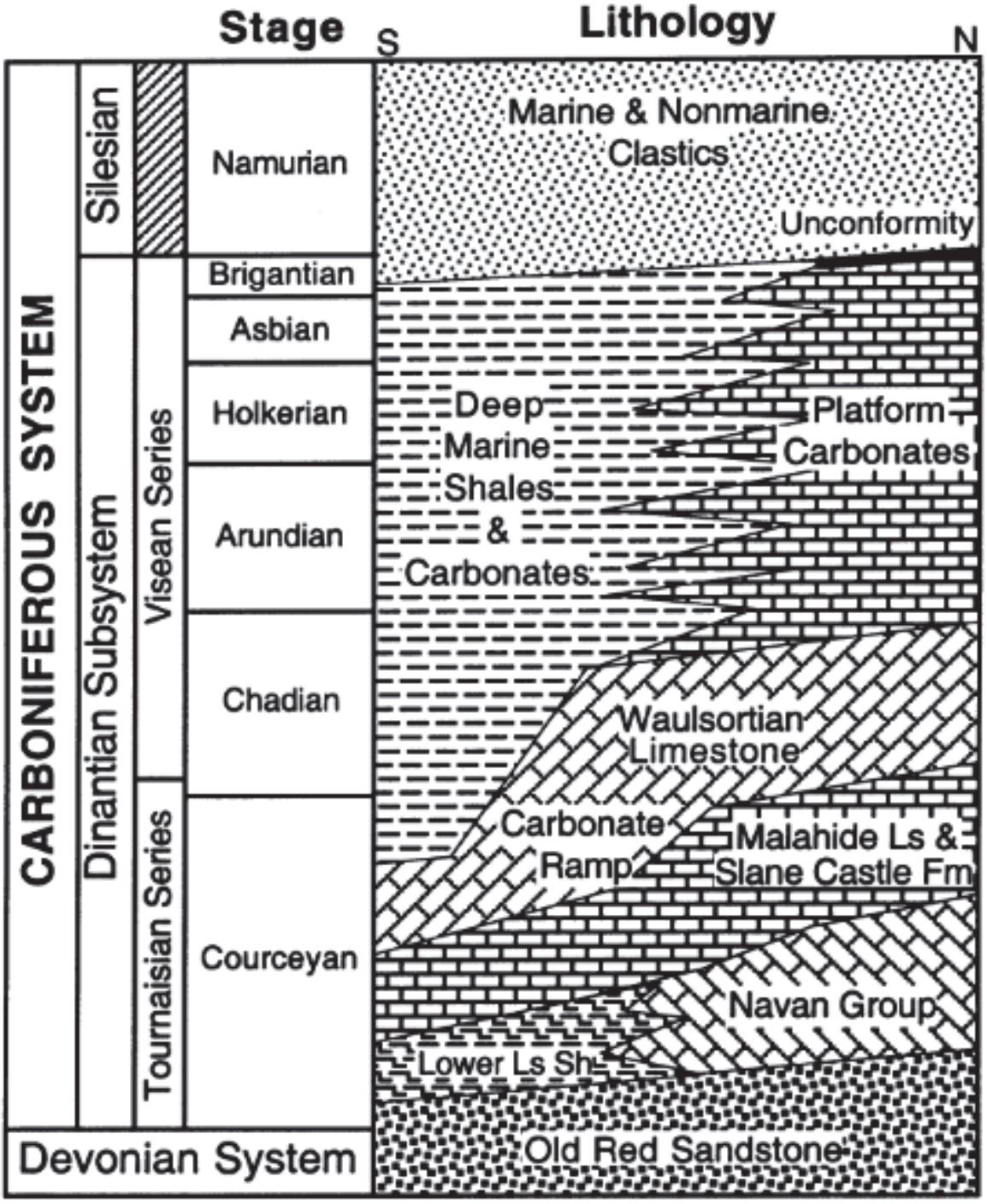

Figure 3 – Coluna geológica mostrando estratos e relações de fácies do *Irish Midlands*. Fonte: Gregg *et al.* (2001). Notar posição do Lower Limestone shale, carbonatos argilosos equivalente ao sul do Grupo Navan, que hospedam o depósito de Mallow.

O vulcanismo intrusivo no *Irish Midlands* é registrado no sudoeste da Irlanda, onde outros depósitos de cobre estão hospedados registrados no Carbonífero Inferior entre o Chadian e o Asbian (Fig, 3) (Steed, 1986; Mccusker e Reed, 2013; Wilkinson e Hitzman, 2015; Elliott *et al*., 2019). O depósito de Cu-Ag-Hg de Gortdrum, similar ao depósito de Tullacondra (Wilbur e Carter, 1986), está

localizado nessa região e contém rochas vulcânicas basálticas de idade Chadian e Asbian do Carbonífero espacialmente associadas com a mineralização (Steed, 1986).

Entre o final do Carbonífero e o Permiano, a Orogenia Herciniana afetou as rochas carbonáticas irlandesas mudando o regime tectônico de extensional para compressional (Hitzman e Large, 1986). A Orogenia Herciniana ocorreu devido à colisão entre os terrenos *Laurussia* (junção da *Avalonia* e *Armorica com Laurencia-Báltica)* e *Gondwana* e consequente fechamento dos oceanos *Rheic, Theic* e *Paleo Tethys* entre o Carbonífero e o Permiano, (Fig. 4) (Matte, 2001; Wilkinson, 2013). A deformação herciniana envolveu metamorfismo, plutonismo e fortes compressões NS (Hitzman e Large, 1986, Wilbur e Carter, 1986) associadas à reativação de falhas caledonianas NE-SW (Johnston 1999). Zonas de empurrões predominaram no sul da Irlanda (Wilbur e Carter, 1986), enquanto cisalhamentos com componentes dextrais E-NE ou N-NE eram também comuns (Johnston 1999). Ao norte da Irlanda, registros dos efeitos dessa compressão são menos comuns e se ocorrem como amplos dobramentos ao longo de eixos EW com falhamentos reversos e de cavalgamento menores (Wilbur e Carter, 1986).

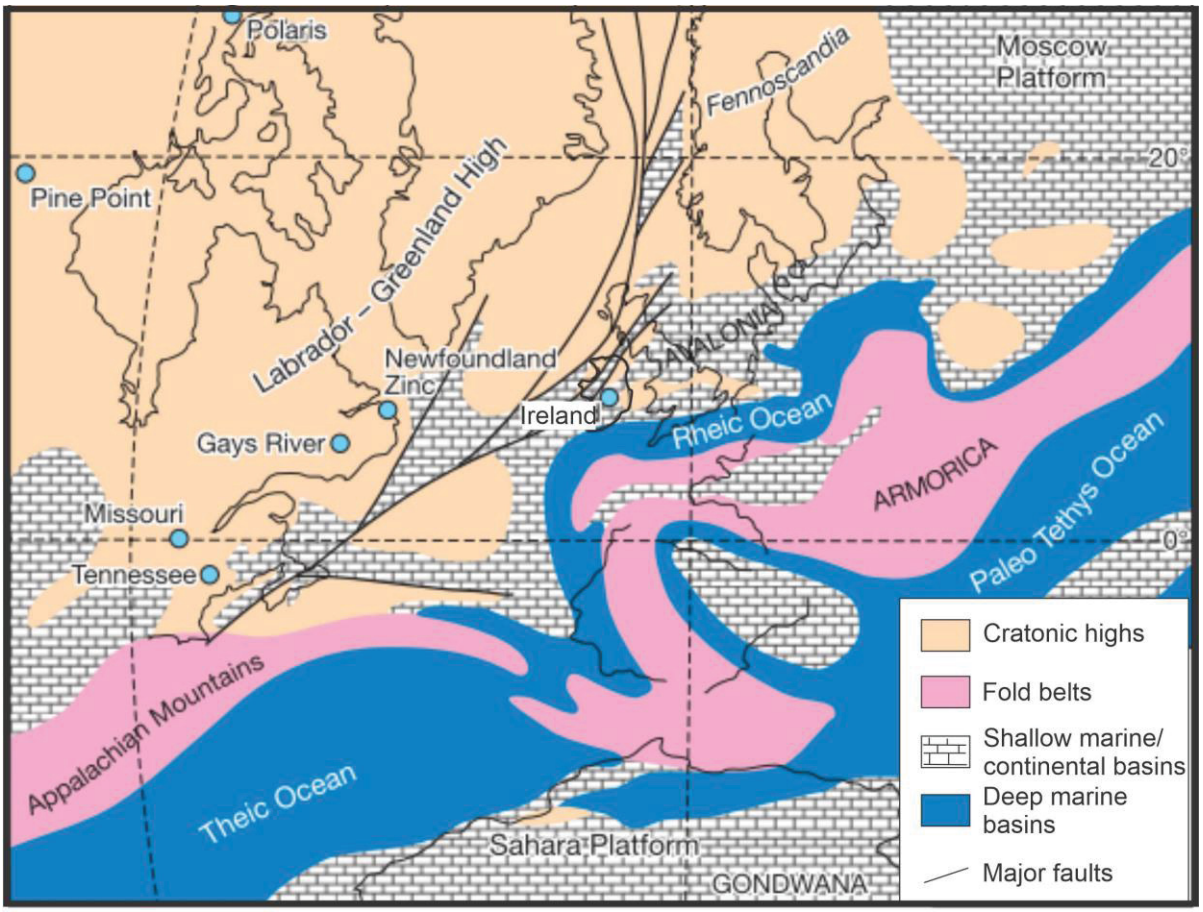

Figure 4 - Reconstrução paleogeográfica do norte da Europa no início do Carbonífero mostrando o encontro entre as placas Laurencia-Baltica e Avalonia (Laurussia) com a Armorica, que posteriormente também colidiram com a Gondwana (canto inferior direito da figura), resultando no fechamento dos oceanos *Theic, Rheic e Paleo Tethys*. O início do fechamento desses oceanos resultou na subsidência da Irlanda e na formação de bacias sedimentares que formaram as rochas hospedeiras dos depósitos de Zn-Pb e Cu-Ag da ilha (Fonte: Wilkinson, 2013).

2.1.1 Mineralização de Zn-Pb no *Irish Ore field*

A mineralização de Zn-Pb do *Irish Ore field* é conhecida principalmente pelos depósitos de Navan, Lisheen e Silvermines (Andrew, 1986b; Anderson *et al*., 1998; Fusciardi *et al*., 2003; Reed e Wallace, 2004; Ashton *et al*., 2015). Esses depósitos apresentam um forte controle estrutural por falhas normais de direção ENE-WSW sendo compostos por corpos de minério *stratabounds* hospedados principalmente nas *hanging walls* das falhas (Fig. 5) (Anderson *et al*., 1998; Ashton *et al*., 2015; Torremans *et al*., 2018; Kyne *et al*., 2019).

No caso dos depósitos Lisheen e Silvermines, os corpos *stratabounds* estão hospedados no *Waulsortian Limestone* ocorrendo em brechas dolomitizadas (Hitzman *et al*., 2002; Lee e Wilkinson, 2002). O depósito de Navan ocorre, por outro lado, em calcários argilosos do Grupo Navan, equivalente ao norte da Irlanda do

Lower Limestone Shale (Anderson *et al*., 1998; Ashton et al., 2015). De modo geral, esses depósitos contêm como principais minerais de minério a galena e esfalerita, e em menor proporção minerais de Cu e As, principalmente próximo as falhas alimentadoras (Anderson *et al*., 1998; Hitzman *et al*., 2002; Fusciardi *et al*., 2003; Torremans *et al*., 2018).

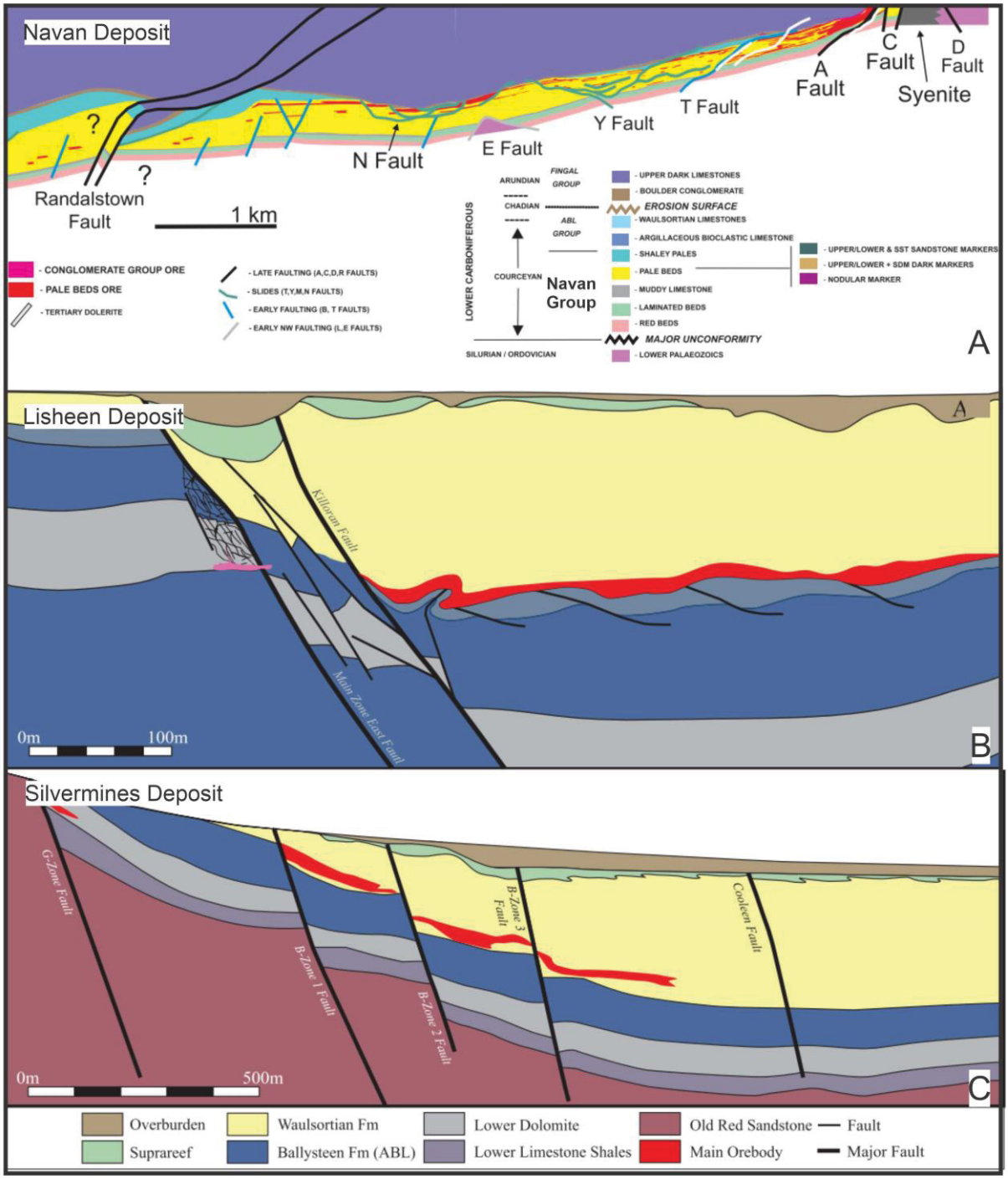

Figure 5 - Seções estratigráficas mostrando as principais caracteristicas dos corpos de minério dos depósitos de Zn-Pb de (A). Navan (Fonte: Ashton *et al*., 2015); (B) Lisheen e (C). Silvermines (Fonte: Kyne *et al*., 2019). Note que os corpos de minério em ambos os depósitos são s*tratabound*, controlados por falhas normais e estão principalmente no *hanging wall* das falhas. O depósito de

Navan está hospedado no *Navan Group* e os depósitos de Lisheen e Silvermines no *Waulsortian Limestone.*

A formação desses depósitos tem sido descrita como ocorrendo durante o início da Orogenia Variscana, em um período de extensão da plataforma irlandesa no Carbonífero Inferior durante a diagênese das rochas hospedeiras. A mineralização ocorreu quando fluido hidrotermal que percolou o embasamento Paleozoico atingiu rochas carbonáticas mais rasas através de falhas normais e misturou-se com salmouras bacteriogênicas marinhas (Boast *et al*., 1981; Anderson *et al*., 1998; Fusciardi *et al*., 2003; Wilkinson *et al*., 2005; Ashton *et al*., 2015; Wilkinson e Hitzman, 2015; Walsh *et al*., 2018). O fluido hidrotermal tem sido considerado como o transportador de Zn e Pb do embasamento Ashton et al. (2015) e Yesares et al. (2019), enquanto as salmouras seriam as principais fontes de enxofre resultando em uma assinatura predominantemente negativa de $\delta^{34}S$ (e.g., Wilkinson, 2013).

Além disso, a formação de *relay ramps* devido a união de falhas normais tem sido considerada um dos principais controles da mineralização (Kyne et al., 2019). *Relay ramps* são formadas quando duas falhas estão próximas o suficiente começando a interagir de modo que com uma continua tensão se formam “rampas” entre as falhas (Fig. 6A) (Fossen e Rotevatn, 2016). Essa continua tensão também é responsável pela formação de fraturas e falhas subsidiárias dentro da rampa, conhecidas por alguns autores como zona de dano *(damage zone)* (Caine *et al*., 1996; Kim *et al*., 2004; Childs *et al*., 2009; Walsh *et al*., 2018). Essas falhas e fraturas subsidiárias aumentaram a permeabilidade vertical das rochas do Carbonífero Inferior da Irlanda, facilitando a percolação vertical dos fluidos mineralizantes próximos às falhas. O contato entre litologias com diferente permeabilidade facilitam a percolação horizontal dos fluidos devido ao contraste entre elas (Fig. 6B-C). (Torremans et al., 2018; Kyne et al., 2019).

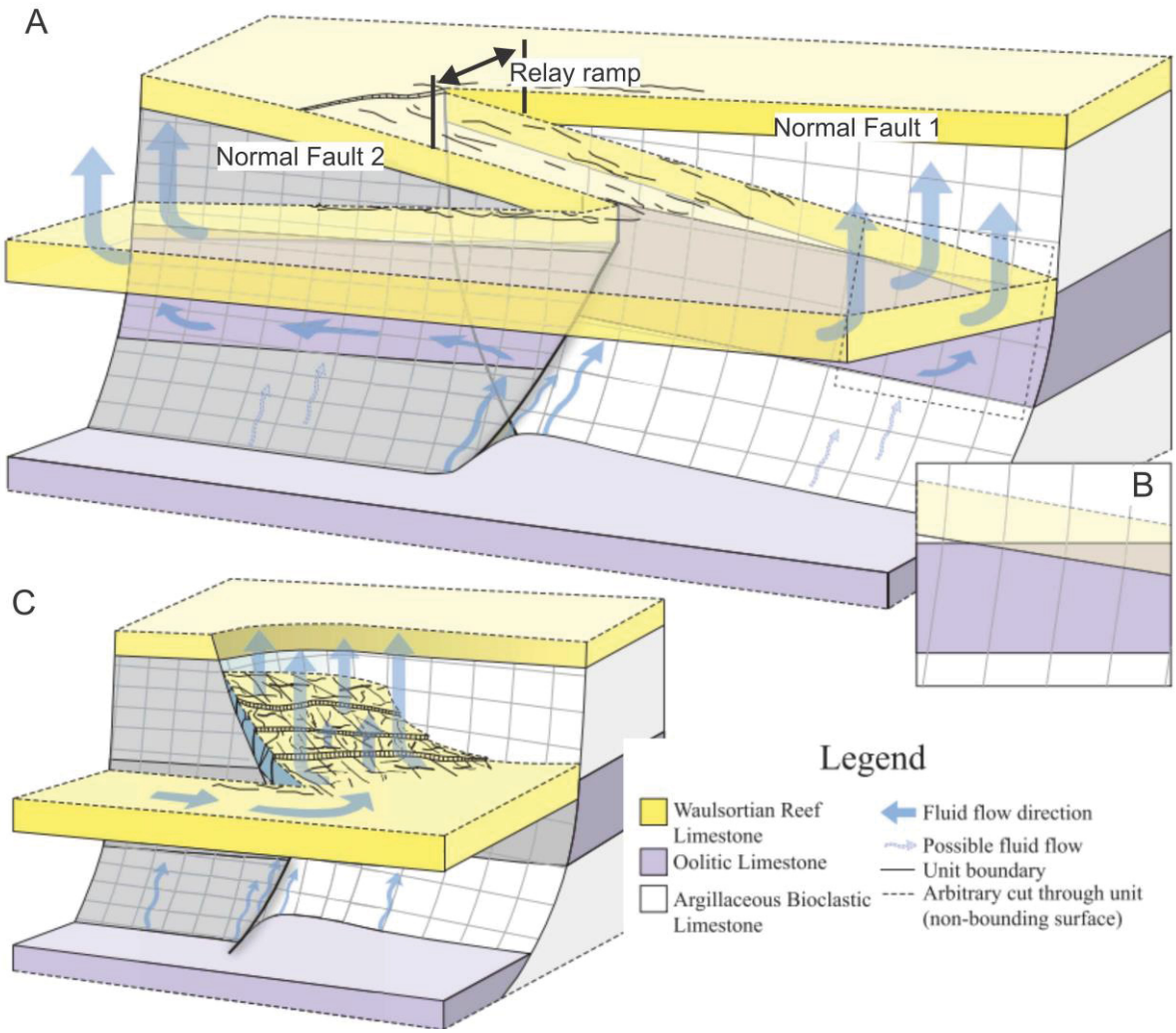

Figure 6 - Esquemas mostrando os sistemas de *relay ramps* tipicamente encontradas *na Irish Ore field.* (A). Figura mostrando *relay ramp* formada entre duas falhas. Notar as direções dos fluidos que são marcadas por percolação vertical controlada por zonas de fraturamento dentro da rampa *(damage zone)* e por percolação horizontal controlada pela estratigrafia; (B). Figura mostrando o contado entre Waulsortian Lm Formation e Oolitic Limestone, unidades que, diferentemente do Argillaceous Bioclastic Limestone, são mais permeáveis e permitem a percolação horizontal do fluido; (C). Figura mostrando com mais detalhes a zona fraturada contendo falhas e fraturas secundárias dentro da *relay ramp* (Fonte: Kyne *et al*., 2019).

2.1.2 Mineralização de Cu-Ag no Irish Ore field

As ocorrências e depósitos de cobre da Irlanda ocorrem principalmente no sul da ilha, hospedados em veios de quartzo do *Munster Basin* (Reilly, 1986; Kinnaird *et al*., 2002; Lang *et al*., 2020), em veios de quartzo, calcita e dolomita, e disseminados do Lower Limestone Shale ou da Formação Ballysteen (Kinnaird et al., 2002). Esses depósitos apresentam controles estruturais ENE (Steed, 1986; Wilbur e Carter, 1986), tais como os depósitos de Zn-Pb, mas estão principalmente localizados em dobras e falhas reversas e transpressionais do final da Orogenia

Variscana (Andrew, 1986a; Steed, 1986; Wilbur e Carter, 1986; Johnston, 1999). Alguns dados isotópicos desses depósitos, entretanto, mostram que eles foram formados no final do Devoniano e início do Carbonífero Inferior e seriam anteriores a essas estruturas, contemporâneos aos depósitos de Zn-Pb (Kinnaird et al., 2002; Lang et al., 2020).

O depósito de Tullacondra é classificado como um dos depósitos disseminados e hospedados em veios do *Lower Limestone Shale* (Wilbur e Carter, 1986). Dentro dessa categoria ainda estão os depósitos de Gortdrum, Aherlow e Ballyvergin (Fig. 7) (Andrew, 1986a; Romer, 1986; Steed, 1986; Duane, 1988). Esses depósitos contêm como minerais de minério calcopirita, bornita, calcocita e menores concentrações de galena e esfalerita. O depósito de Gortdrum, em especial, apresenta mineralização de cobre, associado a Ag e Hg, e está espacialmente relacionado a diques basálticos (Steed, 1986).

Detalhes sobre a gênese desses depósitos e sua relação com os depósitos de Zn-Pb são menos conhecidos na literatura. A gênese do depósito de Tullacondra será discutido abaixo em mais detalhes na seção “Resultados e discussões”.

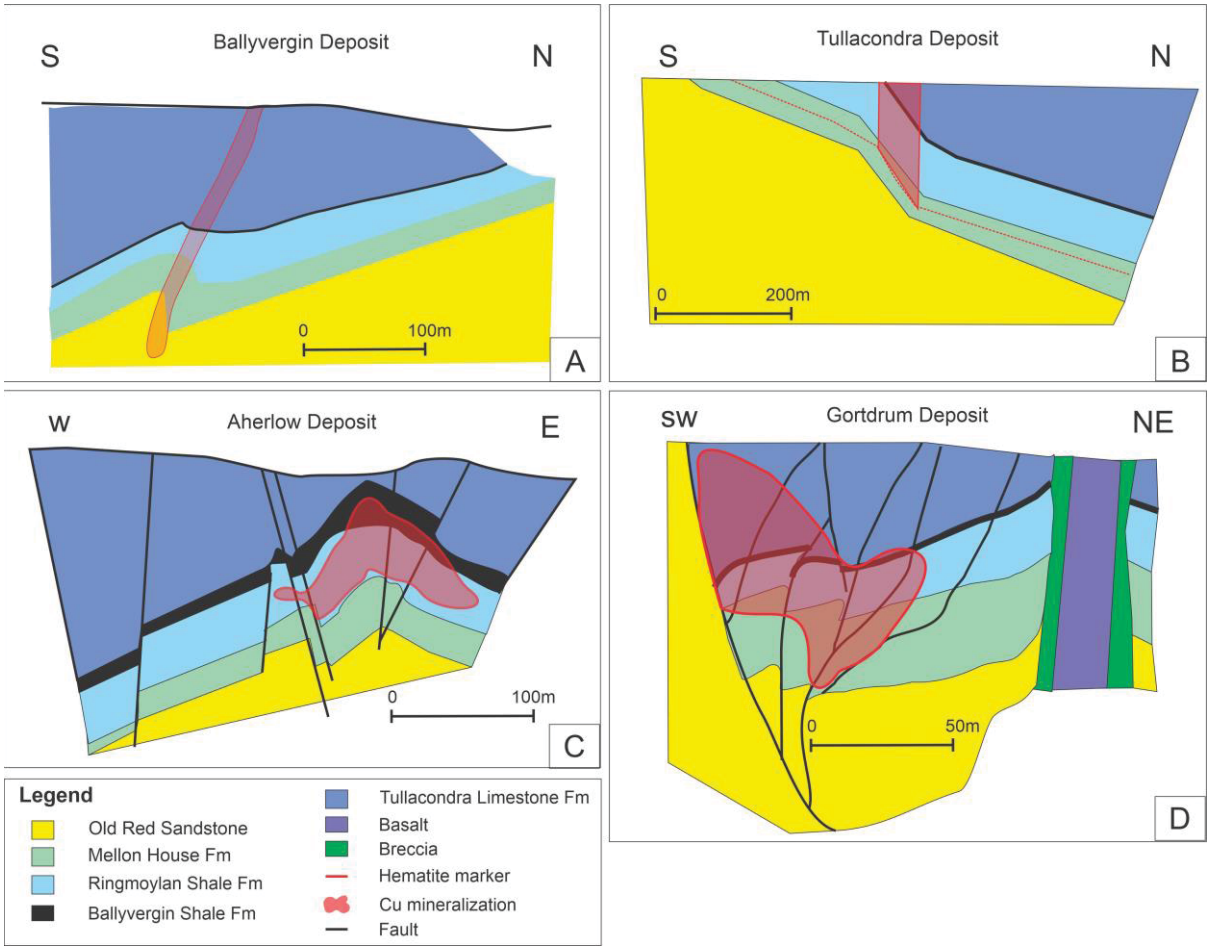

Figure 7 - Seções estratigráficas mostrando os depósitos de cobre de (A) Ballyvergin; (B) Tullacondra; (C) Aherlow; e (D) Gortdrum. Note que a mineralização está em dobras e falhas reversas. As figuras são adaptadas de Johnston (1999). O presente estudo tem o propósito de reavaliar essas feições em Tullacondra e, por isso, a seção estratigráfica de Tullacondra é redesenhadas em "Resultados e Discussões", permitindo novas interpretações.

2.2 GEOLOGIA DO DEPÓSITO DE TULLACONDRA

O depósito de Tullacondra está hospedado na sequência sedimentar do Carbonífero Inferior do *Irish Midlands* (Wilbur e Carter, 1986). Em Tullacondra, a base do depósito é caracterizada pela Bacia de Munster representada pelo *Old Red Sandstone* (ORS). O ORS em Tullacondra consiste em folhelho, arenito, conglomerado e *red beds*, atingindo uma espessura de mais de 500m e recoberta pelo *Lower Limestone Shale* (Hudson e Philcox, 1965; Wilbur e Carter, 1986).

O *Lower Limestone Shale* (LLS) está estratificamente acima do ORS e é a principal unidade do depósito de Cu-Ag de Tullacondra (Wilbur e Carter, 1986) enquanto o Grupo Navan hospeda o depósito de Zn-Pb de Navan no norte da Irlanda. O LLS consiste em rochas siliciclásticas basais que são progressivamente

enriquecidas em calcários no topo e depositadas em um ambiente marinho raso (Hudson e Philcox, 1965; Philcox, 1984). Wilbur e Carter (1986) dividiu o LLS do depósito de Tullacondra em sete subunidades da base para o topo nomeadas como: *Lower* e *Upper Transition Series*, *Uniform Calcarenite, Lower Shaly Calcarenite, Oolitic Calcarenite, Silty Calcarenite* e *Upper Shaly Calcarenite*.

As *Lower e Upper Transition Series* consistem de arenito, conglomerado e siltito intercalados com arenito, siltito e folhelho calcário (Somerville e Jones, 1985; Wilbur e Carter, 1986). De acordo com Wilbur e Carter (1986), na região de Tullacondra o *Lower Transition Series* é composto principalmente por arenito de granulação média enquanto o *Upper Transition Series* é composto principalmente por folhelhos, ambos com cerca de 15 m de espessura cada. Wilbur e Carter (1986) descreveram um horizonte marcador denominado como *Hematite Marker* próximo ao contato entre o Upper e Lower Transition Series que consiste em uma camada fina de cerca de 30cm de espessura que contêm pequenas e frequentemente arredondadas concreções de hematita. Tal marcador foi, também, observado por Somerville e Jones (1985) na Província Limerick, no sudoeste da Irlanda.

Acima das *Transition Series* encontra-se a Formação *Ringmoylan Shale* que é subdividida para o contexto de Tullacondra da base para o topo em *Uniform Calcarenite, Lower Shaly Calcarenite, Oolitic Calcarenite, Silty Calcarenite*, e *Upper Shaly Calcarenite* detalhado na Tabela 2 como reportado por Wilbur e Carter (1986).

Tabela 2 - Estratigrafia do depósito de Tullacondra de acordo com Wilbur e Carter (1986).

	LITHOLOGICAL UNITS		THICKNESS	DESCRIPTION
LOWER CARBONIFEROUS (CORCEYAN)	Kilmaclenine Ls		100m	Pale grey, thick-bedded bioclastic limestone, often shale free
	Tullacondra Ls		35m	Medium grey, crinoidal with thin irregular shale partings, siliceous near base
	Ballyvergin Shale		1m	Fine sandy non-calcareous, green-grey siltstone
	LOWER LIMESTONE SHALE	Upper Shaly Calcarenite	15-20m	Medium grey crinoidal calcarenite, abundant shale partings, siliceous near top
		Silty Calcarenite	2m	Dark grey muddy calcarenite
		Oolitic Calcarenite	9-12m	Interbedded oolites and crinoidal calcarenites
		Lower Shaly Calcarenite	6-9m	Uniform, pale calcarenite with interbedded, shaly crinoidal units
		Uniform Calcarenite	5-6m	Pale massive calcarenite, mostly shale free
		Upper (Shaly) Transition Series	12-15m	Black shales, sandy calcarenites and sandstones - 0.3m Hematitic Horizon near base
		Lower (Sandy) Transition Series	12-15m	Sandstones, shales and conglomerates, often calcareous
DEVONIAN	Old Red Sandstone		> 500m	Shales, quartzitic sandstones, conglomerates and red beds

Acima do LLS está o marcador reginal da Formação *Ballyvergin Shale* com cerca de 1m de espessura em Tullacondra caracterizada por arenosos siltosos não calcários (Wilbur e Carter, 1986). Acima do *Ballyvergin Shale* estão as Formações *Tullacondra Limestone* e *Kilmaclenine Limestone* (Somerville e Jones, 1985; Phillips e Sevastopulo, 1986; Somerville *et al*., 1992; Shearley *et al.*, 1996). A Formação *Tullacondra Limestone* contém cerca de 35m de espessura em Tullacondra e é composta de calcários crinoidais de granulação média com folhelho de espessura fina parcialmente silicoso próximo a base (Wilbur e Carter, 1986). Acima, a Formação *Kilmaclenine* contém cerca de 100m e é composta por calcário bioclástico com baixo conteúdo de argila (Hudson e Philcox, 1965; Wilbur e Carter, 1986).

Acima da Formação *Kilmaclenine*, encontra-se a Formação *Waulsortain Limestone* que tem 450m de espessura em Tullacondra e é composta de calcilutito dolomitizado e contém chert na base (Wilbur e Carter, 1986). Em Tullacondra, a Formação *Waulsortian Limestone* sobreposta pelo Grupo Vulcânico Subulter é composta por rochas piroclásticas com até 100m de espessura (Hudson e Philcox, 1965; Wilbur e Carter, 1986). Além disso, diques de espessura fina intersectam o testemunhos de Tullacondra. Eles foram descritos como diques riolíticos porfiríticos com matriz muito fina, algumas vezes brechados e cortados por veios mineralizados, e hospedados dentro do LLS. Entretanto, devido a ser pobremente

descrito, mais informações sobre esses diques são requeridas para entender sua gênese.

O depósito de Tullacondra está hospedado no centro do flanco norte da anticlinal Kilmaclenine, uma dobra aberta com eixo de direção ENE-WSW. Além disso, falhas de cavalgamento cortam a anticlinal e são interceptadas por falhas de direção NS de alto mergulho (Fig. 8A) (Wilbur e Carter, 1986).

A mineralização em Tullacondra é controlada por uma falha de direção EW de mergulho íngreme, nomeada aqui como Falha Tullacondra (Fig. 8B). Essa falha foi descrita por Wilbur e Carter (1986) como uma monoclinal ou proto-falha interpretada pela mudança abrupta do mergulho de acamamento de 15° a 70° e configura uma zona de dano que abrange superfícies de falhas e fraturas. Seguindo as estruturas regionais, a Falha Tullacondra é truncada ao oeste e leste por falhas de direção NS.

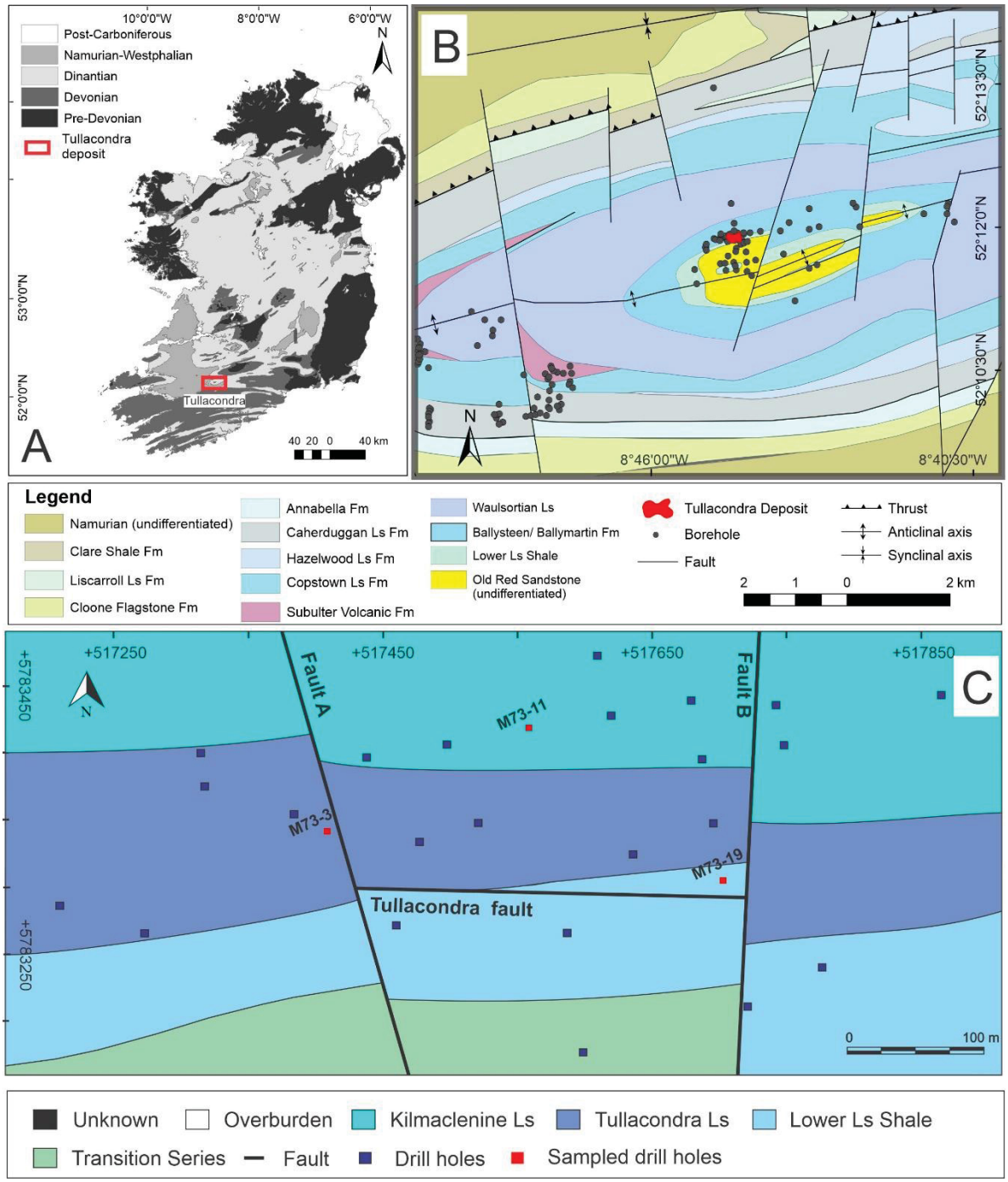

Figure 8 - (A) Mapa geológico da anticlinal Kilmaclenine que hospeda o depósito de Tullacondra mostrando as principais unidades e estruturas. (B) Mapa geológico da área de Tullacondra mostrando a localização dos três furos de sondagens estudados.

3 RESULTADOS E DISCUSÕES – ARTIGO

THE CARBONATE-HOSTED TULLACONDRA CU-AG MINERALIZATION, MALLOW, IRELAND

3.1 ABSTRACT

The Tullacondra Cu-Ag deposit is located on the southern margin of the Lower Carboniferous Irish Midlands orefield, and contains historic reserves of approximately 4.2 Mt of ore at 0.7% copper and 27.5 ppm silver. Despite its small size and low grade, the Tullacondra deposit shares similar characteristics to major Zn-Pb Irish Midlands deposits (Navan, Lisheen and Silvermines). The carbonate-hosted copper deposits of southern Irish Midlands and their relationship with other Irish Midlands deposits, however, has not been researched in any detail. Results from this study indicate that the Tullacondra deposit consists of similar structural and stratigraphic controls, metal affinities, and mineral zonation compared to Zn-Pb deposits within Ireland. Our investigation shows that mineralization within the Tullacondra deposit is primarily controlled by the E-W trending normal Tullacondra Fault, and by a vertical fractured zone, likely related with its relay ramp, and is secondarily influenced by stratigraphy. The abundances of arsenic minerals and Cu, Ag, As, Sb, and Zn are elevated proximal to the fault. In contrast to prior genetic models, which suggested a vertical and a stratabound orebodies, we propose that the Tullacondra deposit consists of three stratabound orebodies. Additionally, two mineral assemblage of disseminated, parallel bedding and dissolution seam-hosted copper mineralization formed during the main ore stage: (1) chalcocite, bornite, and chalcopyrite; (2) arsenopyrite, tennantite, and chalcopyrite. These ore minerals were likely later remobilized and formed vein-hosted chalcocite, bornite, chalcopyrite, and tennantite, charactering a late ore stage.

3.2 INTRODUCTION

The Irish Zn-Pb Orefield hold one of the largest concentrations of Zn and Pb per km² in the world (Singer, 1995). This Orefield includes the Navan, Lisheen, and Silvermines deposits with resources of Zn and Pb of approximately 110 Mt, 22 Mt

and 17 Mt, each deposit respectively (Andrew et al., 1986; Shearley et al., 1996; Ashton et al., 2015). In addition to Zn and Pb, the province also contains significant Cu-Ag reserves that seem to share similar metallogenic controls as the Zn-Pb deposits, such as the same stratigraphic levels, dolomitization, and similar NE to ENE trending structural controls (Steed, 1986; Wilbur and Carter, 1986; Anderson et al., 1998; Johnston, 1999; Hitzman et al., 2002; Wilkinson et al., 2005; Walsh et al., 2018; Lang et al., 2020). However, Cu-Ag deposits, such as Tullacondra, are subeconomic and not enough is known about their formation to assess whether the Irish Orefield could also contain Cu-Ag resources in economic concentrations, waiting to be discovered. Tullacondra, for example, is hosted in shaly limestones overlying oxidized sandstone (Red Beds), deposited during transition from fluvial to marine environments. Therefore, better definition and characteriziation of the processes that govern mineralization at Tullacondra will aid exploration efforts targeting for copper, and help determine the hidden potential of economic copper mineralization associated with the Irish Orefield.

This study presents a detailed assessment of the geology of the Tullacondra Cu-Ag deposit, based on drill hole descriptions, whole-rock chemistry, petrography, SEM-EDS analyses, and semi-qualitative micro X-ray fluorescence element mapping across key textures. On the basis of this data, we demonstrate that mineralization at the Tullacondra deposit has similar metallogenic controls, and contains similar mineralogy and geochemical signatures to the Zn-Pb deposits within the Irish Orefield. However, our results also indicate that the Tullacondra deposit represents a proximal zone of mineralization where dissolution seams failed to evolve into fully brecciated zones, and thus unlikely to accumulate important amounts of sulfides.

3.3 SAMPLES AND METHODS

In this study, we modelled the geology of the mine, geometry of the orebodies, and distribution of metals using Leapfrog Geo software, based on data compiled of 28 drilled over 30 years across the Tullacondra area. This database includes historical drilling and assay data of Cu and Ag that was collected originally by the Munster Base Metals company from 1969 to 1986 from the Tullacondra quarry and currently made available by Geological Society of Ireland (GSI). Moreover, we collected 48 samples from the Diversified Asset Holdings Proprietary Limited core shed. These holes covered a transect (W-E) across the deposit and represent the core ore zone and a peripheral ore zone .They were selected to show the contrasts between proximal and distal mineralized zones. Hence, these samples provide a representation for all of the different mineralized units present at Tullacondra from different parts of the deposit. Petrographic examinations, whole-rock analysis for major and trace element abundances, and micro X-ray fluorescence imaging were conducted for the purpose of characterizing the mineral and textural associations and geochemical variability across the deposit. Polished sections were produced from these samples, which were examined via transmitted and reflected light microscopy, and subsequently investigated by semi-quantitative identification through SEM-EDS analysis at the Laboratório de Análises de Minerais e Rochas (LAMIR) of the Universidade Federal do Paraná (UFPR).

Samples were pulverized in a Widia pan mill at the Laboratório de Análises de Minerais e Rochas (LAMIR) of the Universidade Federal do Paraná (UFPR), the pan was decontaminated by milling with quartz between each sample. Thirty-eight rock pulps were sent to the ALS Global laboratory for major and trace elements. These pulps were fused into lithium tetraborate beads and were analyzed using different instruments: (1). ICP-AES using four acid digestion and loss on ignition (LOI) determined through the furnace (major elements and Ag, Cd, Co, Cu, Li, Mo, Ni, Pb, Sc, and Zn); (2). ICP-MS using acid digestions consisting of nitric, hydrochloric, and hydrofluoric acids (Ba, Ce, Cr, Cs, Dy, Er, Eu, Ga, Gd, Hf, Ho, La, Lu, Nb, Nd, Pr, Rb, Sm, Sn, Sr, Ta, Tb, Th, Tm, U, V, W, Y, Yb, and Zr), and through aqua regia digestion (As, Bi, Hg, In, Re, Sb, Sc, Te, and Tl), and finally, (3). the Leco furnace method was utilized for determination of total carbon and sulfur contents. The major

elements (Al_2O_3, SiO_2, CaO, MgO, TiO_2 and K_2O) are within the detection limit. Thus, the lower and upper detection limits of these elements are Ag (0.5-100 ppm), As (0.1-250 ppm), Cu (0.2-10000 ppm), Pb (2-10000 ppm), S (0.01-50 %), Sb (0.05-250 pmm), and Zn (2-10000 ppm).

Moreover, elemental maps of 14 sample offcuts, which represent the different lithologies and mineralizing styles, were collected by Edax Orbis micro-XRF instrument at the Center for Environmental Science and Technology (CEST), University of Notre Dame. Analytical parameters included a beam size of 30 µm, 40 kV voltage and 300 µA current (Corcoran et al., 2019; Çimen et al., 2019) Chemical maps were produced for the following elements: Cu, S, Al, Fe, Ca, P, As, K, Mg, Mn, Si, Ti and Zn, and ternary RGB images were subsequently generated using ImageJ software.

3.4 THE IRISH OREFIELD

The basement of the Irish Orefield consists of Precambrian, Silurian, and Ordovician rocks, characterized by metamorphic, metasedimentary, and metavolcanic rocks (Phillips and Sevastopulo, 1986). These rocks were formed, folded and faulted due to the emergence and closure of the Iapetus Ocean during the Caledonian Orogeny in the Lower Paleozoic (Phillips and Sevastopulo, 1986; Soper, 1988).

Overlaying the basement, sedimentary rocks were deposited during the Upper Devonian and Lower Carboniferous due to a S-N marine transgression across Ireland (e.g.,

Wilkinson, 2013). This sedimentary sequence initiated with the deposition of Middle-Upper Devonian siliciclastic sediments in the Munster Basin (Hudson and Philcox, 1965; Gardiner and Maccarthy, 1980) consisting of green to red sandstones, conglomerates, and mudstones (Strogen et al., 1990) deposited under fluvial conditions (Graham, 1983).

The Lower Carboniferous records a gradual transition from a continental to a shallow marine environment when the carbonate shelf began to dominate with the S to N marine transgression and further extension across the Irish Midlands (Phillips and Sevastopulo, 1986) The lowermost Carboniferous units are composed mainly of argillaceous limestone which are less siliciclastic in the north, the Navan Group, and

more siliciclastic in the south, the Lower Limestone Shale (LLS), as observed in the study area (Fig. 9) (Philcox, 1984; Anderson et al., 1998). Above the LLS lie the Ballymartin Formation and the Ballysteen Formation (Somerville and Jones, 1985; Phillips and Sevastopulo, 1986; Somerville et al., 1992; Shearley et al., 1996). The Ballymartin Formation consists of medium-grained argillaceous bioclastic limestone and calcareous shale. The Ballysteen Formation consists of locally dolomitized bioclastic limestone containing low clay contents. Overlying these units is the Waulsortian Limestone Formation, which is typically composed of dolomitized reef micritic limestone containing bioclasts (Hudson and Philcox, 1965; Strogen and Somerville, 1984; Lees and Miller, 1985; Somerville and Jones, 1985; Gregg et al., 2001). The depositional environment of the Waulsortian Limestone is considered deeper than the previous formation (Strogen and Somerville, 1984), deposited up to 200 m of depth between the photic and aphotic zone (Lees and Miller, 1985). Moreover, associated with this extensional period of the Lower Carboniferous, mafic intrusions and volcanoclastic rocks are common mainly in the southwest Irish Midlands towards the Limerick area (Steed, 1986; Mccusker and Reed, 2013; Wilkinson and Hitzman, 2015; Elliott et al., 2019).

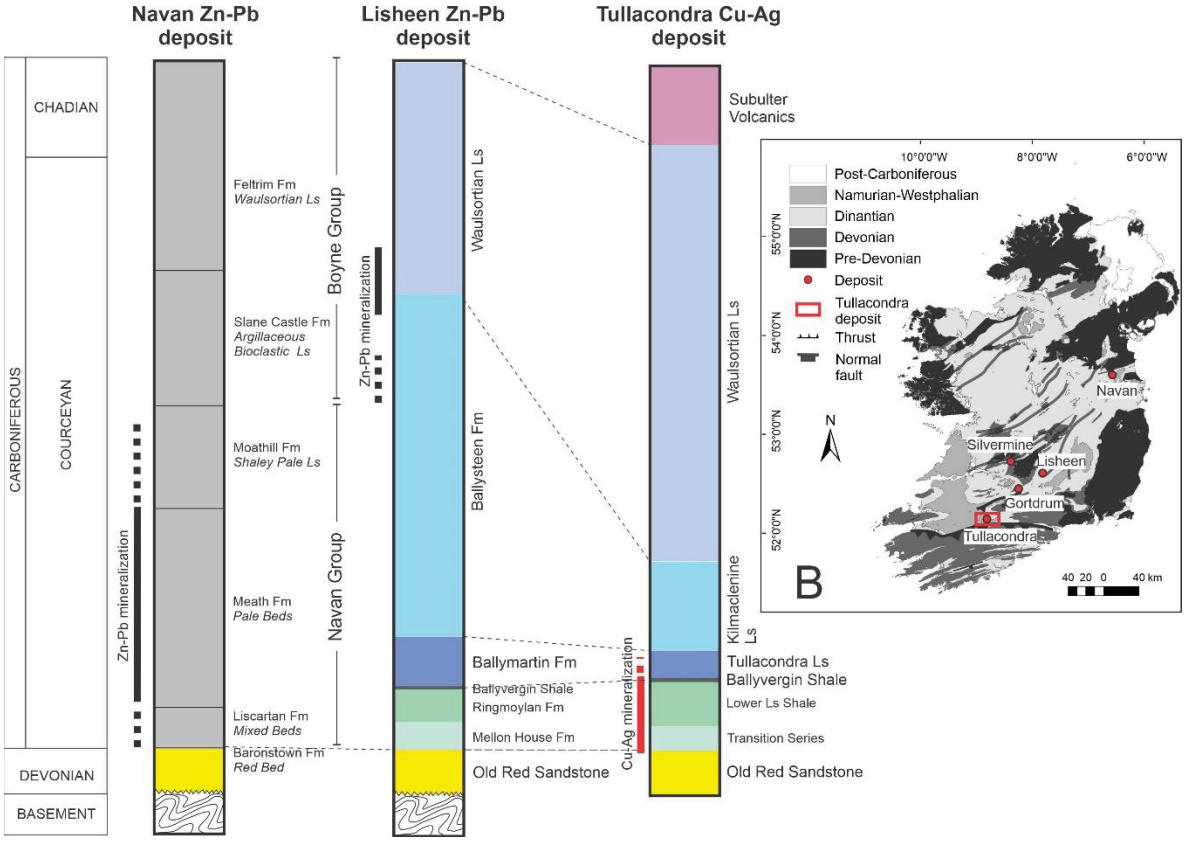

Figure 9 – (A) Stratigraphic columns for the Navan, Lisheen, and Tullacondra deposits showing the lateral stratigraphic variation and the main host lithologies. The Waulsortian Limestone and Navan

Group host the Lisheen and Navan deposits, respectively, while the Lower Limestone Shale hosts the Tullacondra deposit. Note also that the Lower Limestone Shale occurs in deposits from southern Ireland with different names and is laterally correlated with the Navan group. The Navan deposit column is based on Philcox (1984), Strogen et al. (1990), and Ashton et al. (2015). The column for the Lisheen deposit is based on Somerville and Jones (1985), Shearley et al. (1996), and Hitzman et al. (2002), and for the Tullacondra deposit on Hudson and Philcox (1965) and Wilbur and Carter (1986). (B) Geological map of Ireland showing the main stratigraphic units and deposits. Note the localization of the Tullacondra in southern Ireland. Navan, Lisheen and Silvermines are important sources of Zn-Pb whilst Gortdrum and Tullacondra contain Cu-Ag.

The host rocks deposition of the Irish deposits is marked by synchronous ENE-trending faults formed during the reactivation of the Caledonian basement faults during the Carboniferous extensional period (Coller, 1984; Johnston et al., 1996). These structures are characterized by normal faults, which have developed relay ramps and damage zones allowing the increase of the permeability of the rocks (Walsh et al., 2018). Later, during the Late Carboniferous and Upper Permian, the Variscan Orogeny led to inversion causing folding, thrusting and reactivation of these structures (e.g., Cooper et al., 1984; Cooper et al., 1986).

3.5 THE TULLACONDRA DEPOSIT

3.5.1 Stratigraphy

The base of the Tullacondra deposit consists of Old Red Sandstone shales, sandstones, conglomerates and red beds. The Lower Limestone Shale (LLS) is overlies the ORS and is the main host unit of the Tullacondra Cu-Ag deposit (Wilbur and Carter, 1986). Wilbur and Carter (1986) divided the LLS from the Tullacondra deposit into seven subunits from bottom to top: Lower and Upper Transition Series, Uniform Calcarenite, Lower Shaly Calcarenite, Oolitic Calcarenite, Silty Calcarenite and Upper Shaly Calcarenite, which is the more detailed nomenclature we adopted in this work.

Although the Transition Series belongs to the Lower Limestone Shale (Wilbur and Carter, 1986), we separated the data of the Transition Series from the others LLS subunits, because they contrast petrologically and chemically. The Lower and Upper Transition Series, also known as Mellow House elsewhere in Ireland, consist of 30 m thick sandstone, conglomerate and siltstone interbedded with calcareous sandstone, siltstone, and shale (Somerville and Jones, 1985; Wilbur and Carter, 1986). According to Wilbur and Carter (1986), in Tullacondra the Lower Transition

Series is medium-grained (sand) whereas the Upper Transition Series is shale-dominated, both about 15 m thick. Wilbur and Carter (1986) described a 30 cm thick horizon termed as Hematite Marker, of unknown significance, next to the contact between the Upper and Lower Transition Series that consists of iron-oxide stained rounded clasts. Such marker was also reported by Somerville and Jones (1985) in the southwestern Ireland.

The other five subunits belonging to the LLS, also known as Ringmoylan Shale Formation are detailed in Table 2 (Tabela 2) such as reported by Wilbur and Carter (1986). Overlying the LLS is the regional marker the Ballyvergin Shale which is ~1 m thick at Tullacondra (Wilbur and Carter, 1986), the Tullacondra Limestone and Kilmaclenine Limestone as equivalents to the Ballymartin Formation and the Ballysteen Formation, respectively (Somerville and Jones, 1985, Phillips and Sevastopulo, 1986; Somerville et al., 1992; Shearly et al. 1996). The Tullacondra Limestone is 35 m thick at Tullacondra comprising medium-grained crinoidal limestone with thin irregular shale partings and a siliceous base (Wilbur and Carter, 1986). Above it, the Kilmaclenine Limestone is about 100m thick at Tullacondra and comprises bioclastic limestone containing low clay contents (Hudson and Philcox, 1965; Wilbur and Carter, 1986).

The upper Waulsortian Limestone Formation is 450 m and is overlain by the Subulter Volcanic Group that is composed from dark, thin-bedded pyroclastic rocks up to 100 m thick (Hudson and Philcox, 1965; Wilbur and Carter, 1986). Thin dykes cutting drill holes are locally described in historical logging from Tullacondra. They were described as porphyritic rhyolitic dykes with very fine-grained matrix, sometimes brecciated, cut by mineralized veins and hosted within the mineralized LLS. Due to being poorly described, further information about these dykes is required to improve the understanding of them.

3.5.2 Structural and ore body geology

The Tullacondra Cu-Ag deposit is hosted in the northern flank of the Kilmaclinine anticline central area, an open fold with an ENE-WSW trending hinge. Hinge-parallel thrust faults cut the anticline and are intersected by roughly N-S trending steep faults (Fig.10 A-C) (Wilbur and Carter, 1986).

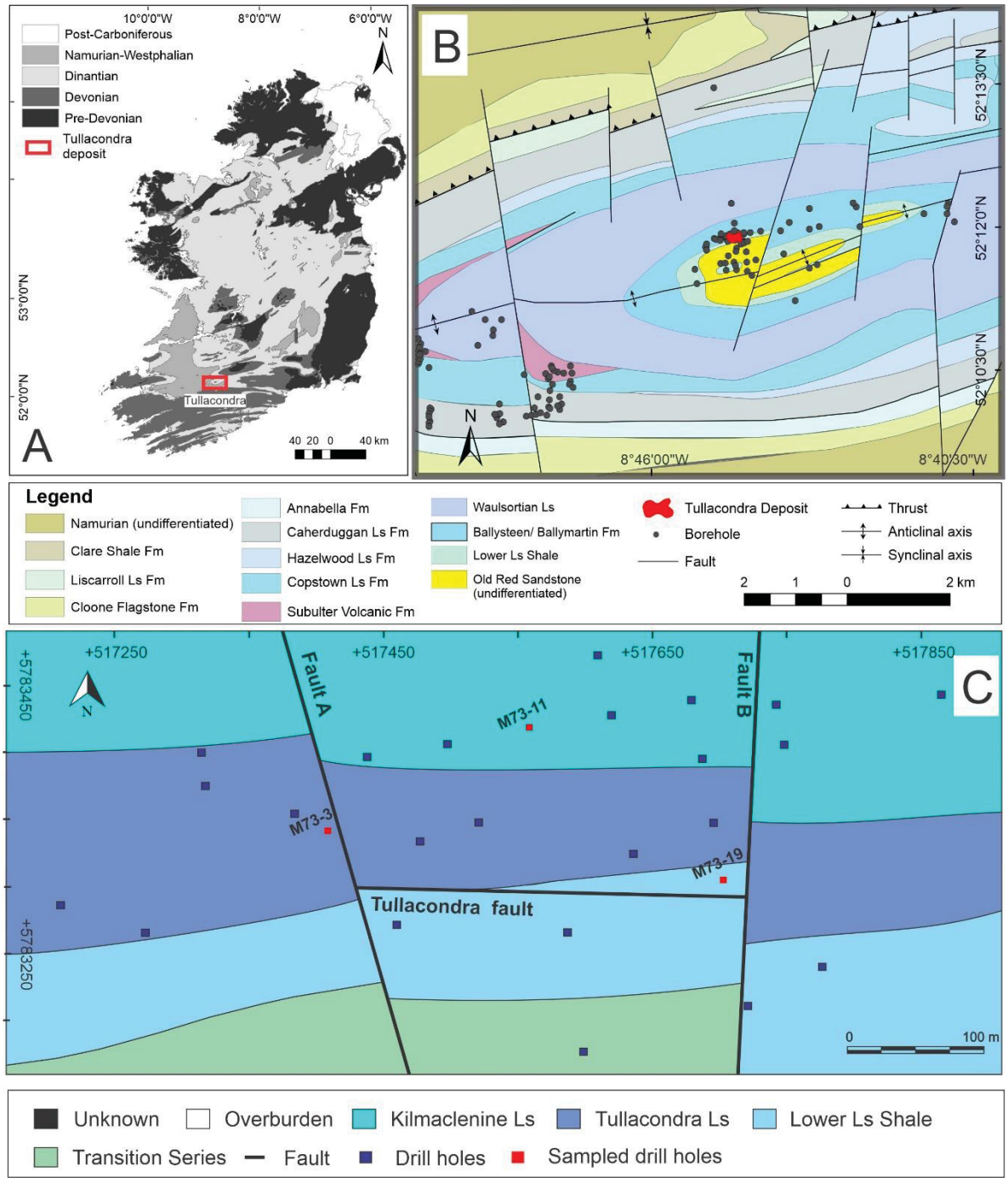

Figure 10 - (A) Geological map of Ireland showing the main stratigraphic units and the localization of the Tullacondra deposit. (B) Geological map of the Kilmaclenine area showing the localization of the drill holes and the Tullacondra quarry (red area), the main units and structures, such as the Kilmaclinine anticline. (C) Local geological map of the Tullacondra quarry showing the main structural features highlighting EW- (Tullacondra Fault) and NS- (Faults A and B) trending faults and lithologic sequence that host the Orebodies. Maps based on data available by the Geological Survey Ireland.

The Tullacondra deposit is controlled by a steeply dipping, 250 m long, ~E-W trending fault referred to as the Tullacondra Fault (Fig. 10C, 11A-B, 12A-B). This fault was described by Wilbur and Carter (1986) as a monocline, interpreted from an abrupt changing of bedding dip from 15° to 70°. Parallel to the Tullacondra Fault,

there is a damage zone comprised of multiple fault surfaces. Following the regional structural pattern, the Tullacondra Fault is truncated to the west and east by steep ~N-S trending faults and limit the extension of the orebody in an E-W direction, named as Fault A and Fault B. The western fault shows normal displacement with a throw of ~20 m calculated from drilling data, whereas the eastern fault displacement is largely observed by changes in bedding angle.

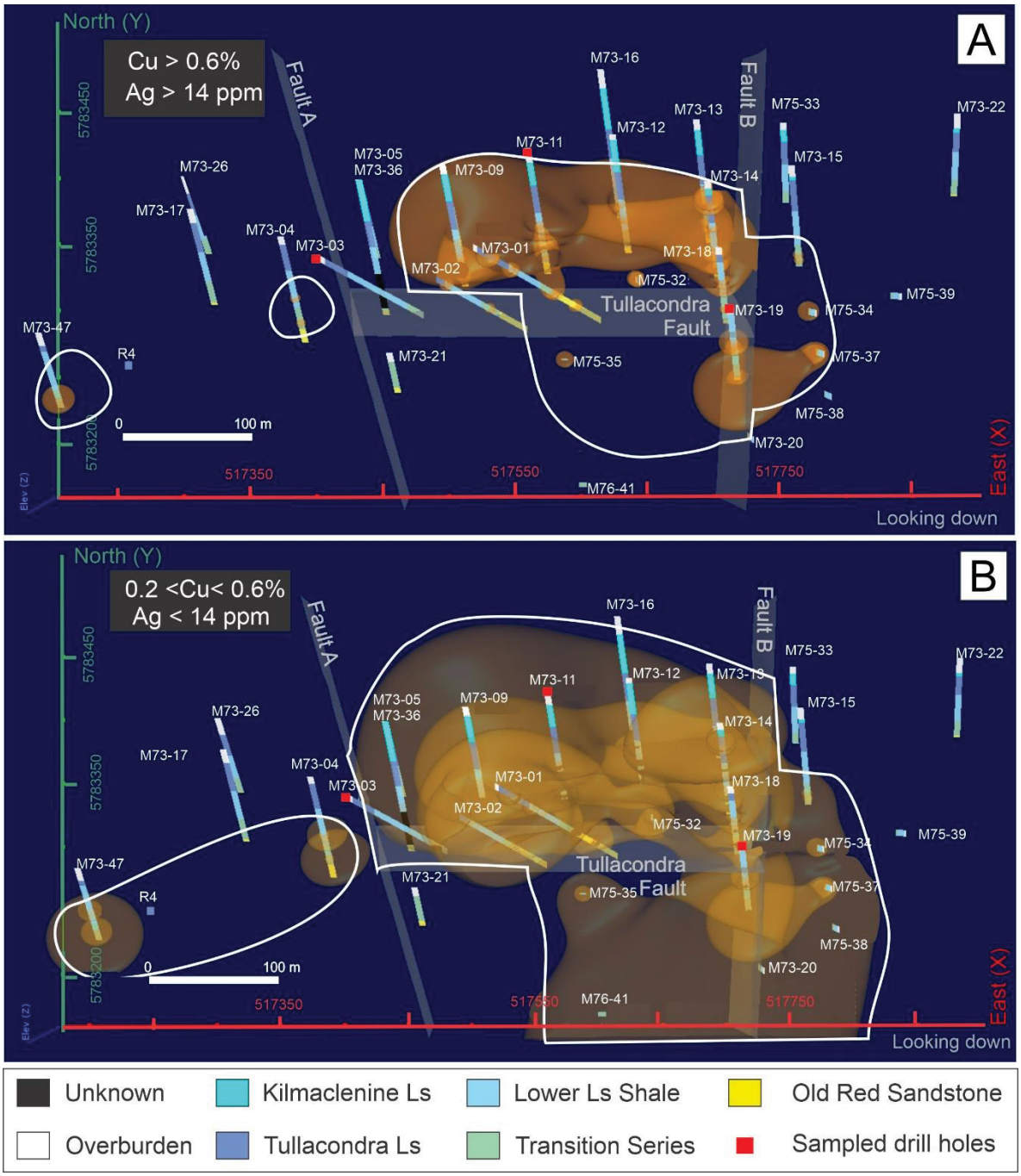

Figure 11 – (A) Ore shell representing the core zone with Cu> 0.6% and Ag > 14 ppm (B) Ore shell representing the peripheral zone with 0.2% < Cu < 0.6% and Ag < 14 ppm.

The concentration of Cu and Ag varies spatially throughout the deposit, as observed in Figures 11A and 11B depicting the distribution of assay results for Tullacondra drill holes. As can be seen in these Figures, the highest values of Cu and Ag are hosted in the rocks between two N-S faults. Unlike most copper results, which are low to moderate south of the Tullacondra Fault, silver and copper has elevated concentrations in this area and low values beyond the external limits of the N-S bounding faults. The mineralized area is subdivided in this study into a core zone (Cu > 0.6 %; Ag > 14 ppm, Fig. 11A) and a peripheral zone (0.2< Cu < 0.6%; Ag < 14 ppm ppm, Fig 11B) in order to understand the main petrological and geochemical differences between the proximal and distal areas. Thus, the petrography and geochemistry of samples from two drill holes (M73-11 and M73-19) of the core zone and from a drill hole (M73-03) were studied.

The Cu-Ag mineralization is characterized by disseminated, bedding-parallel, dissolution seams- and minor veins in three stratabound orebodies connected by a lower grade near-vertical zone (damage zone) (Fig. 12A-F). These orebodies were determined by isograd contours by our visual estimation from the company data of different cross sections containing Cu (> 0.6; 0.6-1.78 %) and Ag (> 10ppm; 20-383 ppm), part of the legacy data from the Munster Basin Metals assay database available by the Geological Survey Ireland. The data indicates three envelopes named as orebody 1, 2 and 3 with grades mentioned bellow and of approximately 300 m length, 250 m wide and 10 m thick each. In addition, isograde contours of Cu from 0.4 to 0.7% and Ag from 10 to 30 ppm indicate the near-vertical mineralized zone (Fig. 12C-F). However, the lack of systematic sampling and assaying of core means it is difficult to further understand grade distribution at Tullacondra. This secondary vertical zone shows higher Cu values in proximity to the damage zone of the Tullacondra Fault, which led Wilbur and Carter (1986) to interpret these stacked orebodies as a single vertical orebody of 370m by 40m and 120m depth comprising the bulk of mineralization at Tullacondra.

3.5.2.1 Orebody 1 (Transition Series - hosted orebody)

The orebody 1 is defined by a stratabound lens located in the Lower and Upper Transition Series. It averages 150 ppm Ag and 0.6% Cu according to Wilbur and Carter (1986), and containing the highest silver grades mainly in the southern

part of the deposit (up to 383 ppm Ag). Sulfide paragenesis determined by petrography of 11 samples in the orebody 1 is zoned with respect to the peripheral and core ore zones: a) core zone containing tennantite > chalcopyrite - bornite - chalcocite and b) peripheral zone containing chalcopyrite > tennantite – arsenopyrite.

3.5.2.2 Orebody 2 (Lower Limestone Shale-hosted orebody)

This orebody averages 30 ppm Ag and 0.7% Cu according to historical assays and is hosted in the subunits of the Lower Limestone Shale which overlying the Transition Series. In contrast to the orebody 1, the petrography of 20 samples of the orebody 2 lacks zonation and contains sulfide paragenesis characterized by chalcopyrite – bornite – chalcocite > tennantite, and traces of pyrite;

3.5.2.3 Orebody 3 (Tullacondra Limestone-hosted Orebody*):*

This orebody represents a smaller portion of the deposit, which ended up under-represented in this study with only 4 samples, and averages 24 ppm Ag and 0.7% Cu. It is characterized predominantly by chalcocite, bornite, and chalcopyrite (> 50 % of the ore minerals), traces of pyrite, and arsenic minerals are absent.

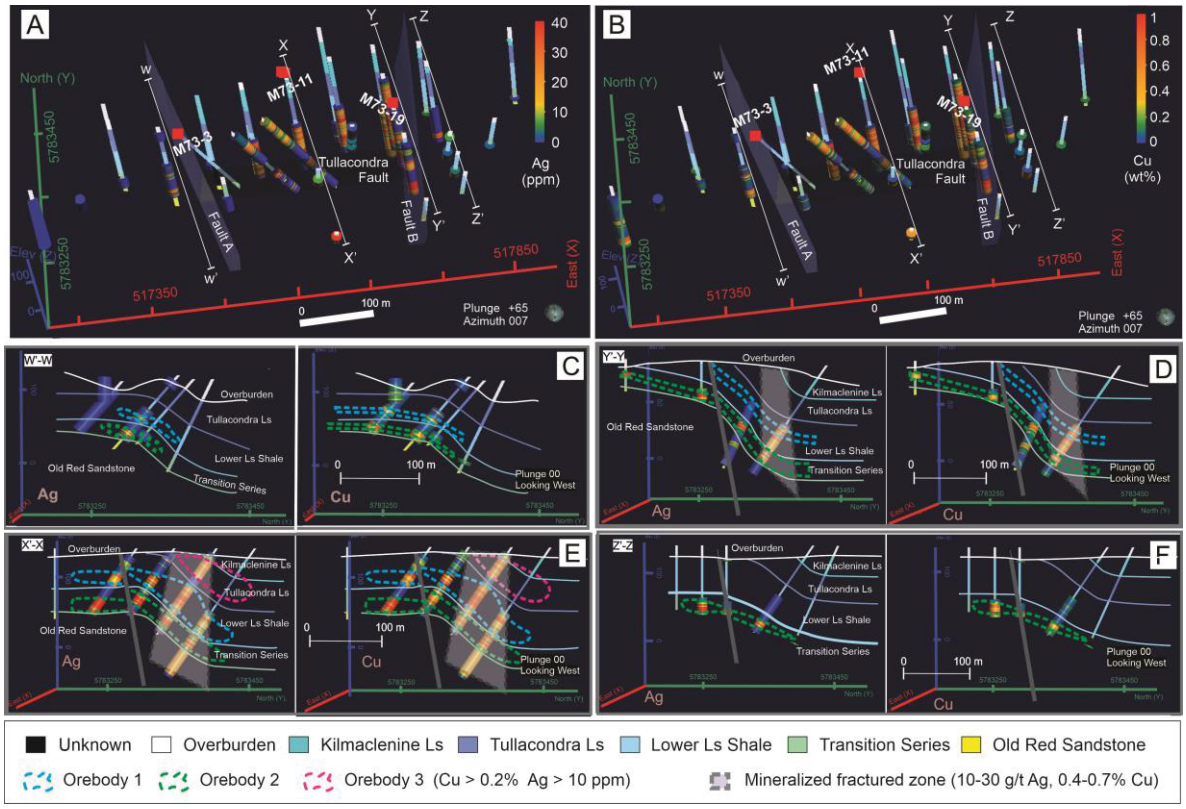

Figure 12 – Localization of core holes, faults and the distribution of Cu (A) and Ag (B). Figures C-F are cross sections of the Tullacondra deposit showing the localization of the Cu (> 0.6%) and Ag (> 10 ppm) mineralization determinated by our visual estimation. (C) Cross section W-W' located in the western part of the deposit. (D) and (E) Cross sections X-X' and Y-Y'' located in the center of the deposit. (F) Cross section Z-Z' shows eastern deposit. Note the occurrence of three orebodies and a near vertical mineralized fractured zone.

3.5.3 Ore-related textures

The Tullacondra deposit contains a limited variety of ore-related textures (Table 1), which we divided into: (1) disseminated and bedding-parallel; (2) dissolution seam-hosted; (3) vein-hosted.

3.5.3.1 Disseminated and bedding-parallel sulfides and sulfosalts:

Disseminated and bedding parallel sulfides are pervasive throughout the Tullacondra deposit and represent the main ore texture characterized by fine to medium-grained chalcocite, bornite, chalcopyrite, tennantite, arsenopyrite, and pyrite. Disseminated textures are associated with host calcarenite, dolomitized calcarenite and sandstone, and they occur replacing bioclasts and oolites and pore infill (Fig. 13A-C); in contrast, bedding parallel are associated with shaly units whereby sulfides occur along bedding planes (Fig. 13D-F). Disseminated and

bedding parallel textures are also common and spatially associated with zones of stylolite-hosted and vein-hosted sulfides and sulfosalts.

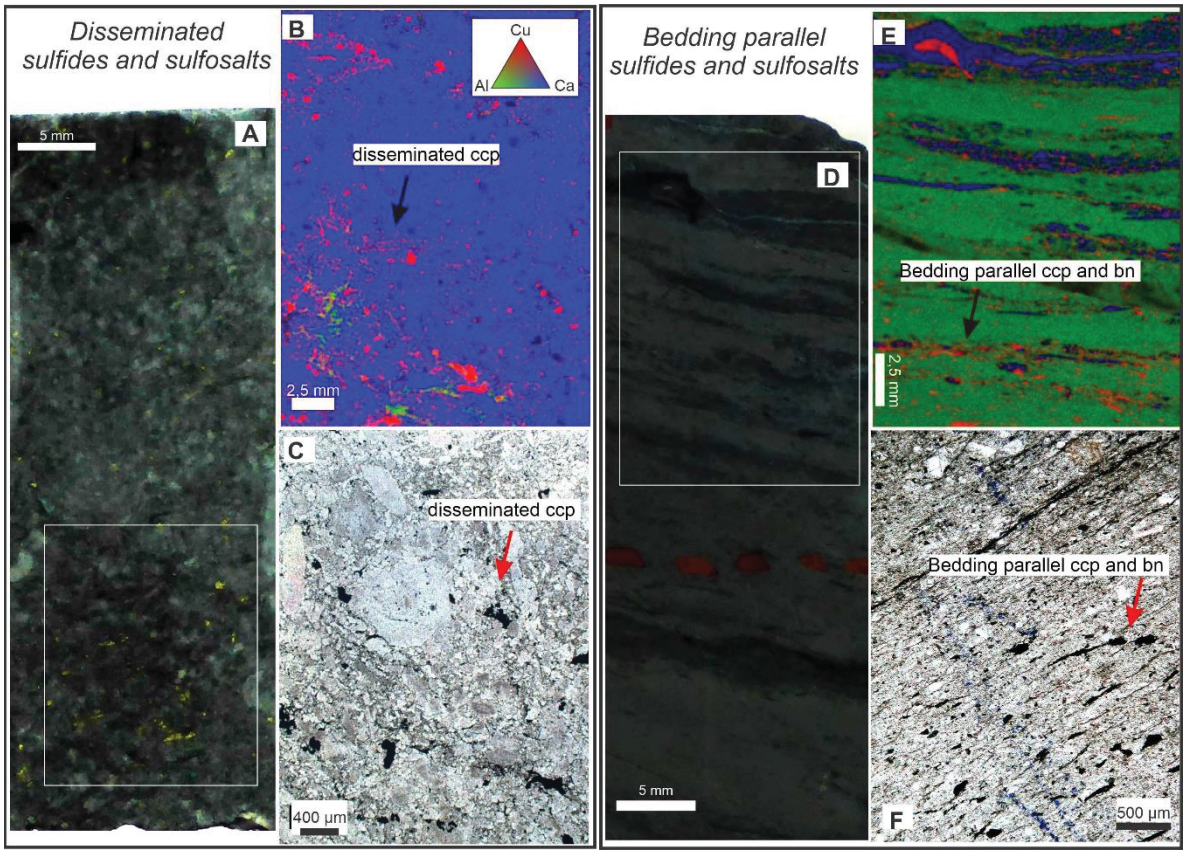

Figure 13 – (A, D) Hand sample images; (B, E) Semi-quantitative chemical maps obtained by micro X-ray fluorescence analysis indicating the variation in the abundances of Cu, Ca, and Al, and (C, F) their respective photomicrographs. The figures (A), (B), and (C) show disseminated sulfide and sulfosalts, whilst the figures (D), (E) and (F) show bedding parallel texture.

3.5.3.2 Dissolution seam-hosted

Dissolution seam-hosted ores are in general more sulfide-richer (up to 5%) compared to disseminated and bedding parallel textures (Table 1). Dissolution surfaces occur in shaly calcarenite, calcareous sandstone, and shale as single or swarms of bedding-oblique to bedding-parallel anastomosed dissolution seams (non-serrated), which can be mineralized and subordinate barren seams (serrated). These seams can be up to 1 cm thick (thicker in some cases) and filled by very fine- to medium-grained phyllosilicates, quartz and traces of very fine-grained oxides. The medium-grained mica within the seams at times shows a preferred orientation defining a bedding-parallel dissolution cleavage. Dissolution seams can evolve to incipient breccias, which are characterized by fine-grained matrix surrounding calcitic

clasts and, in the peripheral zone, has partially dolomitized clasts. These clasts are fine- to coarse-grained and subrounded to subangular containing sharp to irregular contact with the matrix. Ore minerals commonly occur along dissolution seams and within breccias on the boundaries between calcitic clasts and matrix (Fig. 14A-C). Additionally, several clasts are slightly rotated, flatted and, in several shaly areas, symmetrically elongated with anastomose contours or showing a slightly asymmetric shape.

3.5.3.3 Vein-hosted

Vein-hosted ore contains anhedral coarse-grained to fine-grained chalcocite, bornite, chalcopyrite, and tennantite within medium-grained sparitic calcite and ferroan dolomite that is approximately 1 cm thick (Fig. 14D-F). The mineral composition of the vein is the same as that of the host rock and the veins cut the host rock. Thus, dolomitized samples contain ferroan dolomite whilst non-dolomitized samples contain calcitic vein. Furthermore, the same ore minerals observed in the host rocks occur within the veins that cut the host rock.

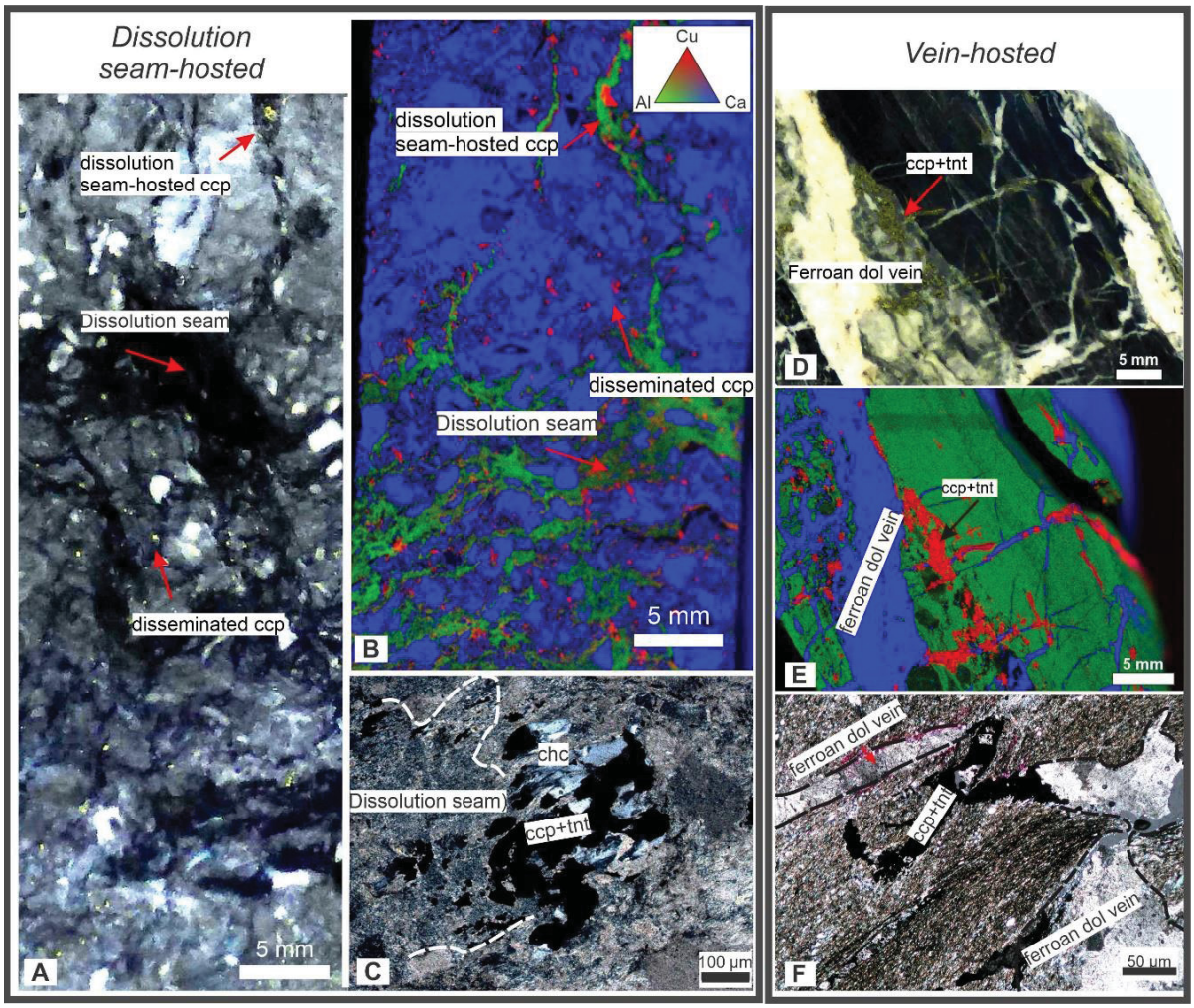

Figure 14 - (A, D) Hand sample images; (B, E) Semi-quantitative chemical maps obtained by micro X-ray fluorescence analysis indicating the variation in the abundances of Cu, Ca, and Al and (C, F) their respective photomicrographs. The figures (A), (B), and (C) show dissolution-hosted sulfide and sulfosalts. Note the very fine-grained quartz and phyllosilicates matrix filling the breccia-like seams. The figures (D), (E) and (F) represent vein-hosted sulfides and sulfosalts with chalcopyrite and tennantite within a ferroan dolomite vein.

3.5.4 Host rock and authigenic minerals

The host rocks consist of calcareous sandstone and shale, marl and calcarenite from the Lower Limestone Shale and Tullacondra Limestone. The main host rock minerals are calcite, quartz, phyllosilicates whilst feldspar, rutile, zircon, monazite, barite, hematite and ilmenite are traces. Calcite is the main mineral in the Tullacondra Limestone and Lower Limestone Shale, and most likely formed during sedimentary deposition and diagenesis, but it also occurs as cement in the Transition Series and Old Red Sandstone. It is characterized by coarse- to medium-grained bioclasts, oolites, and sparite, and occurs as micritic or microsparitic cement and in coarse-grained sparitic veins (Fig. 15A). Additionally, calcite commonly occurs

as clasts of breccias associated with dissolution seams (Fig. 15B-C). Calcite veins usually are up to 1 cm and occur oblique or parallel to the bedding.

After calcite, quartz and phyllosilicates are most common detrital mineral group recorded in the Tullacondra deposit. They are medium-grained and occur along with the whole deposit. Whereas quartz is sub-rounded, micas are subhedral to euhedral bedding-parallel. (Fig. 15D). Moreover, in very fine-grained samples, a sericitic mixture containing quartz occurs within the matrix material along dissolution seams and incipient breccias (Fig. 15B-D). SEM-EDS and micro-XRF analyses show that sericite contains Fe, Mg, Ti and K.

Traces of potassic feldspar, barite, monazite, and zircon also occur and form medium- to fine-grained, subrounded grains occurring mainly in sandstone from the Old Red Sandstone and Transition Series. These minerals lack clear paragenetic evidences for their relationship with the ore mineralization, although barite is an important gangue mineral elsewhere in the Irish Orefield (e.g. Ashton et al. 2015, Anderson et al. 1998). Hematite and ilmenite are likely a detrital mineral characterized by medium- to fine-grained crystals restricted in the Old Red Sandstone. They are elongate, bedding-parallel crystals together with medium-grained potassic mica and ilmenite. Hematite and ilmenite are likely a detrital mineral characterized by medium- to fine-grained crystals restricted in the Old Red Sandstone. They are elongate, bedding-parallel crystals together with medium-grained potassic mica and ilmenite. Hematite occurs at the base of the Tullacondra Limestone with malachite and covellite.

Authigenic minerals are represented mainly by quartz and dolomite. In the uppermost units, such as Tullacondra Limestone and Upper Shaly Calcarenite, hydrothermal/diagenetic quartz/chalcedony replaces bioclasts and oolites, and occurs in veinlets. Moreover, chalcedony is also described as encircling calcite and ore minerals. A second generation of hydrothermal, well-formed fine- to medium-grained, subhedral and euhedral quartz occurs in dolomitized rocks filling voids, within calcite veins (Fig. 15E) and are present in the orebody 2 from the peripheral zone. The paragenetic relationship between this hydrothermal quartz and ore minerals is not clear. Furthermore, this generation of euhedral-subhedral quartz commonly contains micro inclusions of a yet unidentified high birefringence mineral.

Ferroan dolomite in our sample set is restricted to peripheral zone. It occurs either partially replacing bioclasts, in micritic cement with calcite, or completely

replacing calcarenite in medium-grained euhedral-subhedral crystals (Fig. 15F), and in sparitic veins. Planar dolomite occurs solely in samples from the Upper Shaly Calcarenite and Oolitic Calcarenite. Besides quartz and dolomite, in trace amounts medium-grained anhedral apatite and fine-grained chlorite are spatially associated to the ore minerals

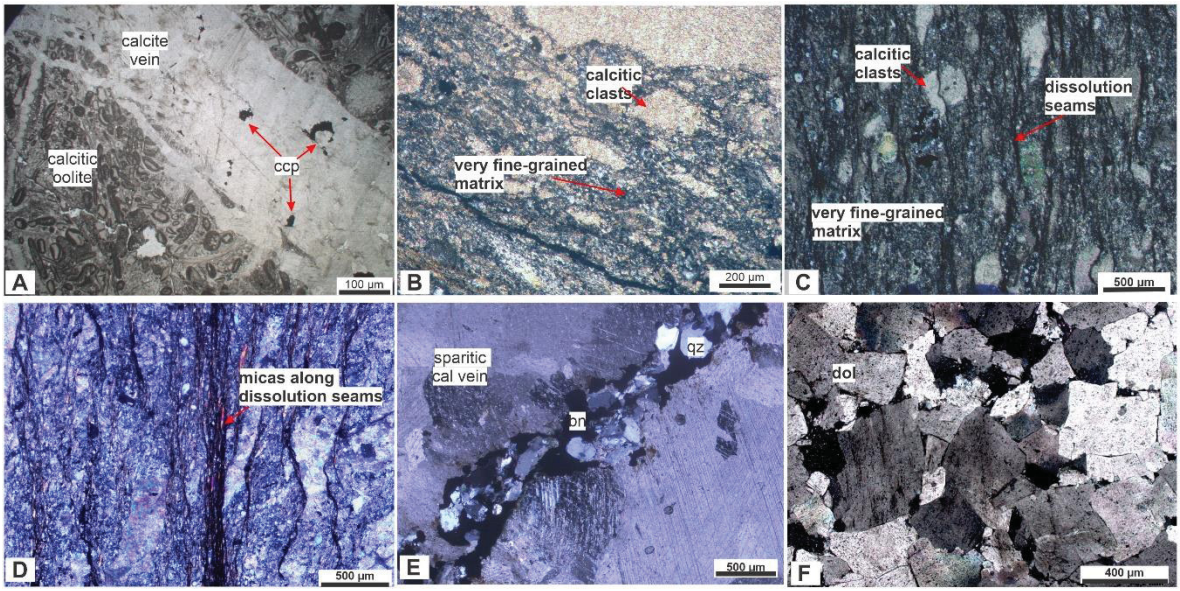

Figure 15 - Photomicrographs illustrating gangue mineral textures and hydrothermal alterations. (A) Oolitic calcarenite and a calcite vein containing anhedral chalcopyrite. (B) Calcitic clasts surrounding by very fine-grained matrix. (C) Calcite clasts cut by dissolution seams in a very fine-grained matrix. (D) Very-fine grained matrix with mica along dissolution seams. (E) Bornite hosted in calcitic vein associated with quartz. (F) Planar dolomite.

3.5.5 Ore Minerals

Fine- to medium-grained iron, copper and arsenic sulfides and sulfosalts are the main ore minerals present in the Tullacondra deposit. These are hosted in the Tullacondra Limestone, Lower Limestone Shale, and Transition Series, and absent in the Old Red Sandstone. Minor supergene minerals such as malachite, hematite, and covellite are also recorded in the Tullacondra Limestone but they are outside the scope of this study.

The ore minerals are described below and listed according to the paragenetic sequence (Fig. 16):

a) Pyrite
b) Cct+bn+ccp
c) Ccp+tnt+apy

d) Ccp+cct+bn+tnt+apy

3.5.5.1 Pyrite

Pyrite occurs locally and is characterized by fine- to medium-grained subhedral and euhedral disseminated pyrite, replacing bioclasts or within dissolution seams of dissolution seams, and is recorded in the Tullacondra Limestone- and Lower Limestone Shale-hosted peripheral and core zone (Fig. 16A). Its chronological relationship with other ore minerals is unclear. Chemical and micro X-ray fluorescence analysis show that the pyrite contains both As and Pb.

3.5.5.2 Chalcocite, bornite, and chalcopyrite

This assemblage marks the first generation of chalcocite, bornite, and chalcopyrite. These minerals are fine- to medium-grained, anhedral, and are usually clustered. They are determined by disseminated, bedding parallel and along stylolite crystals replacing limestone (Fig. 16B-D). Chalcopyrite usually occurs as exsolution lamellae within bornite (8D). Although these minerals occur throughout the three orebodies, they are more abundant in the two uppermost lenses and show distinct lateral variation. The core zone samples contain these copper sulfides in all three orebodies. Peripheral samples, however, show higher modal abundances of bornite and chalcopyrite sulfides when hosted in either the Tullacondra Limestone or Lower Limestone Shale, and negligible contents within the Transition Series.

3.5.5.3 Tennantite, arsenopyrite, and chalcopyrite

The first generation of arsenopyrite and tennantite and second generation of chalcopyrite are present as fine- to medium-grained subhedral to anhedral phases. They are disseminated, along dissolution seams, and are usually when replacing limestone. These generations are characterized by minerals that overprint the first generation of copper sulfides (Fig. 16E-F) and are often rimmed by sub-hedral quartz and chalcedony. These minerals occur mainly in the Transition Series-hosted core zone, whereas the lenses hosted in the Lower Limestone Shale core and peripheral zones contain subordinate occurrences. The peripheral Tullacondra Limestone-hosted orebody is devoid of tennantite and arsenopyrite. Furthermore,

chalcopyrite and traces of arsenopyrite are the only ore minerals found in peripheral dolomitized calcarenite (Fig. 16G).

3.5.5.4 Chalcocite, bornite, tennantite and arsenopyrite, and chalcopyrite

These are medium- to coarse-grained and hosted in sparitic calcite and dolomite veins (Fig. 16H-I). Dolomite veins occur solely in the peripheral ore bodies. Overall, the vein-hosted ores have the same mineralogy as the host rock. In addition, chalcocite and bornite veins ores are associated with apatite and chlorite. Moreover, EDS-SEM analyses show that vein-hosted tennantite contains minor amounts of Ni, Co, and Bi in the lowermost sample from the peripheral zone.distal.

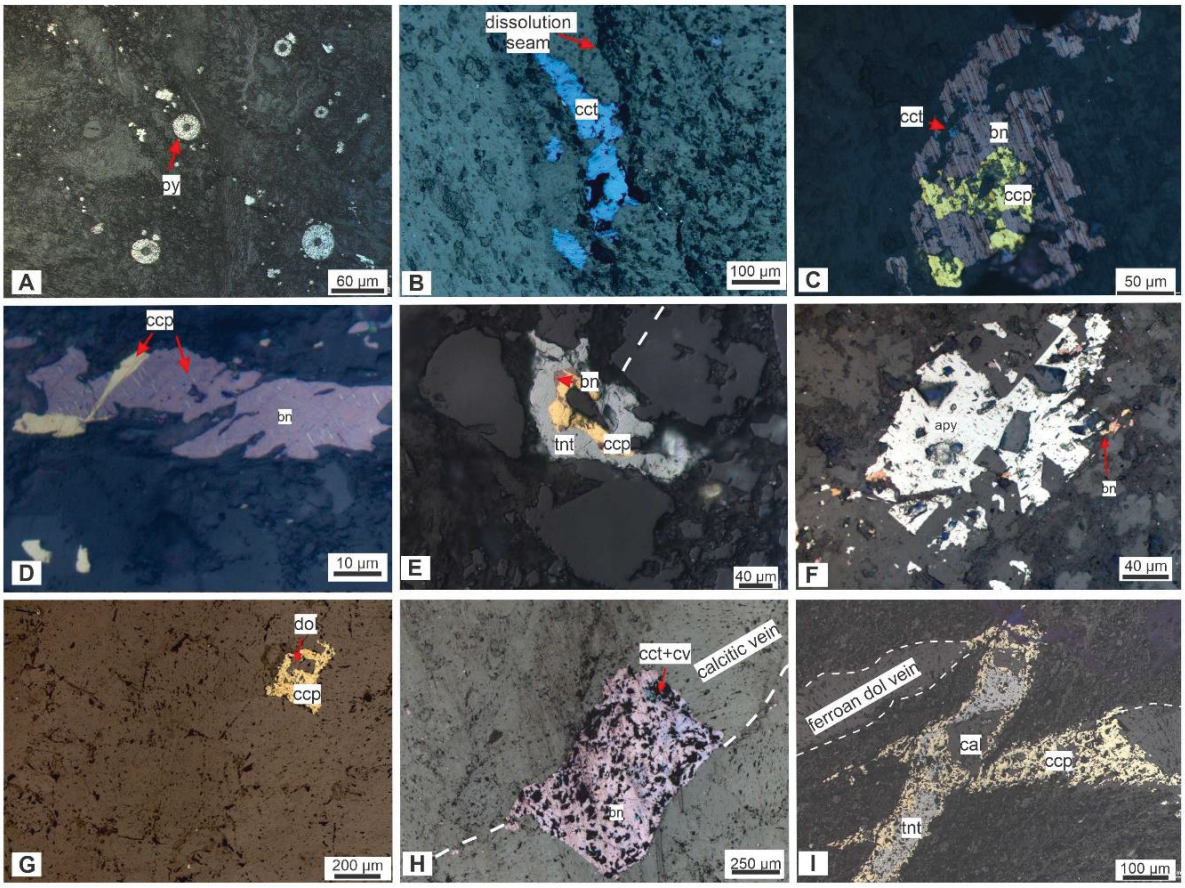

Figure 16 - Photomicrographs with ore textures from the Tullacondra deposit. (A) Pyrite (py) replacing bioclasts. (B) Chalcocite (cct) along with stylolite. (C) Chalcocite, bornite (bn), and chalcopyrite (ccp) clustered. (D) Lamellae of chalcopyrite within bornite. (E) Tennantite (tnt) overprinting chalcopyrite and bornite. (F) Arsenopyrite (apy) overprinting bornite. (G) Chalcopyrite encircling dolomite (dol). (H) Bornite and chalcocite (cc) hosted in a sparitic calcite vein. (I) Chalcopyrite with tennantite hosted in a ferroan dolomite vein.

3.5.6 Geochemistry

Geochemical data in this study are represented through box-and-whiskers plots (Fig. 17) to show chemical variations related to stratigraphic units. Box-and-whiskers plots illustrate the data by dividing it into four parts each containing 25% of the total. The lowermost (Q1) and uppermost 25% (Q4) brackets are represented as whiskers whereas the boxplot represents the central 50%, divided by the median line into Q2 and Q3. Outliers are defined by values above of Q3+1.5*(Q3-Q1) and only units with a representative number of samples were depicted, which excluded the ORS and the Silty Calcarenite.

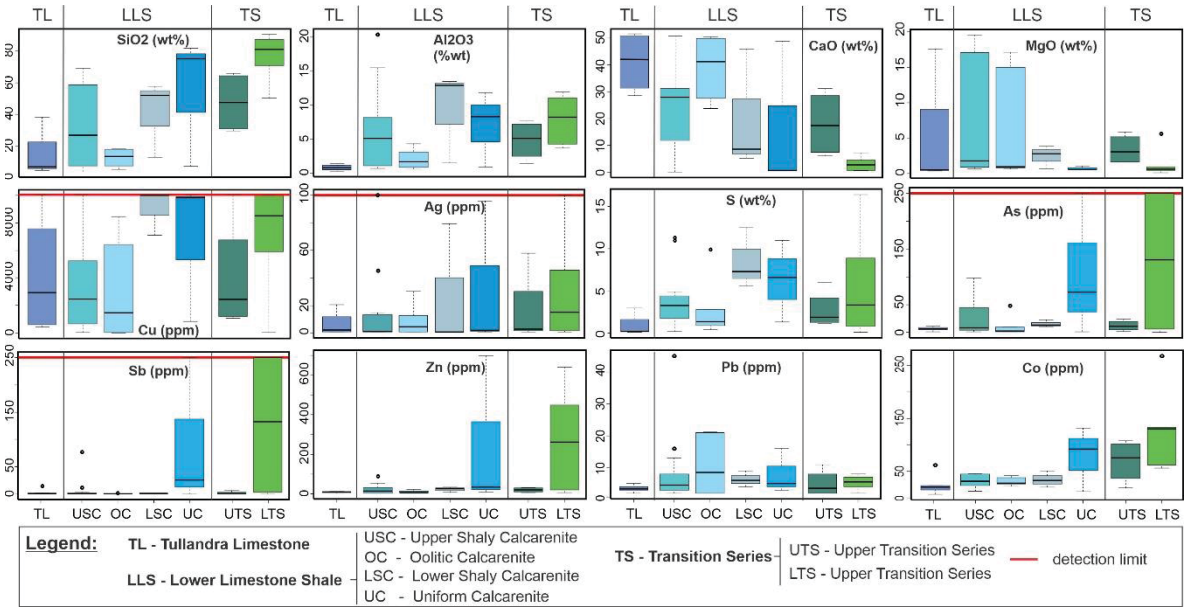

Figure 17 – Box and whiskers plots showing the geochemical variation between groups of units of the Tullacondra deposit.

The Transition Series contains seven samples from the Lower Transition Series and four samples from the Upper Transition Series. Both show high values of Al_2O_3 (6.6%; 1.4-11.9%) and SiO_2 (65.18%; 29.7-90.5%), although ranges are comparatively higher in the Lower Transition Series. On the other hand, the Upper Transition series shows higher concentrations of carbonate-associated elements than the Lower Transition Series. The Lower and Upper Transition Series contain CaO values from 0.82 to 26.3% with average of 9.3% and MgO from 0.14 to 5.88 with average of 2.2%. The Lower Transition Series contains the highest concentration of ore-related metals from our dataset compared to other units (Fig. 17) with particularly anomalous values of As (0.5 to above 250 ppm), Sb (0.12 to

above 250 ppm) and Zn (6 to 640 ppm). Cobalt is anomalous in both Transition Series units in comparison with uppermost ones with concentration of 19 to 268 ppm.

The Lower Limestone Shale Formation is represented by three assays of the Uniform Calcarenite, three of the Lower Shaly Calcarenite, six of the Oolitic Calcarenite and fifteen of the Upper Shaly Calcarenite. For the LLS, the Figure 17 shows variable values of SiO_2 (30.7%; 3.83 to 81.8%) but a general depletion upwards. The Al_2O_3 contents are fluctuating (5.6%; 0.54 to 20.4%) enriched in the Upper Shaly Calcarenite and Lower Shaly Calcarenite. Important variations of MgO values (5.2%; 0.5 to 19.5%) are registered in these units whereas MgO is consistently low throughout the Transition Series. The metals are usually very low in the overlying units of the Transition Series, except for the Uniform Calcarenite which contain the highest concentration of As, Sb, Zn and Co of the Lower Limestone Shale. In the Lower Limestone Shale, As values range from 2 above 250 ppm, Sb from 0.06 above 250 ppm, Zn from 3 to 397 ppm, and Co from 12 to 132 ppm. On the other hand, Pb contains very low values and the highest concentrations are in the Oolitic Calcarenite (2 to 21 ppm) and in the Upper Shaly Calcarenite (2 to 45 ppm). The Tullacondra Limestone (TL) is represented by four samples from the drill hole M73-3 which indicate high values of CaO (34.4%; 28.3-51.6%) and low Al_2O_3 (0.65%; 0.27-1.1%) with variable SiO_2 contents (23.8%; 5 to 38.5%) with a low median compared to other units.

The geochemical data are also depicted as bivariate plots (Fig 18) to allow chemical comparison between the core and peripheral orebodies 1, 2, and 3, and barren samples and, thus, help define metal trends in relation to stratigraphy and orebodies.

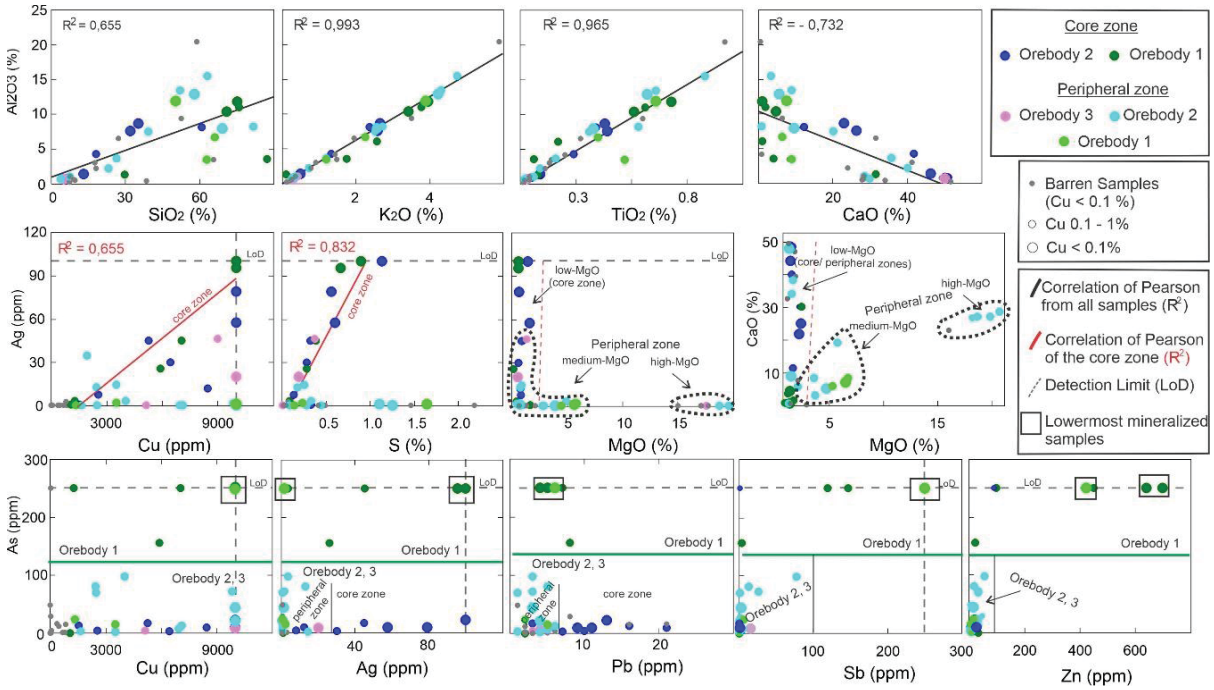

Figure 18 - Bivariate plots showing the geochemical behaviors of the host rocks (CaO, SiO_2, K_2O, Al_2O_3, TiO_2, MgO), main metals and chemical components associated with the mineralization (Cu, Ag, As, Sb, Zn, Pb, S) in different orebodies and barren samples, and core and peripheral zones. The mineralized samples contain > 0.1 % Cu and the barren samples contain < 0.1% Cu.

The correlation of host rock forming elements are depicted in the first line of graphs from Figure 18. Similarly to the box-plots, the bivariate plots show high SiO_2 content in the siliciclastic Transition Series, moderate to high values in the Lower Limestone Shale units and lower contents in the Tullacondra Limestone. High values of Al_2O_3 (0.27-20.4%), K_2O (0.1-5.89%) and TiO_2 (0.01-0.92%) occur in shale-rich units such as the Lower and Upper Shaly Calcarenite and, additionally, show very strong linear correlation with Pearson coefficient > 0.9 and a slightly less linear correlation with SiO_2. The CaO content is higher in the Tullacondra Limestone and uppermost sub-units of the Lower Limestone Shale compared with those from the Lower Limestone Shale, which is also reflected in the negative correlation between CaO and Al_2O_3.

The geochemistry of the core and peripheral zones is illustrated in the second and third lines (Fig. 18). The core zone shows slightly positive correlation of Ag vs Cu (R^2=0.655) and Ag vs S (R^2=0.832). On the other hand, MgO lack correlation with ore-related metals, represented by the plot against Ag. Magnesium oxide shows the lowest concentration (<1%) in the core zone whilst CaO is variable and higher in the orebody 2. The core zone from orebodies 1 and 2 contains variable values of Cu and Ag, whilst other ore-related metals (As, Sb, Zn and Pb), show significant variations

across different orebodies. The orebody 1 is comprised by the highest values of As, Sb, Zn, and low of Pb. Contrarily, the orebody 2 show the lowest values of As, Sb, Zn and the highest of Pb. The orebody 3 from the core zone was not sampled.

The peripheral zone does not show any clear chemical correlation between the ore-related metals as shown by Figure 18. This zone contains medium- (1 to 8%) and high-MgO (17.05 to 19.55%) concentrations. The highest MgO content occurs in calcareous samples from the orebody 2, although medium-MgO is also observed in shaly facies from the orebody 1. The peripheral zone contains variable values of Cu and the lowest concentrations of Ag. Lower values of As, Sb, Zn and Pb are recorded in the zone from both orebodies 1, 2, and 3.

Furthermore, three samples from the same stratigraphic level show similar geochemical behavior. They are from the lowermost mineralized part of the core and peripheral zones (orebody 1) and contain values of Cu, As, and Sb above the detection limit and the highest concentration of Zn.

3.6 DISCUSSION

3.6.1 Host rocks and post-depositional alteration

The mineralogical and geochemical data are consistent with the interpretation that the Tullacondra orebodies are hosted in rocks deposited during a marine transgression (Philcox, 1986; Turner et al., 2019). Host rocks show elevated contents of SiO_2 at the base of the sequence, consistent with siliciclastic-dominant sediments, which decrease up sequence along with an increase in the CaO abundance due to the progressive dominance of limestones and marls (Fig. 17-18). The abundance of calcite is important in the host rocks because ore minerals seem to replace carbonates. They occur predominantly in limestones and marls and subordinately in shales, sandstones and arkoses with carbonate cements replacing the cement or bioclasts (Fig. 15A-C), in agreement with the low Cu content of calcareous-poor rocks of the Old Red Sandstone. Similar replacement of calcareous rock for sulfide is deemed an ore-controlling factor in the Navan deposit, which is hosted in the same time equivalent stratigraphic level as the Tullacondra deposit (Anderson et al., 1998; Peace et al., 2003). Albeit not hosted in the Lower Limestone Shale Formation but in the stratigraphically higher Waulsortian Limestone, the

Lisheen and Silvermines deposits are dominated by sulfide replacement of dolomitized breccias (Hitzman et al., 2002; Lee and Wilkinson, 2002).

Pervasive dolomitization plays important role in controlling the Zn-Pb mineralization in the Lisheen and Silvermines deposits (Hitzman et al., 2002; Lee and Wilkinson, 2002). Medium-grained euhedral replacing the Waulsortian limestone is described as a product of early diagenesis during regional dolomitization (Gregg et al., 2001). In the Irish type deposits, regional dolomitization was an important process because it increased the permeability and porosity of the host rocks consequently allowing for mineralization (Hitzman et al., 2002). At Tullacondra, however, the samples investigated suggest that pervasive dolomitization is limited to pre-mineralization euhedral dolomite within one section of the peripheral zone. In this zone, dolomite is engulfed by a second generation of chalcopyrite (Fig. 16G). Additionally, dolomitized samples contain the lowest Ag concentration, with most of them below the detection limit (< 0.5 ppm). Pervasively dolomitized samples of the Tullacondra deposit also contain authigenic quartz, likely due to overgrowth of very fine-grained quartz matrix during dolomitization, and consistent with the occurrence of euhedral quartz between dolomitized bioclasts. Overgrowths of quartz containing inclusions and evidenced replacing others minerals also occurs in Navan (Anderson et al., 1998; Peace et al., 2003), Silvermines (Reed and Wallace, 2004) and Gortdrum (Steed, 1986) albeit seemly unrelated to the mineralization.

Unlike pervasive dolomitization, dissolution seams containing localized dolomite are important in hosting ore minerals, although most dissolution seams in various parts of the deposit are largely barren. This suggests that the fluid flow process responsible for the genesis of dissolution seams belongs to a pre-ore stage. Moreover, the development of such seams seems not to be tectonic, because these features are mostly parallel to the bedding and not oblique such as tectonic seams. Thus, we interpret that the seams were formed by a pre-ore process related to diagenesis and burial, which caused several features, such as dissolution of calcite along surfaces that were largely bedding parallel, localized dolomitization, enrichment of detrital phyllosilicates and quartz, and development of incipient brecciation.

Incipient into localized breccias (Fig. 14A-C, 15B-D). The breccia textures resemble the breccias in Navan (Peace et al., 2003) and the Black Matrix Breccia in the Waulsortian limestone formed by dissolution processes (Hitzman et al., 2002;

Wilkinson et al., 2011). Brecciation at Tullacondra, however, is more localized and incipient compared to other Irish deposits and, therefore, failed to evolve into fully brecciated zones and thus became unlikely to accumulate important amounts of sulfides.

Another important post-depositional feature of the Tullacondra ores is the concentration of phyllosilicates of inconclusive origin along dissolution seams (Fig. 15D). Our geochemical data suggests that phyllosilicates are controlling the abundance of Al_2O_3 in Tullacondra rocks, although feldspars occur within siliciclastic rocks, and Al_2O_3 contents show a strong positive correlation with both K_2O and TiO_2 (Fig. 18). These significant correlations are also observed in other, barren or mineralized, Irish Lower Carboniferous rocks (Wilkinson et al., 2011; Turner et al., 2019), and suggest that K-Ti-bearing phyllosilicates are common throughout the Irish Midlands and Munster basin.

Whether these phyllosilicates are detrital or authigenic in origin remains a contentious point. A strong argument for their detrital origin may be related to their occurrence as bedding-parallel crystals within barren sandstones and shales of the Old Red Sandstone and Lower Limestone Shale units. The origin of phyllosilicates present within dissolution seams, however, are difficult to interpret as clearly detritic albeit the whole-rock geochemistry throughout dissolution-seams-bearing rocks, shales, and sandstones show similar patterns of positive correlations between Al_2O_3, K_2O and TiO_2 contents. The latter feature suggests that the phyllosilicates, which controls the abundance of these elements, are largely the same type across all lithologies. Therefore, authigenic phyllosilicate is not directly correlated to mineralization but regions with strong mineralization tend to have zones with abundant phyllosilicates as at Tullacondra and at other Irish Midlands deposits.

3.6.2 Ore formation controls

The formation of the orebodies (Fig. 11-12) shows similar structural controls, with NE to EW trending faults also controling Zn-Pb mineralization in the Midlands (e.g., Johnston et al., 1996; Hitzman, 1999; Ashton et al., 2015). In spite of our limited structural assessment of the Tullacondra deposit, geological modelling using drill hole data along with core logging has allowed for evaluation of the spatial correlation between orebodies and the fractured zone of the Tullacondra Fault (Fig.

12). Thus, mineralizing fluids could have percolated through this highly fractured vertical zone and allowed the precipitation of sulfides. In the Irish Orefield, fault damage zones and their increased vertical permeability are interpreted as an important mineralization control that allows vertical and lateral fluid flow (Fossen and Rotevatn, 2016; Walsh et al., 2018). Perhaps, the strain that led to such brittle deformation and the consequent fractured zone is due to the formation of relay ramps (Walsh et al., 2018), as proposed for Lisheen and Silvermines (Torremans et al., 2018; Walsh et al., 2018). It is important to emphasize, nevertheless, that our data show the presence of the Tullacondra Fault but they are insufficient to diagnose association to relay-ramps. The role of the Tullacondra Fault as an important channel for mineralizing fluids is corroborated by the highest concentrations of Cu, Ag, As, Sb and Zn, and predominance of arsenic-bearing sulfides in proximity to the fault, and their decreasing concentrations distal (peripheral zone) from the damage zone. Similar metal distibution is documented elsewhere in the Irish Orefield (Blakeman et al., 2002; Fusciardi et al., 2003; Wilkinson et al., 2005; Torremans et al., 2018)

In addition to these controls, the Lower Limestone Shale shows favorable mineralization conditions, because it offers reducing conditions due to reductant-bearing rocks in contact with underlying Red Beds (oxidized rocks). Furthermore, three samples from the lowermost part of the Transition Series show highest values of Cu, As, Sb and Zn. The lowermost part of the Transition Series is close to the transitional contact with the Old Red Sandstone. This might indicate that a likely redox-boundary were present between these units and can be responsible for the mineralization of elevated concentration of metals in this stratigraphic level.

Moreover, the Transition Series contains the first units bearing important amounts of carbonates that an upward-flowing fluid would meet, thus allowing the dissolution of carbonates and deposition of metals. Progression of upwards flow would allow mineralizing fluids to meet less siliciclastic rocks, which allowed further deposition of base metals in a second, upper, orebody. Thus, sharp contrasts in permeabilities and porosities of host rocks may have acted as a stratigraphic conduit/trap system to focus fluids. This hypothosis is consistent with the high concentration of metals observed within the Lower Limestone Shale. A similar explanation was proposed by Peace et al. (2003) for ores formed at the contact between bioclastic grainstone and dolomitic siltstone in the Navan deposit.

Additionally, secondary porosity associated bedding-parallel dissolution seams likely also played an important role in the formation of Tullacondra stratabound Orebodies.

In addition to the EW trending Tullacondra Fault, rocks of the Tullacondra region are cut by ~NS strike-slip faults in the Variscan Orogeny (Cooper et al., 1986; Wilbur and Carter, 1986). Additionally, several petrographic evidences show posterior deformation, such the occurrence of flatted clasts with slight asymmetric shape in incipient breccias, dissolution cleavage, and undulatory extinction and located new grain boundaries in quartz. Thus, several structures might have been reactivated in the ending of the Variscan Orogen during the thrusting and folding and those deformations were recorded.

3.6.3 Paragenetic sequences and geochemical footprint

The paragenetic sequence discussed below is represented in Figure 19. Pyrite can belong to the first stage of mineralization, as has been suggested for the main generation of pyrite in other Irish deposits (Hitzman et al., 2002; Peace et al., 2003; Reed and Wallace, 2004; Wilkinson et al., 2005; Yesares et al., 2019). On the other hand, it is not possible to determine precisely due to the lack of spatial association with other ore minerals and sulfur isotopic analysis. In other deposits from the Irish Orefield, the earliest pyrite has been described as colloform and is replaced by sphalerite, galena, chalcopyrite, and tennantite (Hitzman et al., 2002). Additionally, the low sulfur isotope ratios for this early pyrite compared to others ore minerals suggest that this generation of iron sulfide formed by bacteriogenic sulfate reduction on the seafloor (Anderson et al., 1998; Wilkinson et al., 2005). Contrarily, trace iron sulfide mineralization may also occur in the main and later ore stages in the Irish Midlands (e.g., Peace et al., 2003; Wilkinson et al., 2005; Yesares et al., 2019).

The textural relationships defined by chalcocite, bornite, and chalcopyrite at Tullacondra indicate that these largely precipitated together in the paragenetic sequence, suggesting that the bulk of Tullacondra ores precipitated within an episodic fluid flow event. Moreover, a close association between these minerals is also observed in the Tynagh and Gortdrum deposits (Boast et al., 1981; Steed, 1986; Duane, 1988). Additionally, these minerals occur predominantly in the shallowest orebodies (2 and 3), whereas they are minor in the deepest orebody 1.

Fine- to medium-grained disseminated and dissolution seam-hosted tennantite, arsenopyrite, and chalcopyrite deposited over copper sulfides suggest that arsenic sulfide and sulfosalts (and a second generation of chalcopyrite), which overprinted previously formed ore minerals, and locally are associated with medium-grained authigenic quartz and chalcedony (Fig. 14C). In contrast to copper sulfides, arsenic minerals are primarily found in the lowermost core zone of the Tullacondra Deposit and decrease upwards. Interestingly, the opposite is observed in the Gortdrum Cu-Ag-Hg deposit, where bornite and chalcocite are predominant in the lowermost parts whilst arsenic minerals are more common is the uppermost units (Steed, 1986).

Therefore, we propose that the main-ore stage comprised the mineralization of different assemblage minerals for the Tullacondra Deposit: (1) Copper sulfide mineralization and (2) tennantite and arsenopyrite sulfide and sulfosalts mineralization. The first mineralization involved the deposition of chalcocite, bornite, and chalcopyrite. The evolution of the mineralizing fluid over time or variations in other ore controls such as chemical, structural or stratigraphic ones allowed the deposition of arsenic minerals in deeper units, and overprinting prior sulfides. In contrast, iron and copper sulfides mineralization took place mainly in shallower stratigraphic units. Chalcopyrite is common in both stages indicating that copper was present in the fluid throughout the mineralization process, but changes in fluid composition/pressure must have occurred in order for the crystallization of other phases of chalcopyrite to take place.

Vein-hosted ores cutting other ore types suggest that they are a late-stage product of remobilization of ore minerals. Additionally, vein-hosted ores consist of the same gangue and ore minerals compared to their host orebody, and the ore minerals in veins are in some cases associated with quartz (Fig. 16G). For example, two types of coarse-grained sparitic veins occur at Tullacondra and their mineral composition is equivalent with the host rock: (1) dolomitic veins are restricted to dolomitized rocks; and (2) calcite veins are hosted within calcareous rocks. The disseminated, parallel or dissolution seams ore minerals are the same both within and surrounding (outside) the veins. Additionally, these veins may also have formed during completely different periods of time (ages) when compared with the timing of ore mineralization, and for this reason isotopic studies are needed to better understand their genesis.

Galena and sphalerite are largely absent at Tullacondra, unlike other base metal deposits in Ireland, where they are the main ore minerals. This might suggest that metallogenic conditions differed from those associated with Navan, Silvermines, and Lisheen. Additionally, lead concentration is highest in the core zone at the top of the Lower Limestone Shale, and throughout the Irish Orefield, lead is elevated in the proximal zones (Fusciardi et al., 2003; Torremans et al., 2018). Thus, although lead content is elevated in proximal zones (core zone), as expected, the absence of notable galena and sphalerite shows that: (1) the fluid lacked the appropriate physicochemical conditions to deposit lead and zinc minerals in the Tullacondra deposit, and/or (2) the fluid that formed the Tullacondra orebodies was extremely poor in Lead and Zinc.

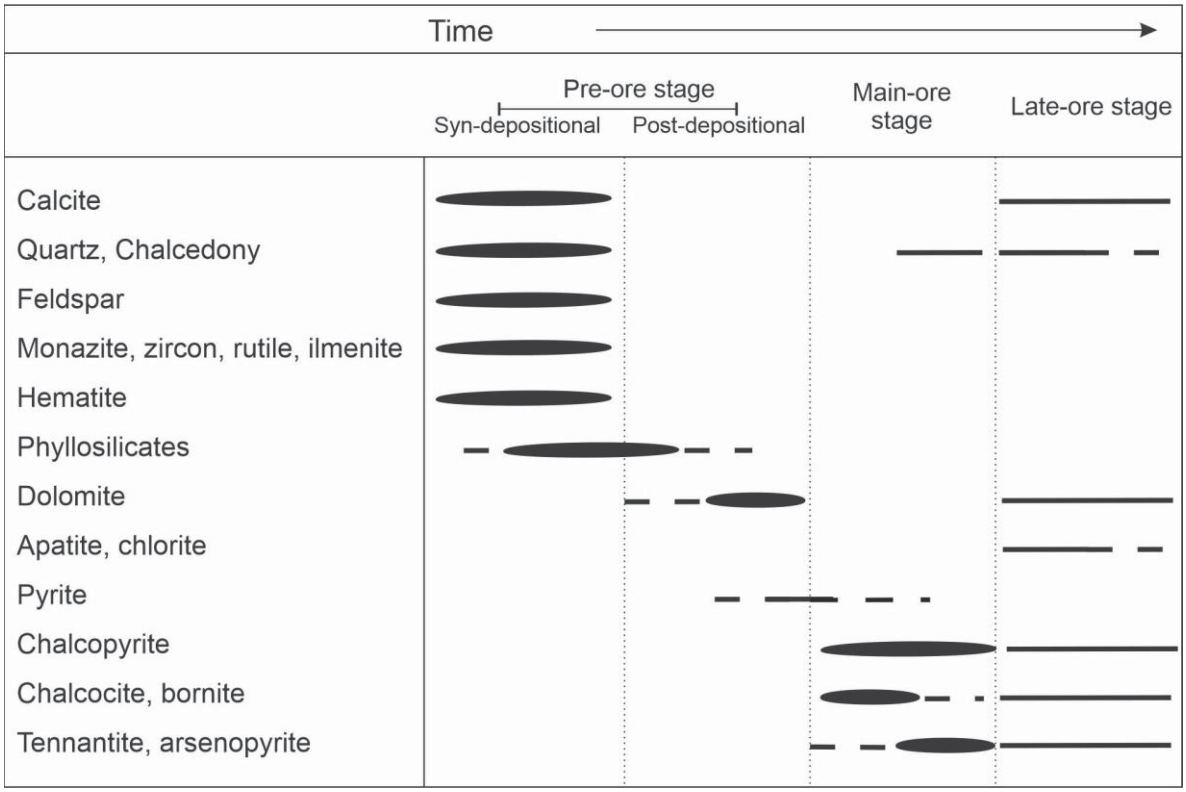

Figure 19 – Proposed paragenetic sequence of the Tullacondra deposit.

In contrast, mineralizing conditions were favorable to the deposition of silver. However, EDS and petrographic analyses carried out on all of the copper and arsenic ore minerals did not identify which mineral phase(s) contains silver. Chemical correlations show that Ag is closely related to sulphur, thus to sulfides and/ or sulfossalts, and slightly related to Cu, whilst a chemical correlation between Ag

and As is not clear. Wilbur and Carter (1986) described the native silver mineralization in the Tullacondra deposit and confirmed that tennantite is not argentiferous. Similarly, at the Gortdrum Cu-Ag-Hg deposit, native silver is associated with Hg or occurs with copper minerals, such as stromeyerite (CuAgS) (Steed, 1986). In contrast, silver in other Irish Zn-Pb deposits is primarily hosted in As and Sb sulfosalts and galena (Derry et al., 1965; Hitzman et al., 2002; Pracht and Sleeman, 2002; Wilkinson et al., 2005; Wilkinson et al., 2011).

3.6.4 Comparison with other Irish Midlands deposits

Based on structural and stratigraphic similarities, we propose that the Tullacondra deposit formed in the same metallogenetic context as that giving rise to other Irish Zn-Pb deposits (e. g. Wilbur and Carter, 1986; Hitzman, 1999; Hitzman et al., 2002; Lee and Wilkinson, 2002).

In summary, the formation of the Irish Zn-Pb deposits took place in a period of extension within the Irish platform during the Lower Carboniferous. The sulfides mineralized during the diageneses of the Carboniferous host rocks, and metal-bearing hydrothermal fluids flowed from Paleozoic basement through normal faults mixed with shallow marine bacteriogenic brines enriched in H_2S (Anderson et al., 1998; Boast et al., 1981; Fusciardi et al., 2003; Wilkinson et al., 2005; Ashton et al., 2015; Walsh et al., 2018; Wilkinson and Hitzman, 2015). Both fluids have been considered sources for sulfur, although the bacteriogenic brines are regarded as the primary source, and their origin determined by sulfur isotopic analyses. The hydrothermal fluid is characterized by heavier S isotope signatures ($\delta^{34}S>0‰$) (Anderson et al., 1998; Ashton et al., 2015; Boast et al., 1981; Wilkinson et al., 2005; Wilkinson, 2013), whilst the bacteriogenic brines contain negative values (-26 to -4‰ in Navan for example, Ashton et al., 2015). Given that the Tullacondra deposit is part of the Irish Orefield metallogenetic region, we postulate that this model also corroborates our observations/results reported here for the Tullacondra deposit. Specifically, this involves a Cu- and Ag-bearing hydrothermal fluid that percolated through the Tullacondra Fault and subsequently mixed with a bacteriogenic brine originating from the limestones of the Lower Limestone Shale. However, further isotopic studies are required to corroborate this interpretation, and to determine which fluid was predominant in the formation of each ore mineral phase present at

Tullacondra. For example, Yesares et al. (2019) determined distinct sulfur isotopic compositions for various sulfide phases in the Tara Deep, at Navan.

Possible metal sources for the Tullacondra deposit are either (1) The Old Red Sandstone or (2) The Lower Paleozoic basement. According to Kinnaird et al. (2002) and Wilkinson et al. (2005), the main source of Cu is most likely the Old Red Sandstone, which is thicker in southern Ireland than elsewhere. Bleaching of the Old Red Sandstone close to mineralized areas indicates stripping of Cu, As, Ni, and Co from this unit by fluid flow(Everett et al., 2003; Wilkinson et al., 2005). Alternatively, Kinnaird et al., (2002) proposed that the Lower Paleozoic basement might be more Cu-rich in southern Ireland, and therefore the source for Cu. This interpretation is consistent with isotopic data demonstrating that Zn and Pb in Navan and Lisheen deposits are leached from the underlying Lower Paleozoic metasedimentary basement (e.g., Ashton et al., 2015; Yesares et al., 2019).

Another possible influence on Tullacondra's mineralization is the magmatic activity recorded in the Limerick basin, northwest of the studied area (Steed, 1986; Mccusker and Reed, 2013; Wilkinson and Hitzman, 2015; Elliott et al., 2019). Sub-volcanic rocks at Tullacondra are represented by at least two dikes with associated breccias cutting through mineralized limestones. Thin-bedded pyroclastic rocks are hosted in the upper part of the Waulsortian Limestone termed as Sulbuter volcanic, and likely represent a younger magmatic event (Wilbur and Carter, 1986). Elliott et al. (2019) observed that the Zn-Pb mineralization is the highest grade proximal to the igneous bodies in the Limerick basin, and is characterized by more positive S isotope values compared to those from the Navan and Lisheen deposits. Hence, this feature suggests that the volcanic rocks acted as pathway and sulfur source for the mineralizing fluids. The observation that magmatic activity during the Lower Carboniferous was stronger in southern Ireland let Wilkinson and Hitzman (2015) to suggest that circulation of metal-rich fluids was driven by heat transfer.

Additionally, Irish Type deposits have been considered to share more similarities with SEDEX deposits than with MVT, and further studies could indicate if the Tullacondra deposit also shows such similarities. Just like the SEDEX deposits, the Irish Type deposits are formed in intracratonic environment, with syn-sedimentary faults acting as conducts, similar metal and mineral zonations, thermohaline convections, and spatial and temporal association with magmatic activities (Wilkinson, 2013). The primary contrasts between these models (i.e,

SEDEX) and the Irish Type deposits are the fact Irish Type deposits experienced mineralization in a shallow marine environment, whilst SEDEX deposits are typically formed in deeper marine setting. In addition, bacteriogenic sulfate reduction (BSR) is a predominant process in the Irish deposits, whereas thermochemical sulfate reduction (TSR) is prevalent in SEDEX deposits. This contrast in sulfate reduction process is evidenced by predominantly negative sulfur isotope signatures for the Irish deposits, and mainly positive sulfur isotope signatures for SEDEX deposits (Wilkinson, 2013). Thus, further isotopic studies of the ore mineralization will better constrain the origin of the Tullacondra deposit.

3.6.5 Genetic model

We propose that the genesis of the Tullacondra deposit can be divided into pre-ore, main-ore and late-ore stages (Figure 20) based on the interpretation of our data in comparison with previous models of mineralization in the Irish ore fields (Wilkinson et al., 2005).

3.6.5.1 Pre-ore stage

This stage is characterized by the onset of EW-trending normal faulting (Tullacondra Fault) contemporaneous with the deposition of the Irish Midlands Basin and with other syn-sedimentary normal faults related to the extensional tectonic controlling Zn-Pb deposition within the Irish Midlands (Andrew 1986; Steed, 1986; Hitzman et al., 2002; Ashton et al., 2015). The formation of the Tullacondra Fault likely resulted in subsidiary faults and the associated damage zone, which later would serve as conduits for mineralizing fluids. This stage is also marked by incipient dolomitization of the Upper Shaly Calcarenite and Oolitc Calcarenite, uppermost sub-units of the Lower Limestone Shale, in the peripheral zone of the Tullacondra area. Additionally, textural features of Tullacondra dolomite such as copper sulfides engulfing dolomite and dissolution seams occurring in non-mineralized rocks indicate that most dissolution and dolomitization took place prior to the main mineralization stage. The dissolution seams were likely formed due the percolation of acidic fluids that increased the permeability of the host rock. These features are similar to pre-ore early diagenetic dolomitization recorded in the Waulsortian Limestone in Lisheen and

Silvermines (Fig. 20A) (Gregg et al., 2001; Hitzman et al., 2002; Lee and Wilkinson, 2002).

3.6.5.2 The Main-ore stage

This stage is characterized by the evolution of normal faulting and development of the damage zone, which allowed enhanced vertical permeability and the consequent flow of mineralizing fluids. Stratigraphic contacts marked by permeability contrast were also important by focussing horizontal fluid flow and the precipitation of stratabound lenses (Fig. 20B). This stage includes sulfide deposition by mixing of metal-bearing fluids ascending through the damage zone before meeting a reductant, such as a reduced sulfur brine. These metal-bearing hydrothermal fluids were in equilibrium with the carbonate-poor oxidant ORS but started precipitating limited amounts of copper-sulfides at the most basal reduced carbonate-bearing unit Transition Series of the Irish Midlands Basin. From then on, the fluid flowed laterally and upwards precipitating various orebodies along stratigraphic boundaries with strong permeability contrasts such as the shaly and sandy Transition Series, the calcarenite interbedded with shale and the silicious base with the other calcareous parts of the Tullacondra Limestone. Vertical and horizontal fluid flow additionally generated the metal zonation observed in Tullacondra with chalcocite, bornite and chalcopyrite deposited all throughout Tullacondra orebodies and were overprinted by tennantite, arsenopyrite and another generation of chalcopyrite also associated with chalcedony. A horizontal zonation is also recorded with higher concentration of metals in the core zone, considered therefore the proximal zone, and the decline of metals and arsenic minerals in the peripheral zone (distal) (Fig. 20C).

3.6.5.3 The Late-ore stage

This stage is marked by remobilization of ore minerals in sparitic calcite and dolomite veins, which, locally, also contain apatite, chlorite and quartz. This remobilization took place either in extensional stages or during the inversion of the basin in the late Variscan (Fig. 20D). The N-S trending faults, which offset

Tullacondra orebodies and limit its extension along E-W might be related with this stage.

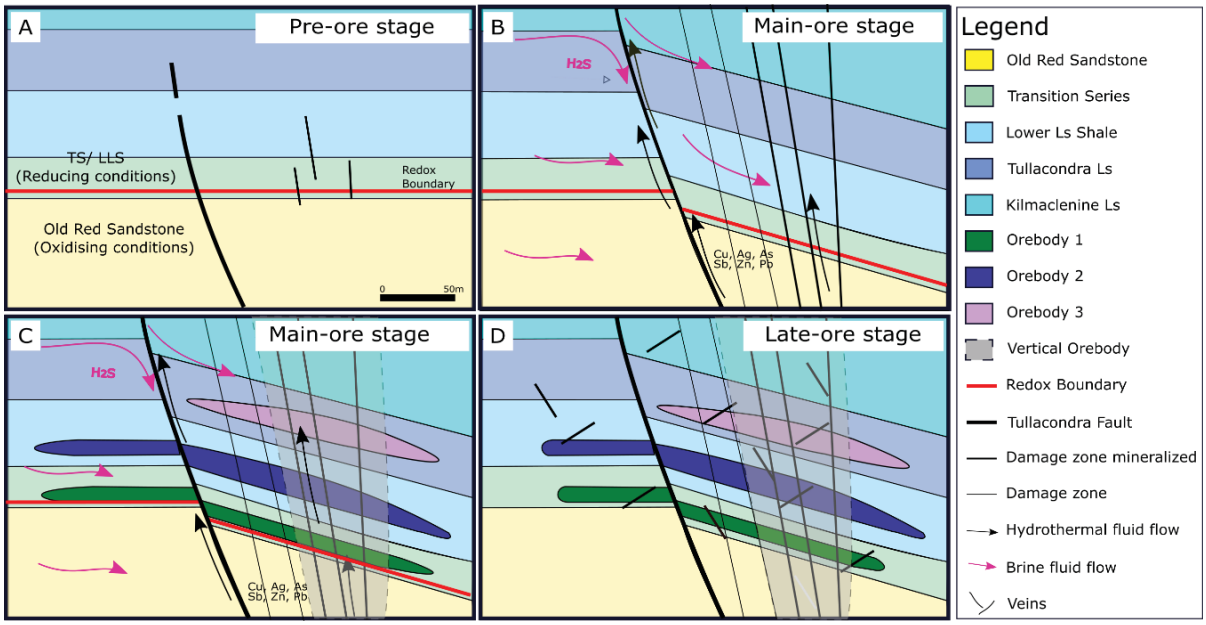

Figure 20 – Sketch showing the model of mineralization proposed by authors. Similarities between the Tullacondra Cu-Ag with other Zn-Pb deposits suggest that the mineralization of these deposits involved the same fluids, contrasting by involved metals. This model was based on Wilkinson et al. (2005) and on our interpretation discussed above. (A) Pre-ore stage and beginning of the faulting and formation of the damage zone. (B) Main-ore stage and evolution of the faulting and increase of the damage zone. Note the two fluids associated to the mineralization as proposed by Wilkinson et al. (2005): 1. Bacterogenic marine brine carrying H_2S and 2. Metal-bearing hydrothermal fluid carrying Cu, Ag, As, Sb, Zn and Pb. The dolomitization and dissolution seams took place in this stage (C) Main-ore stages: mixture of the fluids and mineralization of the three orebodies. (D) Late-ore stage: remobilization of the ore minerals in veins.

3.7 CONCLUSION

Based on drill hole descriptions, geochemistry and petrographic studies, SEM-EDS analyses and micro-XRF imaging, we conclude that the genesis of the Tullacondra Cu-Ag deposit can be attributed to very similar controls to those proposed for formation of Irish Midlands Zn-Pb deposits, in spite of the differences in metal abundances. Moreover, both the Irish Zn-Pb deposits and the Tullacondra Cu-Ag deposit formed during percolation of metal-bearing fluids through a normal fault (Tullacondra Fault) and its associated damage zone. We suggest, based on prior studies of the Irish Midlands, that the mixing of this upwards-flowing metal-bearing fluid with a horizontally-flowing sulfur-bearing brine induced the deposition of three stratabound lenses deposited orebodies preferentially along the redox boundary and zones of permeability contrast. Ore deposition along the damage zone added a

secondary vertical component to the ore geometry. Moreover, dissolution seams seem to have an important mineralization control acting as pathway to the mineralizing fluid. The main mineralization is characterized by deposition of (1) early chalcocite, bornite and chalcopyrite; and (2) later deposition of arsenopyrite and tennantite and a second generation of chalcopyrite associated with chalcedony and medium-grained quartz took place in orebodies proximal to the Tullacondra Fault (core zone). The post-main ore stage is characterized by remobilization of metals and depositions within carbonate veins.

Dissolution seams have an important role in hosting mineralization and allowing the deposition of disseminated sulfides in the Tullacondra deposit. However, unlike Lisheen and Silvermines where a progression from dissolution seams leads towards breccias, brecciation within host rocks of the Tullacondra Deposit was limited, perhaps also limiting the concentration of important amounts of sulfides.

The present study shows that Cu-Ag deposits can occur genetically associated with major Irish Zn-Pb deposits and enrichment of As, Sb, Zn and Pb can be an indicator of Cu and Ag mineralization. Moreover, the presence of dolomitized rocks and dissolution features close to the contact between the ORS and LLS and to an E-W trending fault is also a good indicator that mineralizing fluids were focused in this location. This association can help exploration efforts into targeting for copper and realizing the full potential of the Irish Orefield.

4 CONSIDERAÇÕES FINAIS

Esse trabalho ajudou a redefinir a geologia do depósito de Cu-Ag de Tullacondra, somente detalhada por Wilbur e Carter (1986), mostrando que este se encaixa no mesmo contexto metalogenético que importantes depósitos de Zn-Pb *Irish-type*. Assim como os depósitos de Zn-Pb de Navan, Lisheen e Silvermines, Tullacondra é definido por corpos de minério *stratabounds* controlados por falhas de direção EW e por uma zona de dano associado a *relay ramps.* Tullacondra mostra também nítidas zonações química e petrográfica observadas em outros locais da Irlanda e associadas a brechas de dissolução.

Esses mesmos padrões observados em Tullacondra devem se repetir em outras ocorrências de Cu-Ag hospedados na *Irish Midlands,* tais como Gortdrum, Aherlow e Ballyvergin. Isso indica que a mineralização de cobre fez parte de um

contexto metalogenético maior que também formou os grandes depósitos de Zn-Pb. Assim, ocorrências de Zn-Pb que se assemelham ao *Irish-type,* podem conter cobre associado.

Portanto, assim como para Zn e Pb, as ocorrências de Cu no sul da Irlanda devem-se provavelmente a mistura de dois fluidos: (1) salmouras bacteriogênicas marinhas contendo H_2S e (2) hidrotermais carregando metals de Cu, Ag, As, Sb, Zn, Pb entre outros, do embasamento. Esses fluidos percolaram falhas normais e zonas de danos, e a mineralização se deu durante a diagênese das rochas hospedeiras. A interpretação sobre a origem dos fluidos é provisória e deve ser constatada ou não por futuros trabalhos.

4.1 RECOMENDAÇÕES E TRABALHOS FUTUROS

Apesar de definirmos uma relação genética próxima entre os depósitos de Zn-Pb e Cu *Irish-type,* a fonte e evolução dos fluidos mineralizantes do cobre precisam ser melhor estudadas. Com esse intuito, pretendemos, em parceria com o iCrag (Irish Centre for Research in Applied Geosciences), realizar análises isotópicas de enxofre para verificar a principal origem do enxofre e dos fluidos mineralizantes. Para isso, amostras representativas das diferentes assembléias de minerais de minério foram selecionadas pela autora da tese e enviadas para o iCrag na Irlanda. Na Irlanda, isótopos de enxofre dos diferentes sulfetos e sulfosais serão analisados. Além disso, análises isotópicas de carbono, oxigênio e samário/neodímio já foram realizadas na Universidade de Notre Dame nos Estados Unidos. Essas analises representam os diferentes tipos de carbonatos (calcita sedimentar, dolomita hidrotermal e calcita e dolomita de veios), e foram escolhidos dos diferentes corpos de minéios. Esses dados permitirão entender melhor a natureza dos fluidos mineralizadores e de que forma eles perturbaram as assinaturas diagenéticas dos carbonatos plataformais onde esses sulfetos estão hospedados.

Os dados isotópicos mencionados acima são dos depósitos de Tullacondra e de Gortdrum. Destes dados, pretende-se submeter mais dois artigos de minha coautoria e de autoria do professor orientador. O segundo artigo deve-se referir a metalogênese do depósito de Gortdrum, semelhante ao que foi feito para Tullacondra no presente trabalho. Os dados geoquímicos e de microfluorescencia

de raios-X também foram realizados em amostras de Gortdrum. Com esses dados e da petrografia, o segundo artigo será elaborado. O terceiro artigo deve unir todos os dados isotópicos de ambos depósitos e determinar melhor as origens dos fluidos e do enxofre. Dada a maior participação de intrusões como provável caminho para os fluidos do depósito de Gortdrum (Steed 1986), os próximos artigos trarão respostas mais eficazes também sobre a influência magmática.

Além disso, futuros trabalhos devem definir melhor a idade dos veios e a participação magmática do depósito de Tullacondra. A presença de micas autigenicas associadas ou não com a mineralização também é uma questão a ser levantada.

REFERÊNCIAS

ANDERSON, I. K.; ASHTON, J. H.; BOYCE, A. J.; FALLICK, A. E.; RUSSELL, M. J. Ore Depositional Processes in the Navan Zn-Pb Deposit, Ireland. **Economic Geology**, v. 93, p. 535–563, 1998.

ANDREW, C. J. The geological setting and style of mineralization at Ballyvergin, County Clare. In: J. F. Andrew, C. J., Crowe. R.W.A., Pennell., W.M. Pyne. (Org.); **Geology and genesis of mineral deposits in Ireland**. p.475–480, 1986a. Dublin: Irish Association for Economic Geology.

ANDREW, C.J. The tectono-stratigraphic controls to mineralization in the Silvermines area, County Tipperary, Ireland In: J. F. Andrew, C. J., Crowe. R.W.A., Pennell., W.M. Pyne. (Org.); **Geology and genesis of mineral deposits in Ireland**. p.475–480, 1986b. Dublin: Irish Association for Economic Geology.

ASHTON, J. H.; BLAKEMAN, R. J.; GERAGHTY, J. F.; et al. The Giant Navan Carbonate-Hosted Zn-Pb Deposit – A review. In: S. M. Archibald; S. J. Piercey (Orgs.); **Current perspectives on zinc deposits**. p.85–122, 2015. Dublin: Irish Association for Economic Geology.

BLAKEMAN, R. J.; ASHTON, J. H.; BOYCE, A. J.; FALLICK, A. E.; RUSSELL, M. J. Timing of interplay between hydrothermal and surface fluids in the Navan Zn + Pb orebody, Ireland: Evidence from metal distribution trends, mineral textures, and δ 34S analyses. **Economic Geology**, v. 97, n. 1, p. 73–91, 2002.

BOAST, A. M.; COLEMAN, M. L.; HALLS, C. Textural and stable isotopic evidence for the genesis of the Tynagh base metal deposit, Ireland. **Economic Geology**, v. 76, n. 1, p. 27–55, 1981.

CAINE, J. S.; EVANS, J. P.; FORSTER, C. B. Fault zone architecture and permeability structure. **Geology**, v. 24, n. 11, p. 1025–1028, 1996.

CHILDS, C.; MANZOCCHI, T.; WALSH, J. J.; et al. A geometric model of fault zone and fault rock thickness variations. **Journal of Structural Geology**, v. 31, n. 2, p. 117–127, 2009.

ÇIMEN, O.; KUEBLER, C.; SIMONETTI, S. S.; et al. Combined boron, radiogenic (Nd, Pb, Sr), stable (C, O) isotopic and geochemical investigations of carbonatites from the Blue River Region, British Columbia (Canada): Implications for mantle sources and recycling of crustal carbon. **Chemical Geology**, v. 529, p. 1–18, 2019. Elsevier 6al Society Special Publication.

KIM, Y. S.; PEACOCK, D. C. P.; SANDERSON, D. J. Fault damage zones. **Journal of Structural Geology**, v. 26, p. 503–517, 2004.

KINNAIRD, J. A.; IXER, R. A.; BARREIRO, B.; NEX, P. A. M. Contrasting sources for lead in Cu-polymetallic and Zn-Pb mineralisation in Ireland: constraints from lead isotopes. **Mineralium Deposita**, v. 37, p. 495–511, 2002.

KYNE, R.; TORREMANS, K.; GÜVEN, J.; DOYLE, R.; WALSH, J. 3-D modeling of the Lisheen and Silvermines deposits, County Tipperary, Ireland: insights into structural controls on the formation of Irish Zn-Pb deposits. **Economic Geology**, v. 114, p. 93–116, 2019.

LANG, J.; MEERE, P. A.; UNITT, R. P.; et al. The vein hosted copper deposits of the Allihies Mining area, Southwest Ireland - A new structural and chronological evaluation. **Journal of the Geological Society**, 2020.

LEE, M. J.; WILKINSON, J. J. Cementation, hydrothermal alteration, and Zn-Pb mineralization of carbonate breccias in the Irish Midlands: textural evidence from the cooleen zone, near Silvermines, county Tipperary. **Economic Geology**, v. 97, n. 1, p. 653–662, 2002. Disponível em: <https://pubs.geoscienceworld.org/segweb/economicgeology/article-pdf/97/3/653/3497542/653.pdf>. .

LEES, A.; MILLER, J. Facies variation in Waulsortian buildups, Part 2; Mid-Dinantian buildups from Europe and North America. **Geological Journal**, v. 20, p. 159–180, 1985.

MATTE, P. The Variscan collage and orogeny (480–290 Ma) and the tectonic definition of the Armorica microplate: a review. **Terra Nova**, v. 13, p. 122–128, 2001. Disponível em: <http://onlinelibrary.wiley.com/doi/10.1046/j.1365-3121.2001.00327.x/full%5Cnpapers2://publication/uuid/85445613-EAD8-49D7-AE4E-704E3D282C36>. .

MCCUSKER, J.; REED, C. The role of intrusions in the formation of Irish-type mineralisation. **Mineralium Deposita**, v. 48, p. 687–695, 2013.

MONTEIRO, L. V. S.; BETTENCOURT, J. S.; JULIANI, C.; OLIVEIRA, T. F. Geology, petrography, and mineral chemistry of the Vazante non-sulfide and Ambrósia and Fagundes sulfide-rich carbonate-hosted Zn–(Pb) deposits, Minas Gerais, Brazil. **Ore Geology Reviews**, v. 28, p. 201–234, 2006.

PEACE, W. M.; WALLACE, M. W.; HOLDSTOCK, M. P.; ASHTON, J. H. Ore textures within the U lens of the Navan Zn-Pb deposit , Ireland. **Mineralium Deposita**, v. 38, p. 568–584, 2003.

PHILCOX, M. E. Lower Carboniferous lithostratigraphy of the Midlands: Dublin, Irish Association for Economic Geology, 89 p. 1984.

PHILLIPS, W. E. A.; SEVASTOPULO, G. D. The stratigraphic and structural setting of Irish mineral deposits. In: C. J. Andrew; R. W. A. Crowe; S. Finlay; W. M. Pennel; J. . Pyne (Orgs.); **Geology and genesis of mineral deposits in Ireland**. p.1–30, 1986. Dublin: Irish Association for Economic Geology.

PRACHT, M.; SLEEMAN, A. G. **Geology of West Cork**. 2002.

REED, C. P.; WALLACE, M. W. Zn-Pb mineralisation in the Silvermines district ,

Ireland : a product of burial diagenesis. **Mineralium Deposita**, v. 39, p. 87–102, 2004.

REILLY, T. A. A review of vein mineralization in SW County Cork, Ireland. In: J. F. Andrew, C. J., Crowe. R.W.A., Pennell., W.M. Pyne. (Org.); **Geology and genesis of mineral deposits in Ireland**. p.475–480, 1986. Dublin: Irish Association for Economic Geology.

SHEARLEY, E.; REDMON, P.; KING, M.; GOODMAN, R. Geological controls on mineralization and dolomitization of the Lisheen Zn-Pb-Ag deposit, Co. Tipperary, Ireland. **Geological Society, London, Special Publications**, v. 107, p. 23–33, 1996.

SINGER, D. A. World class base and precious metal deposits - a quantitative analysis. **Economic Geology**, v. 90, p. 88–104, 1995. Disponível em: <https://pubs.geoscienceworld.org/segweb/economicgeology/article-pdf/90/1/88/3492138/88.pdf>. .

SOMERVILLE, I. D.; JONES, G. L. I. The Courceyan stratigraphy of the Pallaskenry Borehole, County Limerick, Ireland. **Geological Journal**, v. 20, n. 4, p. 377–400, 1985.

SOMERVILLE, I. D.; STROGEN, P.; JONES, G. L. Biostratigraphy of Dinantian limestones and associated volcanic rocks in the Limerick Syncline, Ireland. **Geological Journal**, v. 27, n. 3, p. 201–220, 1992.

SOPER, N. J. Timing and geometry of collision, terrane accretion and sinistral strike-slip events in the British Caledonides. In: A. L. Harris; D. J. Fettes (Orgs.); **The Caledonian - Appalachian Orogen**. v. 38, p.481–492, 1988. Geological Society Special Publication.

STEED, G. M. The geology and genesis of the Gortdrum Cu-Ag-Hg orebody. In: C. J. Andrew; R. W. A. Crowe; S. Finlay; W. M. Pennel; J. F. Pyne (Orgs.); **Geology and genesis of mineral deposits in Ireland**. p.481–499, 1986. Dublin: Irish Association for Economic Geology.

STROGEN, P.; JONES, G. L.; SOMERVILLE, I. Stratigraphy and sedimentology of lower carboniferous (Dinantian) boreholes from West Co. Meath, Ireland. **Geological Journal**, v. 25, p. 103–137, 1990.

STROGEN, P.; SOMERVILLE, I. The stratigraphy of the Upper Palaeozoic rocks of the Lyons Hill area, county Kildare. **Irish Association for Economic Geology**, v. 6, n. 2, p. 155–173, 1984.

TORREMANS, K.; KYNE, R.; DOYLE, R.; GÜVEN, J. F.; WALSH, J. J. Controls on metal distributions at the Lisheen and Silvermines deposits: Insights into fluid flow pathways in Irish-Type Zn-Pb deposits. **Economic Geology**, v. 113, n. 7, p. 1455–1477, 2018.

TURNER, O.; HOLLIS, S.; GÜVEN, J.; MCCLENAGHAN, S. Establishing a

geochemical baseline for the Lower Carboniferous stratigraphy of the Rathdowney Trend , Irish Zn-Pb orefield. **Journal of Geochemical Exploration**, v. 196, p. 259–269, 2019. Elsevier. Disponível em: <https://doi.org/10.1016/j.gexplo.2018.11.003>. .

WALSH, J. J.; TORREMANS, K.; GÜVEN, J.; et al. Fault-Controlled Fluid Flow Within Extensional Basins and Its Implications for Sedimentary Rock-Hosted Mineral Deposits. **Society of Economic Geologists Special Publications**, v. 21, p. 237–269, 2018.

WHITNEY, D. L.; EVANS, B. W. Abbreviations for names of rock-forming minerals. **American Mineralogist**, v. 95, n. 1, p. 185–187, 2010.

Wilbur D. G., Royall J. J. Discovery of the Mallow copper-silver deposit, County Cork, Ireland. In: Jones M. J. (ed) *Prospecting in areas of glaciated terrain*. Edinburgo. Inst Mining Metall. London 60-70. 1975.

WILBUR, D. G.; CARTER, J. S. Cu -Ag mineralization at Tullacondra , Mallow , Co . Cork . In: C. J. Andrew; R. W. A. Crowe; S. Finlay; W. M. Pennel; J. F. Pyne (Orgs.); **Geology and genesis of mineral deposits in Ireland**. p.501–507, 1986. Irish Association for Economic Geology.

WILKINSON, J. J. Sediment-Hosted Zinc-Lead Mineralization: Processes and Perspectives: Processes and Perspectives. **Treatise on Geochemistry: Second Edition**. 2º ed, v. 13, p.219–249, 2013. Elsevier Ltd. Disponível em: <http://dx.doi.org/10.1016/B978-0-08-095975-7.01109-8>. .

WILKINSON, J. J.; CROWTHER, H. L.; COLES, B. J. Chemical mass transfer during hydrothermal alteration of carbonates: Controls of seafloor subsidence, sedimentation and Zn-Pb mineralization in the Irish Carboniferous. **Chemical Geology**, v. 289, n. 1–2, p. 55–75, 2011. Elsevier B.V. Disponível em: <http://dx.doi.org/10.1016/j.chemgeo.2011.07.008>. .

WILKINSON, J. J.; EYRE, S. L.; BOYCE, A. J. Ore-forming processes in Irish-Type Carbonate-hosted Zn-Pb deposits : Evidence from mineralogy , chemistry , and isotopic composition of sulfides at the Lisheen mine. **Economic Geology**, v. 100, p. 63–86, 2005.

WILKINSON, J. J.; HITZMAN, M. W. The Irish Zn-Pb Orefield: The View from 2014. **Irish Association for Economic Geology**, , n. September 2010, p. 59–72, 2015.

YESARES, L.; DRUMMOND, D. A.; HOLLIS, S. P.; et al. Coupling mineralogy, textures, stable and radiogenic isotopes in identifying ore-forming processes in Irish-Type Carbonate-hosted Zn–Pb deposits. **Minerals**, v. 9, n. 6, p. 335, 2019. Disponível em: <https://www.mdpi.com/2075-163X/9/6/335>. .

Anexo I - Tabela de dados geoquímicos realizados na ALS Global usados para a discussão da geoquímica (Fig.17 e 18)

SAMPLE	SiO2	Al2O3	Fe2O3	CaO	MgO	Na2O	K2O	Cr2O3	TiO2	MnO	P2O5	SrO	BaO	LOI	Total	C	S
DESCRIPTION	%	%	%	%	%	%	%	%	%	%	%	%	%	%	%	%	%
M73-3-027	7.29	1.1	0.94	28.3	17.55	0.07	0.41	<0.01	0.05	0.14	0.03	<0.01	0.01	43	98.89	11.5	<0.01
M73-3-039	5	0.76	0.77	50.1	0.57	0.05	0.28	<0.01	0.03	0.09	0.04	0.04	0.02	40.5	98.25	11.6	0.19
M73-3-069	7.21	0.27	0.32	51.6	0.48	0.05	0.12	<0.01	0.01	0.06	0.03	0.03	0.01	40.6	100.79	11.2	0.03
M73-3-094	38.5	0.5	0.43	34.1	0.38	0.04	0.19	<0.01	0.02	0.12	0.08	0.04	0.15	26.5	101.05	7.44	0.07
M73-3-119	61.1	15.1	2.27	6.13	1.33	0.1	4.91	0.01	0.78	0.02	0.15	0.02	0.14	7.75	99.81	1.37	0.37
M73-3-132	23	2.28	1.02	40	0.88	0.05	0.71	<0.01	0.09	0.13	0.04	0.06	0.02	31.4	99.68	8.53	0.25
M73-3-143	69.1	8.01	2.31	9.59	0.72	0.04	2.56	0.01	0.33	0.04	0.03	0.01	0.03	8.49	101.27	2.25	1.1
M73-3-154	26.4	3.67	1.21	35.7	0.75	0.06	1.19	<0.01	0.16	0.15	0.1	0.05	0.02	29.1	98.56	7.7	0.17
M73-3-162	39.2	7.56	2.02	20.1	4.9	0.03	2.51	0.01	0.31	0.09	0.2	0.01	0.04	21.6	98.58	5.91	0.33
M73-3-196	7.38	1.06	2.07	28.4	18.7	0.02	0.35	<0.01	0.06	0.2	0.05	<0.01	<0.01	40.6	98.89	10.6	0.44
M73-3-203	3.83	0.71	1.47	29.9	19.55	0.02	0.25	<0.01	0.02	0.16	0.03	<0.01	<0.01	43.9	99.84	11.5	0.08
M73-3-218	7.42	1.08	1.55	28.3	17.7	0.06	0.35	<0.01	0.04	0.22	0.06	<0.01	<0.01	42	98.78	10.9	0.03
M73-3-233	63	15.5	2.51	3.32	2.89	0.14	4.74	0.01	0.83	0.04	0.12	<0.01	0.06	7.96	101.12	1.59	0.28
M73-3-241	8.94	0.63	1.4	28.2	17.05	0.07	0.24	<0.01	0.04	0.18	0.05	<0.01	<0.01	41.5	98.3	10.9	0.02
M73-3-254	58.8	20.4	4.26	0.39	2.14	0.19	5.89	0.02	0.92	0.02	0.07	<0.01	0.08	6.66	99.84	0.65	0.41
M73-3-283	9.58	0.54	1.11	27.8	17.1	0.09	0.23	<0.01	0.02	0.12	0.04	<0.01	<0.01	41.4	98.03	11.3	0.14
M73-3-293	18	2.25	1.12	24	15	0.08	0.77	<0.01	0.11	0.14	0.15	<0.01	0.01	36.6	98.23	9.72	0.04
M73-3-318	52.1	13.45	3.37	8.85	2.79	0.05	4.3	0.01	0.61	0.06	0.1	<0.01	0.05	11.3	97.04	2.85	0.73
M73-3-328	57.7	12.9	3.31	5.46	3.89	0.07	4.22	0.01	0.57	0.06	0.09	<0.01	0.05	9.43	97.76	2.64	1.25
M73-3-347	81.8	8.26	1.78	0.79	0.51	0.01	2.71	0.01	0.53	0.01	0.05	<0.01	0.02	2.93	99.41	0.36	1.1
M73-3-364	62.9	3.5	0.95	8.91	5.88	0.01	1.19	0.01	0.47	0.09	0.05	<0.01	0.01	14.3	98.27	4.01	0.23
M73-3-374	66	6.76	1.16	6.39	4.47	0.02	2.25	0.01	0.35	0.04	0.04	<0.01	0.02	11.2	98.71	2.52	0.14
M73-3-393	50.2	11.9	3.23	7.5	5.61	0.05	3.89	0.01	0.61	0.06	0.05	<0.01	0.03	12.7	95.84	3.47	1.64
M73-3-412	90.5	4.24	0.62	0.82	0.66	0.02	1.42	<0.01	0.2	0.01	0.03	<0.01	0.01	2.04	100.57	0.38	0.01
M73-11-290	27.2	6.58	2.35	31.5	1.43	0.21	1.95	0.01	0.27	0.06	0.22	0.05	0.05	26.1	97.98	7.33	0.49
M73-11-296	60.9	8.17	1.28	12.15	0.9	0.5	2.37	0.01	0.34	0.04	0.04	0.03	0.04	11.75	98.52	3.13	0.32
M73-11-312	35.1	8.67	2.43	22.9	1.43	0.22	2.64	0.01	0.38	0.09	0.11	0.04	0.05	18.95	93.02	5.61	1.13
M73-11-319	5.79	0.89	1.12	51	0.65	0.05	0.28	<0.01	0.05	0.11	0.04	0.06	0.02	37.6	97.66	11.3	0.33
M73-11-336	17.45	3.07	1.59	41.2	1.1	0.07	0.91	<0.01	0.13	0.13	0.14	0.05	0.03	33	98.87	9.4	0.09
M73-11-347	7.59	0.97	1	50.2	0.61	0.01	0.33	<0.01	0.05	0.12	0.08	0.04	0.02	38.9	99.92	10.9	0.28
M73-11-359	5.27	0.8	1.12	50.7	0.82	0.01	0.29	<0.01	0.03	0.17	0.05	0.05	0.01	40	99.32	11.4	0.13
M73-11-404	7.33	0.86	1.48	49.1	1.05	0.03	0.3	<0.01	0.05	0.31	0.11	0.05	0.02	37.8	98.49	11.1	0.13
M73-11-422	32	7.62	2.7	26.3	1.63	0.09	2.58	0.01	0.39	0.19	0.1	0.05	0.06	22.9	96.62	6.47	0.6
M73-11-431	29.7	1.4	6.17	31.5	1.67	0.01	0.1	<0.01	0.08	0.57	0.34	0.04	0.01	27	98.59	7.8	0.11
M73-11-442	71	10.4	1.49	4.71	0.63	0.05	3.42	0.01	0.51	0.06	0.07	0.01	0.06	5.64	98.06	1.34	0.89
M73-11-450	86.4	6.06	0.39	0.97	0.14	0.86	2.56	<0.01	0.17	0.01	0.02	0.01	0.11	1.58	99.28	0.29	0.28
M73-11-498	52.6	9.46	3.8	6.28	1.21	0.48	3.51	0.01	0.55	0.13	0.05	0.21	9.19	8.45	95.93	1.8	2.18
M73-11-510	65.6	3.55	1.84	8.19	1.31	0.04	1.48	<0.01	0.14	0.16	0.04	0.11	6.44	9.1	98	2.36	1.46
M-73-19-72	18,05	4,32	2,26	41,8	0,79	0,21	1,33	0,005	0,24	0,15	0,04	0,04	0,02	31	100,26	8,99	0,99
M-73-19-133	13,05	1,45	1,61	46,2	0,67	0,16	0,49	0,003	0,09	0,22	0,03	0,04	0,01	35,3	99,32	10,1	0,56
M-73-19-249	75,1	11,8	1,09	0,91	0,58	0,2	3,95	0,01	0,68	0,02	0,08	<0.01	0,03	3,59	98,04	0,48	0,66
M-73-19-257	75,9	11,05	1,49	1,87	0,94	0,61	3,77	0,009	0,56	0,06	0,06	<0.01	0,04	4,62	100,98	0,9	0,38
M-73-19-296	87,2	3,63	0,66	4,03	0,43	0,33	1,74	0,002	0,06	0,08	0,02	<0.01	0,03	4,62	>102.00	1,07	0,08

SAMPLE	Ba	Ce	Cr	Cs	Dy	Er	Eu	Ga	Gd	Ge	Hf	Ho	La	Lu	Nb	Nd	Pr	Rb	Sm	Sn
DESCRIPTION	ppm	ppm	ppm	ppm	ppm	ppm	ppm	ppm	ppm	ppm	ppm	ppm	ppm	ppm	ppm	ppm	ppm	ppm	ppm	ppm
M73-3-027	95.6	7.9	20	0.49	0.86	0.58	0.31	2	0.97	<5	0.5	0.19	4.2	0.08	1.3	4.5	1.04	11.7	0.94	<1
M73-3-039	153.5	13.3	20	0.42	1.64	1.07	0.42	1.6	2	<5	0.5	0.34	7.6	0.11	1.4	7.4	1.88	8.8	1.74	<1
M73-3-069	104	6.2	20	0.17	0.83	0.52	0.17	0.8	0.89	<5	<0.2	0.15	4.6	0.05	0.4	3.3	0.82	3.3	0.58	<1
M73-3-094	1345	15.5	20	0.43	0.88	0.48	0.94	1.2	1.26	<5	0.2	0.19	7.7	0.06	0.5	8.9	2.21	5.9	1.67	<1
M73-3-119	1190	83.9	80	10.7	4.26	3.04	1.15	22.9	5.04	<5	6.3	0.92	43.2	0.45	20	34.1	9.47	171.5	6.17	4
M73-3-132	185	19.9	20	1.52	1.79	0.97	0.55	3.5	1.87	<5	0.7	0.34	11	0.1	2.3	10.3	2.68	25.6	1.89	<1
M73-3-143	283	24	50	6.03	1.47	0.98	0.35	12.3	1.49	<5	2.7	0.34	15.3	0.21	9.8	9.3	2.67	88.8	1.97	2
M73-3-154	142	39.1	30	2.4	3.41	1.69	0.84	5.3	3.87	<5	1	0.61	21.4	0.2	4.1	18.9	4.91	42.6	3.77	1
M73-3-162	300	90.5	40	3.47	7.87	5.11	1.45	15.7	8.19	<5	9.6	1.69	43.3	0.79	41.5	44	11.55	77.6	8.55	3
M73-3-196	36.6	29.5	20	0.57	3.61	1.72	0.84	1.9	3.76	<5	0.7	0.65	11.5	0.2	1.5	15.8	3.76	11	3.82	<1
M73-3-203	28.4	20.4	20	0.31	2.54	1.56	0.71	1.2	2.92	<5	0.4	0.47	8.8	0.19	0.8	11.3	2.75	7.3	2.63	<1
M73-3-218	26.2	52	20	0.36	6.85	4.27	1.1	2.4	8.09	<5	0.7	1.42	24.9	0.45	2.1	27.3	6.96	9.1	7.08	1
M73-3-233	532	74.2	90	12.25	4.65	2.95	1.04	22.1	5.4	<5	7.2	0.89	35	0.42	15.5	30.9	8.55	181	6.11	3
M73-3-241	17.4	57.5	20	0.33	21.3	10.25	5.64	1.6	22.4	<5	0.5	3.77	14.3	0.76	1	55.4	11.05	5.9	20.3	<1
M73-3-254	671	84.9	110	20.2	3.67	2.52	0.8	28.6	4.32	<5	4.9	0.75	40.8	0.42	17.6	32.9	9.25	234	5.23	4
M73-3-283	16.1	34.6	20	0.23	5.45	2.59	1.81	1.3	6.59	<5	0.3	0.93	10.4	0.23	0.6	23.6	5.36	5.1	6.86	<1
M73-3-293	81.1	26.3	30	1.18	9.08	5.09	1.9	3.3	8.07	<5	1.2	1.84	8.3	0.48	2.3	21.8	4.44	24.1	7.18	1
M73-3-318	451	66.2	90	10.15	3.58	2.43	1.06	18.8	4.69	<5	4.4	0.76	30.3	0.34	11.9	28.2	7.81	158.5	5.34	3
M73-3-328	412	57.9	80	9.82	3.4	2.26	0.89	17.8	4.29	<5	6.3	0.65	26.8	0.27	11.1	24.2	6.65	145.5	5.04	2
M73-3-347	221	42.5	50	2.73	3.36	2.64	0.45	11.4	2.96	<5	16.8	0.81	20.7	0.46	16.5	17.1	4.69	79.5	3.44	3
M73-3-364	94.3	41.6	50	0.95	6.78	4.78	1.21	3.8	6.49	<5	10.2	1.4	20.7	0.58	8.9	22	5.56	31.7	4.84	1
M73-3-374	150	67.2	50	2.68	5.78	3.52	1.59	9.1	6.71	<5	6.2	1.23	33.1	0.45	7.3	37.6	9.36	66.2	7.73	1
M73-3-393	250	81.1	80	7.87	9.06	4.94	1.63	16.7	10.3	<5	6.8	1.79	48.2	0.6	11.9	46.7	11.7	130	10.15	2
M73-3-412	91.2	36.4	30	1.51	0.91	0.57	0.54	4.8	1.81	<5	4.4	0.17	17.5	0.12	3.6	16.8	4.65	44	2.52	1
M73-11-290	410	32.8	50	5.68	2.83	1.56	0.71	9.9	3.36	<5	2.1	0.53	17	0.19	6.5	16.8	4.19	79.3	3.58	2
M73-11-296	353	37.1	50	9.47	2.27	1.39	0.48	12	2.52	<5	2.7	0.44	18.9	0.2	9.9	15.5	4.31	92.8	2.95	2
M73-11-312	480	39.6	50	8.72	2.74	1.75	0.65	13.1	3.23	<5	3	0.59	21.1	0.23	9.1	18.1	4.72	104	3.31	2
M73-11-319	145.5	17.9	20	0.62	1.41	0.76	0.37	1.3	1.73	<5	0.8	0.26	8.1	0.07	1.3	7.7	1.93	9.8	1.65	<1
M73-11-336	318	36.2	20	4.35	3.49	2.13	0.78	5.1	4.06	<5	1.2	0.72	24.5	0.24	3.4	20	4.8	37.7	3.78	<1
M73-11-347	191	29.2	20	0.92	3.45	1.89	0.76	1.7	3.52	<5	0.4	0.67	14.8	0.19	1.3	15.1	3.71	12	3.33	<1
M73-11-359	100	26.9	10	0.73	2.75	1.47	0.62	1.7	3.18	<5	0.8	0.62	14.5	0.16	1.6	13.7	3.2	10.2	2.62	1
M73-11-404	148	35.8	10	0.79	4.15	2.39	1.09	1.7	5.02	<5	1.2	0.8	18.7	0.21	1.2	19.5	4.43	10.4	3.95	<1
M73-11-422	540	62	50	9.28	4.88	2.85	1.33	12	5.84	<5	4	1	29	0.32	7.5	28.8	7.14	103	5.85	1
M73-11-431	67.4	53.4	20	0.18	5.69	3.3	1.44	3.3	6.11	<5	3.4	1.15	22.3	0.45	2.9	24.5	5.7	2.6	5.48	<1
M73-11-442	503	60.5	50	10.7	2.68	1.48	1.93	15.9	3.29	<5	6.4	0.53	33.3	0.2	11.2	24	6.57	123	3.92	1
M73-11-450	1030	20.9	20	1.83	0.95	0.67	0.3	7.1	1.13	<5	2.9	0.19	9.6	0.08	3.7	9.4	2.38	61.2	1.68	<1
M73-11-498	>10000	61.5	60	6.33	4.55	2.53	<0.03	15.9	5.07	<5	6.7	0.9	29.6	0.33	10.3	28.5	7.16	107.5	5.65	1
M73-11-510	>10000	39.8	20	1.61	4.82	2.63	<0.03	6.6	5.43	<5	2.7	1.01	20	0.27	2.9	23.2	5.41	35.7	4.98	<1
M-73-19-72	200	42,4	30	3,09	4,11	2,06	1,1	6,7	4,61	<5	2,6	0,73	20	0,22	4,9	21,2	5,56	46,1	5,03	1
M-73-19-133	69,7	46,8	20	1	4,76	2,27	1,53	3,3	5,42	<5	1,9	0,81	20,5	0,21	2,1	26	6,88	15,2	5,95	<1
M-73-19-249	277	71	70	5,37	2,95	2,07	0,63	16	3,09	<5	12	0,59	35	0,3	15,2	26,1	8,05	125	4,66	2
M-73-19-257	328	56,4	60	4,16	2,95	1,9	0,57	11	3,27	<5	11	0,6	25,8	0,33	11,7	21,5	6,04	115	3,93	1
M-73-19-296	282	40,7	20	0,72	2,05	1,24	0,45	3	1,89	<5	1,2	0,4	22,6	0,13	1,6	14,7	4,47	37,2	1,9	<1

SAMPLE	Sr	Ta	Tb	Th	Tm	U	V	W	Y	Yb	Zr	As	Bi	Hg	In	Re	Sb	Se	Te	Tl	Ag	Cd	Co	Cu	Li	Mo	Ni	Pb	Sc	Zn
DESCRIPTION	ppm	ppm	ppm	ppm	ppm	ppm	ppm	ppm	ppm	ppm	ppm	ppm	ppm	ppm	ppm	ppm	ppm	ppm	ppm	ppm	ppm	ppm	ppm	ppm	ppm	ppm	ppm	ppm	ppm	ppm
M73-3-027	20.9	0.2	0.15	1.34	0.13	1.07	21	65	6.4	0.62	20	4.2	1.5	0.042	0.006	0.001	2	1.2	0.01	0.04	<0.5	<0.5	15	5130	10	2	3	3	1	6
M73-3-039	329	0.2	0.27	1.41	0.15	1.79	17	106	10.3	0.77	18	8.6	2.92	0.105	0.011	0.009	14.6	1.8	0.02	0.12	20.2	<0.5	23	>10000	10	8	3	5	1	12
M73-3-069	256	0.1	0.13	0.28	0.11	0.44	10	42	5.6	0.49	5	11.5	0.13	0.045	<0.005	0.001	0.73	1.2	0.01	0.02	0.5	<0.5	7	463	10	1	1	2	1	8
M73-3-094	319	0.2	0.18	0.49	0.09	0.27	11	437	5.4	0.33	6	0.9	0.28	0.06	0.043	0.009	0.17	0.3	0.01	0.05	3.1	<0.5	62	782	10	4	5	3	1	3
M73-3-119	135.	1.5	0.75	13.25	0.45	2.52	98	116	20.9	3.1	217	8.3	4.26	<0.005	0.02	0.035	0.39	0.2	0.03	0.13	46.6	<0.5	20	9000	20	22	33	4	12	23
M73-3-132	451	0.3	0.29	1.57	0.15	0.62	18	189	9.6	0.94	24	2.1	2.61	0.114	0.012	0.019	0.22	1.1	0.01	0.07	14.5	<0.5	23	3510	10	10	7	4	2	9
M73-3-143	113	0.8	0.26	5.71	0.21	1.4	57	266	8.4	1.24	87	44.3	2.93	0.017	0.019	0.033	1.93	1.1	0.04	0.11	1.4	<0.5	46	>10000	10	26	19	3	6	15
M73-3-154	372	0.5	0.59	2.62	0.28	0.86	30	143	18.2	1.63	38	80.6	0.06	0.062	0.018	0.003	12.35	0.7	0.03	0.06	13.1	<0.5	31	2450	10	5	12	5	3	17
M73-3-162	70.6	2	1.31	9.54	0.83	3.98	48	244	43.7	5.57	437	97.6	2.83	0.031	0.048	0.018	77	0.5	0.07	0.08	3.7	0.5	45	4010	20	16	15	3	6	55
M73-3-196	23.9	0.2	0.61	1.95	0.28	0.8	17	148	18.5	1.6	25	8	0.04	0.008	0.02	0.006	4.4	0.4	0.01	0.21	0.7	<0.5	27	6930	10	24	4	5	1	3
M73-3-203	31.8	0.2	0.45	1.77	0.29	0.34	13	49	15.9	1.26	11	3.9	0.16	0.022	0.017	0.001	0.63	1	0.01	0.05	<0.5	<0.5	14	1650	<10	4	2	<2	2	3
M73-3-218	28.1	0.2	1.19	1.62	0.58	0.89	14	68	40.2	3.27	29	1.7	0.08	0.013	0.03	0.001	0.22	0.9	0.01	0.02	<0.5	<0.5	17	654	10	1	4	2	2	3
M73-3-233	29.8	1.3	0.75	12.2	0.46	2.81	100	216	23.6	2.96	255	70.2	0.18	<0.005	0.019	0.002	0.7	<0.2	0.01	0.09	<0.5	<0.5	45	2470	30	4	35	<2	13	33
M73-3-241	35.4	0.2	3.69	1.86	1.17	0.34	14	184	109.5	6.5	16	4	1.73	0.029	0.059	0.18	0.32	0.6	<0.01	0.11	<0.5	<0.5	39	65	10	60	8	6	1	3
M73-3-254	32.7	1.5	0.61	13.5	0.42	2.66	138	51	19.6	2.55	173	28.7	0.37	0.038	0.012	0.001	0.64	<0.2	0.03	0.1	<0.5	<0.5	24	41	50	3	42	8	16	46
M73-3-283	29.8	0.2	1.04	1.44	0.35	0.24	14	162	30.6	1.84	13	48.5	0.23	0.064	0.045	0.004	0.66	0.4	<0.01	0.19	<0.5	<0.5	38	9	<10	2	5	<2	1	3
M73-3-293	30.3	0.4	1.47	3.98	0.68	1.07	29	108	46.1	4.05	40	2	0.42	0.036	0.03	0.003	0.09	0.6	0.02	0.03	<0.5	<0.5	22	21	10	4	4	2	3	6
M73-3-318	39.4	0.9	0.63	9.08	0.37	2.05	92	119	19.1	2.42	159	13.2	0.22	0.06	0.031	<0.001	0.9	0.7	0.01	0.11	<0.5	<0.5	20	7120	30	7	32	6	12	34
M73-3-328	24	1	0.6	9.01	0.37	2.29	76	325	17.7	1.85	215	22.2	0.41	0.099	0.023	<0.001	1.15	0.8	0.01	0.15	<0.5	<0.5	51	>10000	10	10	20	4	10	26
M73-3-347	9.3	1.8	0.48	8.24	0.45	3.11	37	796	20.4	3.19	622	72.7	9.79	0.09	0.012	0.024	25.6	0.5	0.01	0.05	1.7	<0.5	92	9830	10	17	13	3	6	34
M73-3-364	13.3	0.9	1.11	5.06	0.7	3.8	21	782	48	4.38	412	15	1.44	0.019	0.019	0.001	0.76	0.6	<0.01	0.09	2.4	<0.5	108	3510	<10	2	15	5	3	6
M73-3-374	12.1	0.8	1.02	4.95	0.53	1.43	37	786	33	3.24	237	23.6	2.35	0.051	0.016	<0.001	5.99	0.3	<0.01	0.05	<0.5	<0.5	96	1350	<10	1	14	2	6	16
M73-3-393	17.4	0.9	1.56	9.44	0.73	3.19	74	158	47.5	4.36	243	>250	14.8	0.391	0.055	0.03	>250	0.6	0.02	0.15	1.5	3.8	56	>10000	10	34	26	6	10	422
M73-3-412	3.6	0.7	0.18	2.56	0.12	0.78	21	1160	4.5	0.72	176	0.5	0.01	0.012	<0.005	0.001	0.12	<0.2	<0.01	0.05	<0.5	<0.5	129	18	10	1	14	2	2	6
M73-11-290	437	0.6	0.47	4.8	0.24	1.44	45	137	14.6	1.46	65	>250	0.12	0.246	0.025	<0.001	1.07	0.6	0.03	0.05	<0.5	<0.5	35	15	40	1	19	45	6	89
M73-11-296	233	0.8	0.39	5.98	0.26	1.43	66	265	11.7	1.43	100	17.2	1.68	2.42	0.015	0.016	0.13	1	0.05	0.08	45	<0.5	46	5250	20	20	24	3	7	12
M73-11-312	356	0.7	0.49	6.41	0.24	1.42	59	151	14.8	1.77	99	22.4	0.26	0.077	0.023	0.003	0.07	1	0.09	0.05	>100	<0.5	32	>10000	30	7	27	13	8	20
M73-11-319	486	0.2	0.26	1.39	0.12	1.72	13	39	8.5	0.81	29	12.9	0.06	0.229	<0.005	<0.001	0.47	0.8	0.01	0.02	0.9	<0.5	13	1520	10	2	4	16	1	8
M73-11-336	503	0.2	0.63	2.56	0.31	0.85	27	131	23.7	1.89	42	16.2	0.06	0.106	0.013	0.001	0.16	0.9	0.04	0.04	<0.5	<0.5	26	375	20	2	7	21	3	15
M73-11-347	431	0.1	0.56	2.49	0.23	0.79	23	140	18.3	1.58	19	3.7	2.44	0.269	0.006	0.009	0.06	0.9	0.01	0.03	30	<0.5	29	6420	10	12	2	7	2	6
M73-11-359	439	0.1	0.48	1.63	0.22	0.55	11	135	16.3	1.45	26	4.3	0.69	0.079	0.01	<0.001	0.24	1	0.01	<0.02	8	<0.5	26	2540	10	3	4	10	1	8
M73-11-404	448	0.1	0.68	2.41	0.29	0.62	17	46	23.1	1.86	41	15.1	0.01	0.179	0.006	<0.001	0.1	1.1	0.02	<0.02	0.6	<0.5	12	843	10	3	6	16	1	10
M73-11-422	460	0.5	0.88	6.9	0.39	1.73	62	123	25.3	2.45	142	10.3	1.74	0.095	0.033	0.011	0.23	0.2	0.03	0.09	57.6	<0.5	19	>10000	20	8	17	11	8	26
M73-11-431	357	0.2	0.99	3.31	0.42	0.72	83	386	30.5	3.12	146	0.5	0.45	0.061	0.032	0.004	0.07	<0.2	0.14	0.04	1	<0.5	55	1070	20	1	12	2	2	33
M73-11-442	123.5	0.9	0.46	7.93	0.24	2.03	65	577	13.6	1.76	234	>250	5.11	2.17	0.019	0.005	>250	<0.2	<0.01	0.1	>100	4.7	62	>10000	10	2	21	4	7	640
M73-11-450	58.2	0.5	0.16	2.83	0.1	1.22	16	1115	4.6	0.73	103	155.5	7.66	0.29	<0.005	<0.001	3.25	0.4	<0.01	0.03	26	<0.5	133	5910	10	2	14	8	2	21
M73-11-498	1715	0.9	0.81	7.08	0.37	1.63	62	306	25	2.43	266	1.6	0.03	0.016	0.026	0.002	0.37	<0.2	<0.01	0.1	<0.5	<0.5	47	13	10	1	25	5	7	18
M73-11-510	1015	0.5	0.87	1.87	0.34	0.48	21	745	28.9	1.82	110	0.7	<0.01	0.029	0.026	<0.001	<0.05	0.5	<0.01	0.02	<0.5	<0.5	98	6	10	1	15	3	2	9
M-73-19-72	449	0,4	0,7	5	0,3	0,91	33	168	20,9	1,81	93	9,5		0,269	0,03	0,008	2,29	0,3	0,04	0,13	12,3	<0.5	42	8460	20	21	12	21	4	22
M-73-19-133	442	0,2	0,72	2,06	0,25	0,64	14	135	23,6	1,85	75	10,2	14,6	0,55	0,034	0,002	0,27	0,6	0,02	0,04	79	<0.5	33	>10000	10	3	13	9	3	8
M-73-19-249	20,6	1,3	0,51	9,35	0,32	2,16	54	790	16,2	2,33	495	>250	0,29	5,53	0,008	0,006	>250	<0.2	0,02	0,11	95,5	5,6	132	>10000	20	5	33	5	7	697
M-73-19-257	36,6	1,2	0,47	7,06	0,32	2,34	33	703	17	1,98	421	>250	0,04	2,87	0,011	0,004	146,5	<0.2	0,01	0,08	45,3	3,3	132	7050	10	14	35	7	6	448
M-73-19-296	44,2	1	0,36	0,94	0,2	0,54	9	1720	12,4	1,09	49	>250	1,6	0,51	0,014	0,009	119	<0.2	0,03	0,08	3,6	0,7	268	1280	10	5	34	5	<1	99

Anexo II – Tabela com dados químicos de Cu e Ag dos diferentes furos de testemunhos da área de Tullacondra realizados pela *Munster Base Metals* de 1969 a 1986 usados para o modelamento geológico (Fig. 11 e 12)

	from	to	Ag	Cu		from	to	Ag	Cu		from	to	Ag	Cu		from	to	Ag	Cu		from	to	Ag	Cu
M-73-01	5,2	6,1	11	0,28	**M-73-04**	97,2	98,8	4	0,33	**M-73-12**	82,6	84,1	19	0,63	**M-73-18**	30,5	32,3	0	0,19	**M-78-47**	54,6	56,1	0,1	0,04
M-73-01	6,1	7,6	6	0,14	**M-73-04**	98,8	100	42	1,02	**M-73-12**	84,1	85,6	23	0,82	**M-73-18**	32,3	33,8	0	0,09	**M-78-47**	56,1	57,6	0,1	0,068
M-73-01	7,6	9,1	6	0,36	**M-73-04**	100	100,9	7	0,25	**M-73-12**	85,6	87,2	15	0,61	**M-73-18**	33,8	36,3	0	0,02	**M-78-47**	57,6	59,1	0,1	0,225
M-73-01	9,1	10,7	8	0,33	**M-73-04**	100,9	102,4	3	0,18	**M-73-12**	87,2	88,7	20	0,58	**M-73-18**	36,3	37,8	0	0,18	**M-78-47**	59,1	60,7	0,1	0,061
M-73-01	10,7	12,2	19	0,43	**M-73-04**	102,4	103,9	19	0,62	**M-73-12**	88,7	90,2	20	0,61	**M-73-18**	37,8	39,3	0	0,02	**M-78-47**	60,7	62,2	0,1	0,07
M-73-01	12,2	13,7	12	0,34	**M-73-04**	103,9	105,5	0	0,1	**M-73-12**	90,2	91,7	32	0,84	**M-73-18**	39,3	40,8	0	0,16	**M-78-47**	62,2	63,7	0,1	0,063
M-73-01	13,7	15,2	14	0,49	**M-73-07**	26,5	29,5	2	0,32	**M-73-12**	91,7	93,3	28	0,72	**M-73-18**	40,8	42,4	24	0,92	**M-78-47**	63,7	65,2	0,1	0,152
M-73-01	15,2	16,8	25	0,75	**M-73-09**	91,7	93,6	0	0,03	**M-73-12**	93,3	94,8	24	1,48	**M-73-18**	43,9	45,4	5	0,31	**M-78-47**	65,2	66,8	0,1	0,027
M-73-01	16,8	18,3	19	0,66	**M-73-09**	93,6	95,1	26	0,8	**M-73-12**	94,8	96,3	35	0,78	**M-73-18**	45,4	46,3	25	0,55	**M-78-47**	66,8	68,3	0,1	0,013
M-73-01	18,3	19,8	16	0,53	**M-73-09**	95,1	96,6	37	1,04	**M-73-12**	96,3	97,8	42	1,38	**M-73-18**	46,3	47,9	36	0,84	**M-78-47**	68,3	69,8	0,1	0,08
M-73-01	19,8	21,3	23	0,79	**M-73-09**	96,6	98,1	20	0,83	**M-73-12**	97,8	99,4	42	1,38	**M-73-18**	47,9	49,7	18	0,45	**M-78-47**	69,8	71,3	0,1	0,019
M-73-01	21,3	22,9	21	0,67	**M-73-09**	98,1	99,7	36	1	**M-73-12**	99,4	100,9	39	1,18	**M-73-18**	49,7	50,9	27	0,6	**M-78-47**	71,3	72,8	0,1	0,023
M-73-01	22,9	24,1	3	0,35	**M-73-09**	99,7	101,2	30	0,97	**M-73-12**	100,9	102,4	21	0,69	**M-73-18**	50,9	51,8	94	1,48	**M-78-47**	72,8	74,4	0,1	0,02
M-73-01	24,1	25,9	2	0,51	**M-73-09**	101,2	102,7	67	1,62	**M-73-12**	102,4	103,9	19	0,79	**M-73-18**	51,8	53,3	24	0,68	**M-78-47**	74,4	75,9	0,1	0,252
M-73-01	25,9	27,4	23	0,92	**M-73-09**	102,7	104,2	61	1,56	**M-73-12**	103,9	105,5	15	0,4	**M-73-18**	53,3	54,9	4	0,01	**M-78-47**	75,9	77,4	0,1	1,66
M-73-01	27,4	29	6	0,27	**M-73-09**	104,2	105,8	54	1,68	**M-73-12**	105,5	107	22	0,56	**M-73-18**	54,9	56,4	14	0,44	**M-78-47**	77,4	78,9	0,1	0,62
M-73-01	29	30,5	7	0,17	**M-73-09**	105,8	107,3	46	1,33	**M-73-12**	107	108,5	24	0,75	**M-73-18**	56,4	57,9	14	0,4	**M-78-47**	78,9	80,5	0,1	0,87
M-73-01	30,5	32	9	0,27	**M-73-09**	107,3	108,8	40	1,01	**M-73-12**	108,5	110	11	0,36	**M-73-18**	57,9	59,4	6	0,75	**M-78-47**	80,5	82	0,1	0,43
M-73-01	32	33,5	12	0,3	**M-73-09**	108,8	110,3	39	1,21	**M-73-12**	110	111,6	8	0,17	**M-73-18**	59,4	62,8	3	0,11	**M-78-47**	82	83,5	0,1	0,292
M-73-01	33,5	35,1	24	0,57	**M-73-09**	110,3	111,9	37	1,21	**M-73-12**	111,6	113,1	15	0,42	**M-73-18**	62,8	64,3	3	0,1	**M-78-47**	83,5	85	0,1	0,405
M-73-01	35,1	36,6	16	0,43	**M-73-09**	111,9	113,4	29	0,91	**M-73-12**	113,1	114,9	21	0,56	**M-73-18**	64,3	65,8	10	0,37	**M-78-47**	85	86,6	0,1	0,127
M-73-01	36,6	38,1	12	0,41	**M-73-09**	113,4	114,9	19	0,54	**M-73-12**	114,9	116,7	20	0,5	**M-73-18**	65,8	67,1	4	0,38	**M-78-47**	86,6	89	0,1	0,108
M-73-01	38,1	39,6	6	0,28	**M-73-09**	114,9	116,4	16	0,48	**M-73-12**	116,7	118,9	14	0,34	**M-73-18**	67,1	68,9	0	0,05					
M-73-01	39,6	41,1	7	0,28	**M-73-09**	116,4	118	19	0,54	**M-73-12**	118,9	120,4	12	0,46	**M-73-18**	68,9	70,4	8	0,31					
M-73-01	41,1	42,7	5	0,26	**M-73-09**	118	119,5	15	0,47	**M-73-12**	120,4	121,9	26	0,84	**M-73-18**	70,4	72,2	18	0,39					
M-73-01	42,7	44,2	8	0,42	**M-73-09**	119,5	121	5	0,72	**M-73-12**	121,9	123,4	33	1,07	**M-73-18**	72,2	73,5	26	0,55					
M-73-01	44,2	45,7	14	0,67	**M-73-09**	121	122,5	4	0,45	**M-73-12**	123,4	125	48	1,5	**M-73-18**	73,5	75	39	0,56					
M-73-01	45,7	47,2	13	0,66	**M-73-09**	122,5	124,1	3	0,29	**M-73-12**	125	126,5	41	1,38	**M-73-18**	75	76,5	86	0,61					
M-73-01	47,2	48,8	14	0,54	**M-73-09**	124,1	125	4	0,46	**M-73-12**	126,5	128	41	1,32	**M-73-18**	76,5	77,4	107	0,72					
M-73-01	48,8	50,3	19	0,76	**M-73-09**	125	125,9	12	0,58	**M-73-12**	128	129,5	26	0,66	**M-73-18**	77,4	78,6	27	0,11					
M-73-01	50,3	51,8	25	0,68	**M-73-09**	125,9	127,4	20	0,49	**M-73-12**	129,5	131,7	34	1,05	**M-73-18**	78,6	79,9	165	0,82					
M-73-01	51,8	53,3	24	0,57	**M-73-09**	127,4	128,9	32	1,08	**M-73-12**	131,7	134,7	24	0,56	**M-73-18**	79,9	81,1	100	0,7					
M-73-01	53,3	54,9	5	0,24	**M-73-09**	128,9	130,5	11	0,72	**M-73-12**	134,7	137,8	29	0,64	**M-73-18**	81,1	82,6	21	0,22					
M-73-01	54,9	56,4	12	0,23	**M-73-09**	130,5	132	18	0,87	**M-73-12**	137,8	140,8	14	0,31	**M-73-18**	82,6	84,1	0	0,02					
M-73-01	56,4	57,9	2	0,01	**M-73-09**	132	133,5	11	0,41	**M-73-12**	140,8	142,3	4	0,19	**M-73-18**	84,1	85,6	0	0,05					
M-73-01	57,9	59,4	3	0,01	**M-73-09**	133,5	135	30	0,97	**M-73-12**	142,3	143,3	6	0,29	**M-73-18**	85,6	87,2	0	0,09					
M-73-01	59,4	61,3	3	0,01	**M-73-09**	135	135,9	53	1,14	**M-73-12**	143,3	146,3	0	0,07	**M-73-18**	87,2	88,7	0	0,13					
M-73-01	61,3	62,5	5	0,24	**M-73-09**	135,9	137,5	52	1,03	**M-73-12**	146,3	150,6	0	0,04	**M-73-18**	88,7	90,2	0	0,03					
M-73-01	62,5	64	24	0,55	**M-73-09**	137,5	138,7	9	0,21	**M-73-13**	90,2	91,7	0	0,04	**M-73-18**	90,2	91,7	53	0,39					
M-73-01	64	65,5	5	0,02	**M-73-09**	138,7	140,2	21	0,56	**M-73-13**	91,7	93,3	5	0,34	**M-73-18**	91,7	92,7	40	0,44					
M-73-01	65,5	67,1	0	0,01	**M-73-09**	140,2	141,7	15	0,59	**M-73-13**	93,3	94,8	4	0,24	**M-73-18**	92,7	94,2	0	0,04					
M-73-01	67,1	68,6	0	0,01	**M-73-09**	141,7	143	12	0,57	**M-73-13**	94,8	96,3	4	0,2	**M-73-18**	94,2	95,7	0	0,01					
M-73-01	68,6	69,8	0	0,01	**M-73-09**	143	144,5	29	0,94	**M-73-13**	96,3	97,8	12	0,45	**M-73-18**	95,7	97,8	0	0,01					
M-73-01	69,8	70,9	0	0,16	**M-73-09**	144,5	145,4	12	0,28	**M-73-13**	97,8	100	20	0,7	**M-73-19**	15,5	18,9	0	0,07					
M-73-01	70,9	71,9	0	0,01	**M-73-09**	145,4	146,6	0	0,16	**M-73-13**	100	101,5	52	1,6	**M-73-19**	18,9	20,4	0	0,01					
M-73-01	71,9	73,5	0	0,01	**M-73-09**	146,6	148,1	0	0,03	**M-73-13**	101,5	103	41	1,28	**M-73-19**	20,4	23,5	0	0,18					
M-73-01	73,5	75	0	0,13	**M-73-09**	148,1	150,3	30	0,84	**M-73-13**	103	104,5	31	1	**M-73-19**	23,5	26,5	9	0,26					
M-73-01	75	76,5	0	0,01	**M-73-09**	150,3	152,4	0	0,17	**M-73-13**	104,5	106,1	9	0,35	**M-73-19**	26,5	29,6	8	0,15					
M-73-01	76,5	78	0	0,01	**M-73-11**	88,4	89,6	0	0,03	**M-73-13**	106,1	107,6	15	0,43	**M-73-19**	29,6	31,1	12	0,33					
M-73-01	78	79,6	0	0,02	**M-73-11**	89,6	91,1	0	0,12	**M-73-13**	107,6	109,1	15	0,44	**M-73-19**	31,1	32,6	5	0,43					
M-73-01	79,6	81,1	0	0,05	**M-73-11**	91,1	92,7	25	0,77	**M-73-13**	109,1	110,6	12	0,38	**M-73-19**	32,6	35,7	0	0,18					
M-73-01	81,1	82,6	0	0,01	**M-73-11**	92,7	93,9	32	1,12	**M-73-13**	110,6	112,2	17	0,54	**M-73-19**	35,7	38,7	0	0,08					
M-73-01	82,6	84,1	0	0,02	**M-73-11**	93,9	95,4	21	0,66	**M-73-13**	112,2	113,7	3	0,16	**M-73-19**	38,7	40,2	4	0,04					
M-73-01	84,1	85,6	0	0,01	**M-73-11**	95,4	96,6	21	0,63	**M-73-13**	113,7	114,9	15	0,48	**M-73-19**	40,2	42,1	35	0,91					
M-73-01	85,6	87,2	0	0,03	**M-73-11**	96,6	98,1	15	0,38	**M-73-13**	114,9	116,4	7	0,22	**M-73-19**	42,1	43,9	37	1,05					
M-73-01	87,2	88,7	0	0,03	**M-73-11**	98,1	99,7	49	1,34	**M-73-13**	116,4	118	12	0,47	**M-73-19**	43,9	45,4	22	0,61					
M-73-01	88,7	90,2	0	0,02	**M-73-11**	99,7	100,9	14	0,39	**M-73-13**	118	119,5	15	0,62	**M-73-19**	45,4	48,5	16	0,36					
M-73-01	90,2	91,7	0	0,04	**M-73-11**	100,9	102,4	32	1,11	**M-73-13**	119,5	121	12	0,25	**M-73-19**	48,5	51,5	13	0,74					
M-73-01	91,7	93,3	0	0,02	**M-73-11**	102,4	103,9	12	0,44	**M-73-13**	121	122,5	16	0,49	**M-73-19**	51,5	54,6	20	0,46					
M-73-01	93,3	94,8	0	0,01	**M-73-11**	103,9	105,5	19	0,56	**M-73-13**	122,5	123,7	14	0,42	**M-73-19**	54,6	56,1	28	0,66					
M-73-01	94,8	96,3	0	0,16	**M-73-11**	105,5	107	26	0,68	**M-73-13**	123,7	125,3	36	1,08	**M-73-19**	56,1	59,1	0	0,04					
M-73-01	96,3	97,5	0	0,01	**M-73-11**	107	108,5	25	0,77	**M-73-13**	125,3	126,8	46	1,26	**M-73-19**	59,1	62,2	0	0,03					
M-73-01	97,5	98,5	0	0,01	**M-73-11**	108,5	110	33	0,97	**M-73-13**	126,8	128,6	9	0,65	**M-73-19**	62,2	65,2	0	0,01					
M-73-01	98,5	100	26	0,43	**M-73-11**	110	111,6	28	0,76	**M-73-13**	128,6	130,1	5	0,2	**M-73-19**	65,2	66,8	0	0,02					
M-73-01	100	100,7	11	0,45	**M-73-11**	111,6	113,1	16	0,65	**M-73-13**	130,1	131,7	32	1,09	**M-73-19**	66,8	68,3	0	0,02					
M-73-01	101	101,3	24	1,24	**M-73-11**	113,1	114,6	14	0,42	**M-73-13**	131,7	133,5	15	0,6	**M-73-19**	68,3	69,8	0	0,04					
M-73-01	101	103	56	0,71	**M-73-11**	114,6	116,1	21	0,78	**M-73-13**	133,5	135	62	0,99	**M-73-19**	69,8	71,3	0	0,11					
M-73-01	103	104,5	26	0,39	**M-73-11**	116,1	117,7	18	0,64	**M-73-13**	135	136,9	56	0,71	**M-73-19**	71,3	72,8	0	0,01					
M-73-01	105	106,1	35	0,82	**M-73-11**	117,7	119,2	18	0,67	**M-73-13**	136,9	138,4	15	0,34	**M-73-19**	72,8	74,4	0	0,01					
M-73-01	106	107,6	71	0,85	**M-73-11**	119,2	120,7	12	0,4	**M-73-13**	138,4	139,9	78	1,17	**M-73-19**	74,4	75,9	117	1,22					
M-73-01	108	109,1	26	0,38	**M-73-11**	120,7	121,9	22	0,66	**M-73-13**	139,9	141,4	17	0,29	**M-73-19**	75,9	77,4	61	1,15					
M-73-01	109	110,6	5	0,15	**M-73-11**	121,9	123,1	12	0,41	**M-73-13**	141,4	143	11	0,2	**M-73-19**	77,4	78,9	58	0,99					
M-73-01	111	112,2	3	0,08	**M-73-11**	123,1	124,7	15	0,69	**M-73-13**	143	144,2	2	0,08	**M-73-19**	78,9	80,5	69	1,14					
M-73-01	112	113,7	2	0,4	**M-73-11**	124,7	126,2	14	0,43	**M-73-13**	144,2	177,4	19	0,41	**M-73-19**	80,5	82	60	0,9					
M-73-01	114	115,2	29	0,24	**M-73-11**	126,2	128	46	1,28	**M-73-13**	177,4	180,4	0	0,08	**M-73-19**	82	83,5	46	0,76					
M-73-01	115	116,7	0	0,06	**M-73-11**	128	129,2	45	1,47	**M-73-14**	8,8	10,4	0	0,08	**M-73-19**	83,5	85	46	0,92					
M-73-01	117	118,3	0	0,03	**M-73-11**	129,2	130,8	4	0,54	**M-73-14**	10,4	11,9	0	0,11	**M-73-19**	85	86,9	51	1,02					
M-73-01	118	119,8	0	0,03	**M-73-11**	130,8	132,3	17	0,74	**M-73-14**	11,9	13,4	5	0,23	**M-73-19**	86,9	89	34	0,86					
M-73-01	120	121,3	0	0,04	**M-73-11**	132,3	133,8	36	0,89	**M-73-14**	13,4	14,9	6	0,26	**M-73-19**	89	90,5	9	0,16					
M-73-01	121	123,1	0	0,09	**M-73-11**	133,8	135	78	1,36	**M-73-14**	14,9	16,2	8	0,48	**M-73-19**	90,5	92	39	0,62					
M-73-01	123	124,4	0	0,05	**M-73-11**	135	136,6	10	0,32	**M-73-14**	16,2	17,7	9	0,15	**M-73-19**	92	93,9	42	1,14					
M-73-01	124	125,7	0	0,17	**M-73-11**	136,6	138,1	20	0,7	**M-73-14**	17,7	19,2	27	0,48	**M-73-19**	93,9	95,4	5	0,17					
M-73-01	126	127,4	0	0,03	**M-73-11**	138,1	139,6	31	1,02	**M-73-14**	19,2	20,7	20	0,43	**M-73-21**	32	33,8	0	0,04					
M-73-01	127	128,9	0	0,04	**M-73-11**	139,6	141,7	23	0,67	**M-73-14**	20,7	22,3	29	0,73	**M-73-21**	33,8	36	0	0,06					
M-73-01	129	129,7	3	0,14	**M-73-11**	141,7	143,6	7	0,31	**M-73-14**	22,3	23,8	27	0,72	**M-73-21**	36	37,2	0	0,33					
M-73-01	130	131,2	15	0,51	**M-73-11**	143,6	144,8	5	0,11	**M-73-14**	23,8	25,3	28	0,84	**M-73-21**	37,2	38,7	0	0,07					
M-73-01	131	131,8	3	0,14	**M-73-11**	144,8	146	0	0,12	**M-73-14**	25,3	26,8	16	0,38	**M-73-21**	38,7	41,8	0	0,05					
M-73-01	132	133,5	8	0,22	**M-73-11**	146	147,5	0	0,17	**M-73-14**	26,8	28,3	19	0,52	**M-73-21**	41,8	44,5	0	0,06					
M-73-01	134	134,1	64	1,7	**M-73-11**	147,5	149	0	0,03	**M-73-14**	28,3	29,9	26	0,71	**M-73-21**	44,5	46,3	0	0,06					

M-73-01	134	135,6	9	0,45	**M-73-11**	149	150,9	0	0,04	**M-73-14**	29,9	31,4	25	0,83	**M-73-21**	46,3	48,8	0	0,03
M-73-01	136	137,2	5	0,16	**M-73-11**	150,9	152,7	0	0,03	**M-73-14**	31,4	32,9	23	0,56	**M-73-21**	48,8	50,3	0	0,47
M-73-01	137	138,7	0	0,03	**M-73-11**	152,7	155,8	0	0,05	**M-73-14**	32,9	34,4	27	0,58	**M-73-21**	50,3	51,8	0	0,03
M-73-01	139	140,2	0	0,1	**M-73-11**	155,8	156,4	0	0,18	**M-73-14**	34,4	36	18	0,42	**M-73-22**	125,9	127	0	0,14
M-73-01	140	141,7	0	0,11	**M-73-11**	156,4	157,9	0	0,12	**M-73-14**	36	37,5	25	0,7	**M-73-23**	0	5,8		
M-73-01	142	143,7	0	0,09	**M-73-11**	157,9	160,6	0	0,08	**M-73-14**	37,5	39	16	0,39	**M-73-23**	5,8	8,8	1	0,23
M-73-01	144	144,6	0	0,08	**M-73-12**	77,7	79,2	0	0,02	**M-73-14**	39	40,5	12	0,39	**M-73-23**	8,8	11,9		0,12
M-73-01	145	145,2	0	0,28	**M-73-12**	79,2	80,5	0	0,19	**M-73-14**	40,5	42,1	13	0,26	**M-73-23**	11,9	14,9		0,09
M-73-01	145	146,8	0	0,02	**M-73-12**	80,5	81,7	7	0,28	**M-73-14**	42,1	43,6	23	0,61	**M-73-23**	14,9	18		0,1
M-73-01	147	148,3	0	0,02	**M-73-12**	81,7	82,6	32	0,98	**M-73-14**	43,6	45,1	0	0,12	**M-73-23**	18	21		0,04
M-73-01	148	150,4	0	0,03	**M-73-12**	82,6	84,1	19	0,63	**M-73-14**	45,1	48,2	0	0,04	**M-73-23**	21	24,1	1	0,32
M-73-01	150	151,5	0	0,02	**M-73-12**	84,1	85,6	23	0,82	**M-73-14**	48,2	50,6	0	0,02	**M-73-23**	24,1	27,1		0,13
M-73-01	152	152,7	0	0,01	**M-73-12**	85,6	87,2	15	0,61	**M-73-14**	50,6	52,4	0	0,14	**M-73-23**	27,1	30,2		0,15
M-73-01	153	154,2	0	0,06	**M-73-12**	87,2	88,7	20	0,58	**M-73-14**	52,4	53,9	0	0,11	**M-73-23**	30,2	33,2		0,16
M-73-01	154	155,9	0	0,08	**M-73-12**	88,7	90,2	20	0,61	**M-73-14**	53,9	55,5	7	0,21	**M-73-23**	33,2	36,3		0,12
M-73-01	156	157,4	0	0,08	**M-73-12**	90,2	91,7	32	0,84	**M-73-14**	55,5	57	24	0,75	**M-73-23**	36,3	39,3		0,15
M-73-01	157	159,1	0	0,08	**M-73-12**	91,7	93,3	28	0,72	**M-73-14**	57	58,5	21	0,64	**M-73-23**	39,3	42,4		0,17
M-73-01	159	159,9	0	0,07	**M-73-12**	93,3	94,8	24	1,48	**M-73-14**	58,5	60	21	0,52	**M-73-23**	42,4	45,4		0,17
M-73-01	160	161,4	0	0,02	**M-73-12**	94,8	96,3	35	0,78	**M-73-14**	60	61,6	18	0,68	**M-73-23**	45,4	48,8		0,17
M-73-01	161	162,9	0	0,02	**M-73-12**	96,3	97,8	42	1,38	**M-73-14**	61,6	63,1	34	1,04	**M-73-24**	0	3,2		
M-73-02	7,6	9,1	2	0,4	**M-73-12**	97,8	99,4	42	1,38	**M-73-14**	63,1	64,6	29	0,82	**M-73-24**	3,2	3,6		0,18
M-73-02	9,1	10,7	2	0,28	**M-73-12**	99,4	100,9	39	1,18	**M-73-14**	64,6	66,4	21	0,68	**M-73-24**	3,6	4,1		0,03
M-73-02	10,7	12,2	3	0,34	**M-73-12**	100,9	102,4	21	0,69	**M-73-14**	66,4	68,3	27	0,76	**M-73-24**	4,1	4,6		0,01
M-73-02	12,2	13,7	3	0,59	**M-73-12**	102,4	103,9	19	0,79	**M-73-14**	68,3	69,8	59	1,78	**M-73-24**	4,6	5,4		0,01
M-73-02	13,7	15,2	3	0,59	**M-73-12**	103,9	105,5	15	0,4	**M-73-14**	69,8	71,3	41	1,33	**M-73-24**	5,4	6,3		0,01
M-73-02	15,2	16,8	3	0,47	**M-73-12**	105,5	107	22	0,56	**M-73-14**	71,3	72,8	49	1,54	**M-73-24**	6,3	7,2		0,01
M-73-02	16,8	18,3	3	0,38	**M-73-12**	107	108,5	24	0,75	**M-73-14**	72,8	74,4	40	1,33	**M-73-25**	13,7	16,7	3	0,32
M-73-02	18,3	19,8	3	0,26	**M-73-12**	108,5	110	11	0,36	**M-73-14**	74,4	75,9	27	0,85	**M-73-26**	114,9	117		0,15
M-73-02	19,8	21,3	2	0,29	**M-73-12**	110	111,6	8	0,17	**M-73-14**	75,9	77,4	29	0,98	**M-73-26**	116,7	120		0,1
M-73-02	21,3	22,9	2	0,14	**M-73-12**	111,6	113,1	15	0,42	**M-73-14**	77,4	78,9	36	1,06	**M-75-32**	6,7	9,1	1	0,1
M-73-02	22,9	24,4	2	0,11	**M-73-12**	113,1	114,9	21	0,56	**M-73-14**	78,9	80,5	31	0,92	**M-75-32**	9,1	10,7	10	0,45
M-73-02	24,4	25,9	2	0,21	**M-73-12**	114,9	116,7	20	0,5	**M-73-14**	80,5	82	23	0,83	**M-75-32**	10,7	12,2	46	1,48
M-73-02	25,9	27,4	2	0,27	**M-73-12**	116,7	118,9	14	0,34	**M-73-14**	82	83,5	20	0,59	**M-75-32**	12,2	13,7	3	0,23
M-73-02	27,4	29	16	0,51	**M-73-12**	118,9	120,4	12	0,46	**M-73-14**	83,5	85	13	0,46	**M-75-32**	13,7	16,8	0	0,1
M-73-02	29	30,5	15	0,38	**M-73-12**	120,4	121,9	26	0,84	**M-73-14**	85	86,6	35	1,14	**M-75-32**	16,8	19,8	1	0,07
M-73-02	30,5	32	18	0,42	**M-73-12**	121,9	123,4	33	1,07	**M-73-14**	86,6	89,6	9	0,27	**M-75-32**	19,8	22,9	1	0,06
M-73-02	32	33,5	31	0,67	**M-73-12**	123,4	125	48	1,5	**M-73-14**	89,6	91,1	19	0,61	**M-75-32**	22,9	25,9	1	0,05
M-73-02	33,5	35,1	15	0,31	**M-73-12**	125	126,5	41	1,38	**M-73-14**	91,1	93	34	0,98	**M-75-32**	25,9	27,4	3	0,06
M-73-02	35,1	36,6	27	0,72	**M-73-12**	126,5	128	41	1,32	**M-73-14**	93	94,8	9	0,31	**M-75-32**	27,4	30,5	20	0,18
M-73-02	36,6	38,1	20	0,53	**M-73-12**	128	129,5	26	0,66	**M-73-14**	94,8	96,3	14	0,39	**M-75-32**	30,5	32	1	0,13
M-73-02	38,1	39	29	0,49	**M-73-12**	129,5	131,7	34	1,05	**M-73-14**	96,3	97,8	3	0,08	**M-75-32**	32	35,1	3	0,09
M-73-02	39	39,9	32	1,08	**M-73-12**	131,7	134,7	24	0,56	**M-73-14**	97,8	99,7	14	0,54	**M-75-32**	48,8	51,8	3	0,02
M-73-02	39,9	41,5	12	0,46	**M-73-12**	134,7	137,8	29	0,64	**M-73-14**	99,7	100,6	12	0,2	**M-75-32**	68,6	71,6	3	0,13
M-73-02	41,5	43	3	0,21	**M-73-12**	137,8	140,8	14	0,31	**M-73-14**	100,6	102,1	27	0,56	**M-75-32**	71,6	73,2	6	0,56
M-73-02	43	44,5	13	0,27	**M-73-12**	140,8	142,3	4	0,19	**M-73-14**	102,1	103,6	49	0,99	**M-75-32**	73,2	74,7	9	1,32
M-73-02	44,5	46	0	0,13	**M-73-12**	142,3	143,3	6	0,29	**M-73-14**	103,6	106,4	73	0,68	**M-75-32**	74,7	76,5	1	0,13
M-73-02	46	47,5	0	0,02	**M-73-12**	143,3	146,3	0	0,07	**M-73-14**	106,4	107,9	49	0,23	**M-75-33**	129,5	131	5	0,16
M-73-02	47,5	49,1	3	0,2	**M-73-12**	146,3	150,6	0	0,04	**M-73-14**	107,9	109,4	128	1,21	**M-75-34**	18,6	20,4	6	0,11
M-73-02	49,1	50,6	6	0,37	**M-73-13**	90,2	91,7	0	0,04	**M-73-14**	109,4	110,3	51	0,69	**M-75-34**	68,3	71,3	2	0,06
M-73-02	50,6	52,1	0	0,16	**M-73-13**	91,7	93,3	5	0,34	**M-73-14**	110,3	112,8	7	0,08	**M-75-34**	71,3	74,4	2	0,07
M-73-02	52,1	53,6	0	0,02	**M-73-13**	93,3	94,8	4	0,24	**M-73-14**	112,8	115,8	4	0,08	**M-75-34**	74,4	77,4	3	0,03
M-73-02	53,6	55,2	0	0,01	**M-73-13**	94,8	96,3	4	0,2	**M-73-14**	115,8	116,7	23	0,29	**M-75-34**	77,4	78,9	383	1,26
M-73-02	55,2	58,2	0	0,18	**M-73-13**	96,3	97,8	12	0,45	**M-73-14**	116,7	119,5	0	0,04	**M-75-34**	78,9	80,5	99	0,85
M-73-02	58,2	61,3	0	0,01	**M-73-13**	97,8	100	20	0,7	**M-73-15**	74,7	76,2	0	0,12	**M-75-34**	80,5	82	65	0,44
M-73-02	61,3	64,6	0	0,01	**M-73-13**	100	101,5	52	1,6	**M-73-15**	76,2	77,7	0	0,07	**M-75-34**	82	84,4	19	0,19
M-73-02	64,6	67,7	0	0,01	**M-73-13**	101,5	103	41	1,28	**M-73-15**	77,7	80,8	0	0,07	**M-75-35**	34,7	37,8	7	0,03
M-73-02	67,7	68,3	4	0,46	**M-73-13**	103	104,5	31	1	**M-73-15**	80,8	83,8	0	0,03	**M-75-35**	37,8	40,8	5	0,05
M-73-02	68,3	69,8	0	0,01	**M-73-13**	104,5	106,1	9	0,35	**M-73-15**	83,8	85,3	0	0,02	**M-75-35**	40,8	42,4	300	1,21
M-73-02	92,7	94,2	0	0,02	**M-73-13**	106,1	107,6	15	0,43	**M-73-15**	85,3	86,9	0	0,14	**M-75-35**	42,4	45,1	139	0,39
M-73-02	94,2	95,4	42	0,62	**M-73-13**	107,6	109,1	15	0,44	**M-73-15**	86,9	89,9	0	0,1	**M-75-35**	45,1	47,9	21	0,56
M-73-02	95,4	96,6	46	0,97	**M-73-13**	109,1	110,6	12	0,38	**M-73-15**	89,9	93	0	0,06	**M-75-35**	47,9	48,8	7	0,16
M-73-02	96,6	98,1	25	0,38	**M-73-13**	110,6	112,2	17	0,54	**M-73-15**	93	94,5	0	0,03	**M-75-36**	123,4	127	0	0
M-73-02	98,1	99,7	13	0,28	**M-73-13**	112,2	113,7	3	0,16	**M-73-15**	94,5	96	0	0,17	**M-75-36**	126,5	130	0	0,1
M-73-02	101	102,1	33	0,78	**M-73-13**	113,7	114,9	15	0,48	**M-73-15**	96	99,1	0	0,03	**M-75-36**	129,5	133	0	0,09
M-73-02	102	103,6	23	0,43	**M-73-13**	114,9	116,4	7	0,22	**M-73-15**	99,1	100,9	0	0,05	**M-75-36**	132,6	136	0	0,07
M-73-02	104	105,2	0	0,13	**M-73-13**	116,4	118	12	0,47	**M-73-15**	100,9	102,4	4	0,28	**M-75-37**	63,7	65,2	3,117	0,02
M-73-02	105	106,7	0	0,07	**M-73-13**	118	119,5	15	0,62	**M-73-15**	102,4	105,5	0	0,03	**M-75-37**	65,2	66,8	2,267	0,07
M-73-02	107	107,6	0	0,05	**M-73-13**	119,5	121	12	0,25	**M-73-15**	105,5	108,5	0	0,02	**M-75-37**	66,8	68,3	6,518	0,29
M-73-02	108	109,4	0	0,04	**M-73-13**	121	122,5	16	0,49	**M-73-15**	108,5	110	0	0,07	**M-75-37**	68,3	69,8	5,951	0,59
M-73-02	109	110,9	9	0,23	**M-73-13**	122,5	123,7	14	0,42	**M-73-15**	110	111,9	0	0,01	**M-75-37**	69,8	71,6	11,34	0,78
M-73-02	111	112,5	0	0,04	**M-73-13**	123,7	125,3	36	1,08	**M-73-15**	111,9	113,4	32	1,01	**M-75-37**	71,6	73,5	40,81	0,77
M-73-02	120	121	0	0,13	**M-73-13**	125,3	126,8	46	1,26	**M-73-15**	113,4	115,8	23	0,29	**M-75-37**	73,5	75	20,69	0,34
M-73-02	121	122,8	0	0,18	**M-73-13**	126,8	128,6	9	0,65	**M-73-15**	115,8	117,3	57	0,46	**M-75-37**	75	76,5	45,91	0,53
M-73-02	123	125	0	0,05	**M-73-13**	128,6	130,1	5	0,2	**M-73-15**	117,3	118,9	17	0,21	**M-75-37**	76,5	78	66,88	0,47
M-73-02	125	125,6	12	0,51	**M-73-13**	130,1	131,7	32	1,09	**M-73-15**	118,9	120,7	50	0,91	**M-75-37**	78	79,6	108,8	1,01
M-73-02	126	127,1	0	0,07	**M-73-13**	131,7	133,5	15	0,6	**M-73-15**	120,7	124,1	0	0,13	**M-75-37**	79,6	80,5	79,35	1,17
M-73-02	127	128,6	0	0,12	**M-73-13**	133,5	135	62	0,99	**M-73-15**	124,1	127,1	0	0,11	**M-75-37**	80,5	82,6	2,267	0,21
M-73-02	129	129,8	0	0,1	**M-73-13**	135	136,9	56	0,71	**M-73-16**	150,9	153,9	0	0,04	**M-75-37**	82,6	84,7	7,935	0,25
M-73-02	130	131,7	14	0,25	**M-73-13**	136,9	138,4	15	0,34	**M-73-16**	153,9	157	0	0,03	**M-75-39**	88,1	91,1	2,267	0,11
M-73-02	132	134,4	0	0,06	**M-73-13**	138,4	139,9	78	1,17	**M-73-16**	157	160	0	0,05	**M-76-41**	16,1	18,3	60,28	0,52
M-73-02	134	135,9	16	0,49	**M-73-13**	139,9	141,4	17	0,29	**M-73-16**	160	163,1	0	0,05	**M-76-41**	18,3	19,8	157,6	0,53
M-73-02	136	137,5	0	0,05	**M-73-13**	141,4	143	11	0,2	**M-73-16**	163,1	166,1	0	0,05	**M-76-41**	19,8	21	44,43	0,33
M-73-02	138	140,2	0	0,05	**M-73-13**	143	144,2	2	0,08	**M-73-16**	166,1	169,8	0	0,06	**M-76-41**	21	23,2	6,226	0,38
M-73-02	140	141,4	4	0,44	**M-73-13**	144,2	177,4	19	0,41	**M-73-16**	169,8	173,1	12	0,2	**M-78-47**	15,2	16,5	0,1	0,018
M-73-02	141	143	0	0,06	**M-73-13**	177,4	180,4	0	0,08	**M-73-16**	173,1	174	4	1	**M-78-47**	16,5	18	0,1	0,02
M-73-04	8,8	11,9	0	0,04	**M-73-14**	8,8	10,4	0	0,08	**M-73-16**	174	177,1	0	0,08	**M-78-47**	18	19,5	0,1	0,014
M-73-04	11,9	14,9	0	0,05	**M-73-14**	10,4	11,9	0	0,11	**M-73-16**	177,1	180,4	0	0,08	**M-78-47**	19,5	21	0,1	0,053
M-73-04	14,9	18	0	0,04	**M-73-14**	11,9	13,4	5	0,23	**M-73-16**	180,4	181,4	37	0,49	**M-78-47**	21	22,6	0,1	0,04
M-73-04	18	19,5	0	0,01	**M-73-14**	13,4	14,9	6	0,26	**M-73-16**	181,4	183,2	0	0,08	**M-78-47**	22,6	24,1	0,1	0,033
M-73-04	56,7	58,2	0	0,04	**M-73-14**	14,9	16,2	8	0,48	**M-73-17**	90,8	92,4	0	0,04	**M-78-47**	24,1	25,6	0,1	0,055
M-73-04	58,2	59,7	0	0,03	**M-73-14**	16,2	17,7	9	0,15	**M-73-17**	92,4	94,2	0	0,04	**M-78-47**	25,6	27,1	0,1	0,082
M-73-04	59,7	61,3	5	0,25	**M-73-14**	17,7	19,2	27	0,48	**M-73-17**	94,2	95,7	0	0,12	**M-78-47**	27,1	28,7	0,1	0,102

M-73-04	61,3	62,8	0	0,02	**M-73-14**	19,2	20,7	20	0,43	**M-73-17**	95,7	97,2	0	0,13	**M-78-47**	28,7	30,2	0,1	0,065
M-73-04	62,8	65,8	0	0,01	**M-73-14**	20,7	22,3	29	0,73	**M-73-17**	97,2	99,7	0	0,07	**M-78-47**	30,2	31,7	0,1	0,102
M-73-04	65,8	67,4	0	0,09	**M-73-14**	22,3	23,8	27	0,72	**M-73-17**	99,7	102,7	0	0,06	**M-78-47**	31,7	33,2	0,1	0,059
M-73-04	67,4	68,9	0	0,08	**M-73-14**	23,8	25,3	28	0,84	**M-73-18**	10,1	11,6	0	0,14	**M-78-47**	33,2	34,7	0,1	0,027
M-73-04	68,9	70,7	30	1,1	**M-73-14**	25,3	26,8	16	0,38	**M-73-18**	11,6	13,1	0	0,15	**M-78-47**	34,7	36,3	0,1	0,02
M-73-04	70,7	72,2	7	0,25	**M-73-14**	26,8	28,3	19	0,52	**M-73-18**	13,1	14,6	0	0,15	**M-78-47**	36,3	37,8	0,1	0,013
M-73-04	72,2	73,8	7	0,3	**M-73-14**	28,3	29,9	26	0,71	**M-73-18**	14,6	16,2	0	0,13	**M-78-47**	37,8	39,3	0,1	0,019
M-73-04	73,8	75,6	1	0,06	**M-73-14**	29,9	31,4	25	0,83	**M-73-18**	16,2	17,7	0	0,15	**M-78-47**	39,3	40,8	0,1	0,022
M-73-04	75,6	77,1	12	0,45	**M-73-14**	31,4	32,9	23	0,56	**M-73-18**	17,7	18,9	4	0,2	**M-78-47**	40,8	42,4	0,1	0,049
M-73-04	77,1	78,6	0	0,05	**M-73-14**	32,9	34,4	27	0,58	**M-73-18**	18,9	19,8	0	0,02	**M-78-47**	42,4	43,9	0,1	0,044
M-73-04	78,6	81,7	0	0,08	**M-73-14**	34,4	36	18	0,42	**M-73-18**	19,8	21,3	14	0,29	**M-78-47**	43,9	45,4	0,1	0,117
M-73-04	81,7	84,7	0	0,07	**M-73-14**	36	37,5	25	0,7	**M-73-18**	21,3	22,9	0	0,03	**M-78-47**	45,4	46,9	0,1	0,134
M-73-04	84,7	91,1	0	0,04	**M-73-14**	37,5	39	16	0,39	**M-73-18**	22,9	24,4	0	0,04	**M-78-47**	46,9	48,5	0,1	0,065
M-73-04	91,1	92,7	0	0,01	**M-73-14**	39	40,5	12	0,39	**M-73-18**	24,4	25,9	0	0,05	**M-78-47**	48,5	50	0,1	0,381
M-73-04	92,7	93,9	11	0,38	**M-73-14**	40,5	42,1	13	0,26	**M-73-18**	25,9	27,4	0	0,04	**M-78-47**	50	51,5	0,1	0,336
M-73-04	93,9	95,1	48	0,78	**M-73-14**	42,1	43,6	23	0,61	**M-73-18**	27,4	29	7	0,22	**M-78-47**	51,5	53	0,1	0,48
M-73-04	95,1	97,2	15	0,49	**M-73-14**	43,6	45,1	0	0,12	**M-73-18**	29	30,5	0	0,09	**M-78-47**	53	54,6	0,1	0,367

ANEXO III – Tabela com dados estratigráficos dos dos diferentes furos de testemunhos da área de Tullacondra realizados pela *Munster Base Metals* de 1969 a 1986 usados para o modelamento geológico (Fig. 11 e 12)

Drill Hole	from	to	Lithology
M-73-01	0.00	5.18	Overburden
M-73-01	5.18	45.42	Tullacondra Limestone
M-73-01	45.42	46.48	Ballyvergin Shale
M-73-01	46.48	67.97	Upper Shaly Calcarenite
M-73-01	67.97	74.07	Oolitic Calcarenite
M-73-01	74.07	83.52	Lower Shaly Calcarenite
M-73-01	83.52	87.78	Uniform Calcarenite
M-73-01	87.78	99.97	Upper Transition Series
M-73-01	99.97	111.10	Lower Transition Series
M-73-01	111.10	168.55	Old Red Sandstone
M-73-02	0.00	7.62	Overburden
M-73-02	7.62	27.43	Kilmaclenine Limestone
M-73-02	27.43	39.01	Tullacondra Limestone
M-73-02	39.01	40.08	Ballyvergin Shale
M-73-02	40.08	61.57	Upper Shaly Calcarenite
M-73-02	61.57	68.58	Oolitic Calcarenite
M-73-02	68.58	81.69	Lower Shaly Calcarenite
M-73-02	81.69	84.73	Uniform Calcarenite
M-73-02	84.73	96.62	Upper Transition Series
M-73-02	96.62	109.27	Lower Transition Series
M-73-02	109.27	146.00	Old Red Sandstone
M-73-03	0.00	7.62	Overburden
M-73-03	7.62	35.36	Tullacondra Limestone
M-73-03	35.36	36.27	Ballyvergin Shale
M-73-03	36.27	81.08	Upper Shaly Calcarenite
M-73-03	81.08	92.35	Oolitic Calcarenite
M-73-03	92.35	105.77	Lower Shaly Calcarenite
M-73-03	105.77	110.34	Uniform Calcarenite
M-73-03	110.34	119.48	Upper Transition Series
M-73-03	119.48	131.37	Lower Transition Series
M-73-04	0.00	8.84	Overburden
M-73-04	8.84	38.56	Tullacondra Limestone
M-73-04	38.56	39.62	Ballyvergin Shale
M-73-04	39.62	63.70	Upper Shaly Calcarenite
M-73-04	63.70	69.19	Oolitic Calcarenite
M-73-04	69.19	76.05	Lower Shaly Calcarenite
M-73-04	76.05	81.38	Uniform Calcarenite
M-73-04	81.38	95.10	Upper Transition Series
M-73-04	95.10	106.22	Lower Transition Series
M-73-04	106.22	121.92	Old Red Sandstone
M-73-05	0.00	42.67	Kilmaclenine Limestone
M-73-05	42.67	68.88	Tullacondra Limestone
M-73-05	68.88	69.04	Ballyvergin Shale
M-73-05	69.04	87.63	Upper Shaly Calcarenite
M-73-05	87.63	97.23	Oolitic Calcarenite
M-73-05	97.23	133.81	UNKNOWN
M-73-05	133.81	135.33	Lower Transition Series
M-73-05	135.33	140.51	Old Red Sandstone
M-73-09	0.00	12.19	Overburden
M-73-09	12.19	45.72	Kilmaclenine Limestone
M-73-09	45.72	81.23	Tullacondra Limestone
M-73-09	81.23	82.30	Ballyvergin Shale
M-73-09	82.30	108.36	Upper Shaly Calcarenite
M-73-09	108.36	111.56	Oolitic Calcarenite
M-73-09	111.56	116.74	Lower Shaly Calcarenite
M-73-09	116.74	119.63	Uniform Calcarenite
M-73-13	80.77	81.99	Ballyvergin Shale
M-73-13	81.99	102.11	Upper Shaly Calcarenite
M-73-13	102.11	111.86	Oolitic Calcarenite
M-73-13	111.86	118.57	Lower Shaly Calcarenite
M-73-13	118.57	123.14	Uniform Calcarenite
M-73-13	123.14	136.09	Upper Transition Series
M-73-13	136.09	149.96	Lower Transition Series
M-73-13	149.96	156.06	Old Red Sandstone
M-73-14	0.00	8.84	Overburden
M-73-14	8.84	17.68	Kilmaclenine Limestone
M-73-14	17.68	52.43	Tullacondra Limestone
M-73-14	52.43	53.34	Ballyvergin Shale
M-73-14	53.34	70.41	Upper Shaly Calcarenite
M-73-14	70.41	79.55	Oolitic Calcarenite
M-73-14	79.55	85.95	Lower Shaly Calcarenite
M-73-14	85.95	91.29	Uniform Calcarenite
M-73-14	91.29	106.38	Upper Transition Series
M-73-14	106.38	119.33	Lower Transition Series
M-73-14	119.33	121.92	Old Red Sandstone
M-73-15	0.00	15.24	Overburden
M-73-15	15.24	19.35	Kilmaclenine Limestone
M-73-15	19.35	57.15	Tullacondra Limestone
M-73-15	57.15	58.52	Ballyvergin Shale
M-73-15	58.52	78.49	Upper Shaly Calcarenite
M-73-15	78.49	88.85	Oolitic Calcarenite
M-73-15	88.85	96.16	Lower Shaly Calcarenite
M-73-15	96.16	100.28	Uniform Calcarenite
M-73-15	100.28	116.74	Upper Transition Series
M-73-15	116.74	128.32	Lower Transition Series
M-73-16	0.00	23.16	Overburden
M-73-16	23.16	72.85	Kilmaclenine Limestone
M-73-16	72.85	108.97	Tullacondra Limestone
M-73-16	108.97	110.03	Ballyvergin Shale
M-73-16	110.03	132.28	Upper Shaly Calcarenite
M-73-16	132.28	144.78	Oolitic Calcarenite
M-73-16	144.78	152.25	Lower Shaly Calcarenite
M-73-16	152.25	157.28	Uniform Calcarenite
M-73-16	157.28	170.54	Upper Transition Series
M-73-16	170.54	183.34	Lower Transition Series
M-73-16	183.34	185.93	Old Red Sandstone
M-73-17	0.00	15.54	Overburden
M-73-17	15.54	49.38	Tullacondra Limestone
M-73-17	49.38	50.44	Ballyvergin Shale
M-73-17	50.44	66.75	Upper Shaly Calcarenite
M-73-17	66.75	71.93	Oolitic Calcarenite
M-73-17	71.93	80.47	Lower Shaly Calcarenite
M-73-17	80.47	82.60	Uniform Calcarenite
M-73-17	82.60	95.10	Upper Transition Series
M-73-17	95.10	107.29	Lower Transition Series
M-73-17	107.29	110.34	Old Red Sandstone
M-73-18	0.00	10.06	Overburden
M-73-18	10.06	18.90	Tullacondra Limestone
M-73-18	18.90	19.81	Ballyvergin Shale
M-73-18	19.81	39.93	Upper Shaly Calcarenite
M-73-18	39.93	53.04	Oolitic Calcarenite
M-73-18	53.04	59.13	Lower Shaly Calcarenite
M-73-26	67.06	83.82	Upper Shaly Calcarenite
M-73-26	83.82	93.57	Oolitic Calcarenite
M-73-26	93.57	102.72	Lower Shaly Calcarenite
M-73-26	102.72	105.77	Uniform Calcarenite
M-73-26	105.77	117.96	Upper Transition Series
M-73-26	117.96	131.06	Lower Transition Series
M-73-26	131.06	133.20	Old Red Sandstone
M-75-36	0.00	17.98	Overburden
M-75-36	17.98	42.67	Kilmaclenine Limestone
M-75-36	42.67	78.79	Tullacondra Limestone
M-75-36	78.79	80.47	Ballyvergin Shale
M-75-36	80.47	94.49	Upper Shaly Calcarenite
M-75-36	94.49	105.16	Oolitic Calcarenite
M-75-36	105.16	111.71	Lower Shaly Calcarenite
M-75-36	111.71	117.20	Uniform Calcarenite
M-75-36	117.20	126.19	Upper Transition Series
M-75-36	126.19	135.03	Lower Transition Series
M-75-32	0.00	6.71	Overburden
M-75-32	6.71	31.39	Upper Shaly Calcarenite
M-75-32	31.39	41.15	Oolitic Calcarenite
M-75-32	41.15	51.51	Lower Shaly Calcarenite
M-75-32	51.51	57.00	Uniform Calcarenite
M-75-32	57.00	71.63	Upper Transition Series
M-75-32	71.63	76.50	Lower Transition Series
M-75-33	0.00	12.19	Overburden
M-75-33	12.19	31.24	Kilmaclenine Limestone
M-75-33	31.24	69.04	Tullacondra Limestone
M-75-33	69.04	70.10	Ballyvergin Shale
M-75-33	70.10	91.44	Upper Shaly Calcarenite
M-75-33	91.44	102.11	Oolitic Calcarenite
M-75-33	102.11	109.42	Lower Shaly Calcarenite
M-75-33	109.42	114.30	Uniform Calcarenite
M-75-33	114.30	129.08	Upper Transition Series
M-75-33	129.08	134.72	Lower Transition Series
M-75-34	0.00	16.76	Overburden
M-75-34	16.76	16.92	Ballyvergin Shale
M-75-34	16.92	38.10	Upper Shaly Calcarenite
M-75-34	38.10	47.70	Oolitic Calcarenite
M-75-34	47.70	57.76	Lower Shaly Calcarenite
M-75-34	57.76	63.40	Uniform Calcarenite
M-75-34	63.40	81.69	Upper Transition Series
M-75-34	81.69	84.43	Lower Transition Series
M-75-35	0.00	4.57	Overburden
M-75-35	4.57	10.82	Oolitic Calcarenite
M-75-35	10.82	20.73	Lower Shaly Calcarenite
M-75-35	20.73	27.13	Uniform Calcarenite
M-75-35	27.13	41.91	Upper Transition Series
M-75-35	41.91	48.77	Lower Transition Series
M-75-37	0.00	14.63	Overburden
M-75-37	14.63	31.39	Upper Shaly Calcarenite
M-75-37	31.39	42.37	Oolitic Calcarenite
M-75-37	42.37	49.68	Lower Shaly Calcarenite
M-75-37	49.68	57.45	Uniform Calcarenite
M-75-37	57.45	76.50	Upper Transition Series
M-75-37	76.50	84.73	Lower Transition Series
M-75-38	0.00	14.63	Overburden
M-79-49	141.43	164.29	Upper Shaly Calcarenite
M-79-49	164.29	180.14	Oolitic Calcarenite
M-79-49	180.14	186.23	Lower Shaly Calcarenite
M-79-49	186.23	190.20	Uniform Calcarenite
M-79-49	190.20	204.52	Upper Transition Series
M-79-49	204.52	234.09	Lower Transition Series
M-79-49	234.09	239.88	Old Red Sandstone
M-85-51	0.00	29.44	Overburden
M-85-51	29.44	34.70	Oolitic Calcarenite
M-85-51	34.70	42.17	Lower Shaly Calcarenite
M-85-51	42.17	46.31	Uniform Calcarenite
M-85-51	46.31	60.80	Upper Transition Series
M-85-51	60.80	62.86	Lower Transition Series
M-85-52	0.00	29.26	Overburden
M-85-52	29.26	37.56	Lower Shaly Calcarenite
M-85-52	37.56	42.06	Uniform Calcarenite
M-85-52	42.06	56.08	Upper Transition Series
M-85-52	56.08	61.87	Lower Transition Series

M-73-09	119.63	133.05	Upper Transition Series	M-73-18	59.13	64.47	Uniform Calcarenite	M-75-38	14.63	34.14	Upper Shaly Calcarenite
M-73-09	133.05	145.39	Lower Transition Series	M-73-18	64.47	77.27	Upper Transition Series	M-75-38	34.14	45.26	Oolitic Calcarenite
M-73-09	145.39	155.45	Old Red Sandstone	M-73-18	77.27	94.03	Lower Transition Series	M-75-38	45.26	53.19	Lower Shaly Calcarenite
M-73-10	0.00	19.51	Overburden	M-73-18	94.03	97.84	Old Red Sandstone	M-75-38	53.19	58.52	Uniform Calcarenite
M-73-10	19.51	46.94	Kilmaclenine Limestone	M-73-19	0.00	8.84	Overburden	M-75-38	58.52	74.98	Upper Transition Series
M-73-10	46.94	83.67	Tullacondra Limestone	M-73-19	8.84	19.66	Upper Shaly Calcarenite	M-75-38	74.98	79.55	Lower Transition Series
M-73-10	83.67	84.73	Ballyvergin Shale	M-73-19	19.66	28.65	Oolitic Calcarenite	M-75-39	0.00	16.46	Overburden
M-73-10	84.73	106.38	Upper Shaly Calcarenite	M-73-19	28.65	46.33	Lower Shaly Calcarenite	M-75-39	16.46	17.22	Tullacondra Limestone
M-73-10	106.38	114.30	Oolitic Calcarenite	M-73-19	46.33	55.93	Uniform Calcarenite	M-75-39	17.22	18.29	Ballyvergin Shale
M-73-10	114.30	120.24	Lower Shaly Calcarenite	M-73-19	55.93	71.17	Upper Transition Series	M-75-39	18.29	43.13	Upper Shaly Calcarenite
M-73-10	120.24	124.97	Uniform Calcarenite	M-73-19	71.17	92.66	Lower Transition Series	M-75-39	43.13	55.02	Oolitic Calcarenite
M-73-10	124.97	137.92	Upper Transition Series	M-73-19	92.66	95.40	Old Red Sandstone	M-75-39	55.02	62.79	Lower Shaly Calcarenite
M-73-10	137.92	151.49	Lower Transition Series	M-73-20	0.00	13.72	Overburden	M-75-39	62.79	69.04	Uniform Calcarenite
M-73-10	151.49	184.71	Old Red Sandstone	M-73-20	13.72	24.08	Upper Shaly Calcarenite	M-75-39	69.04	86.26	Upper Transition Series
M-73-11	0.00	18.29	Overburden	M-73-20	24.08	34.90	Oolitic Calcarenite	M-75-39	86.26	91.14	Lower Transition Series
M-73-11	18.29	46.33	Kilmaclenine Limestone	M-73-20	34.90	45.90	Lower Shaly Calcarenite	M-76-41	0.00	10.67	Overburden
M-73-11	46.33	81.38	Tullacondra Limestone	M-73-20	45.90	50.29	Uniform Calcarenite	M-76-41	10.67	17.68	Upper Transition Series
M-73-11	81.38	82.91	Ballyvergin Shale	M-73-20	50.29	62.03	Upper Transition Series	M-76-41	17.68	36.27	Lower Transition Series
M-73-11	82.91	101.96	Upper Shaly Calcarenite	M-73-20	62.03	75.90	Lower Transition Series	M-76-41	36.27	42.06	Old Red Sandstone
M-73-11	101.96	108.81	Oolitic Calcarenite	M-73-20	75.90	85.34	Old Red Sandstone	M-76-42	0.00	10.06	Overburden
M-73-11	108.81	118.57	Lower Shaly Calcarenite	M-73-21	0.00	12.19	Overburden	M-76-42	10.06	27.43	Old Red Sandstone
M-73-11	118.57	123.14	Uniform Calcarenite	M-73-21	12.19	26.21	FAULT ZONE	M-78-47	0.00	15.24	Overburden
M-73-11	123.14	131.52	Upper Transition Series	M-73-21	26.21	32.77	Upper Transition Series	M-78-47	15.24	21.95	Tullacondra Limestone
M-73-11	131.52	143.56	Lower Transition Series	M-73-21	32.77	46.33	Lower Transition Series	M-78-47	21.95	23.32	Ballyvergin Shale
M-73-11	143.56	144.78	DIKE	M-73-21	46.33	52.73	Old Red Sandstone	M-78-47	23.32	42.06	Upper Shaly Calcarenite
M-73-11	144.78	147.52	Old Red Sandstone	M-73-22	0.00	25.30	Overburden	M-78-47	42.06	51.21	Oolitic Calcarenite
M-73-11	147.52	147.98	DIKE	M-73-22	25.30	32.00	Kilmaclenine Limestone	M-78-47	51.21	55.78	Dike
M-73-11	147.98	160.63	Old Red Sandstone	M-73-22	32.00	63.55	Tullacondra Limestone	M-78-47	55.78	59.44	Lower Shaly Calcarenite
M-73-12	0.00	7.62	Overburden	M-73-22	63.55	64.92	Ballyvergin Shale	M-78-47	59.44	68.12	Uniform Calcarenite
M-73-12	7.62	46.63	Kilmaclenine Limestone	M-73-22	64.92	86.56	Upper Shaly Calcarenite	M-78-47	68.12	77.72	Upper Transition Series
M-73-12	46.63	81.69	Tullacondra Limestone	M-73-22	86.56	95.10	Oolitic Calcarenite	M-78-47	77.72	89.00	Lower Transition Series
M-73-12	81.69	82.60	Ballyvergin Shale	M-73-22	95.10	104.09	Lower Shaly Calcarenite	M-78-48	0.00	12.19	Overburden
M-73-12	82.60	96.93	Upper Shaly Calcarenite	M-73-22	104.09	110.34	Uniform Calcarenite	M-78-48	12.19	25.60	Upper Shaly Calcarenite
M-73-12	96.93	106.98	Oolitic Calcarenite	M-73-22	110.34	126.03	Upper Transition Series	M-78-48	25.60	34.75	Oolitic Calcarenite
M-73-12	106.98	114.91	Lower Shaly Calcarenite	M-73-22	126.03	135.94	Lower Transition Series	M-78-48	34.75	44.35	Lower Shaly Calcarenite
M-73-12	114.91	121.01	Uniform Calcarenite	M-73-22	135.94	138.68	Old Red Sandstone	M-78-48	44.35	49.38	Uniform Calcarenite
M-73-12	121.01	128.63	Upper Transition Series	M-73-24	0.00	10.36	Overburden	M-78-48	49.38	62.79	Upper Transition Series
M-73-12	128.63	142.49	Lower Transition Series	M-73-24	10.36	31.39	Lower Transition Series	M-78-48	62.79	73.15	Lower Transition Series
M-73-12	142.49	150.57	Old Red Sandstone	M-73-24	31.39	34.75	Old Red Sandstone	M-79-49	0.00	25.60	Overburden
M-73-13	0.00	13.72	Overburden	M-73-26	0.00	28.96	Overburden	M-79-49	25.60	110.34	Kilmaclenine Limestone
M-73-13	13.72	44.20	Kilmaclenine Limestone	M-73-26	28.96	66.29	Tullacondra Limestone	M-79-49	110.34	140.21	Tullacondra Limestone
M-73-13	44.20	80.77	Tullacondra Limestone	M-73-26	66.29	67.06	Ballyvergin Shale	M-79-49	140.21	141.43	Ballyvergin Shale